

ISSN 1881-7831 Online ISSN 1881-784X

DD & T

Drug Discoveries & Therapeutics

Volume 17, Number 1
February, 2023



www.ddtjournal.com

DD & T

Drug Discoveries & Therapeutics



ISSN: 1881-7831
Online ISSN: 1881-784X
CODEN: DDTRBX
Issues/Year: 6
Language: English
Publisher: IACMHR Co., Ltd.

Drug Discoveries & Therapeutics is one of a series of peer-reviewed journals of the International Research and Cooperation Association for Bio & Socio-Sciences Advancement (IRCA-BSSA) Group. It is published bimonthly by the International Advancement Center for Medicine & Health Research Co., Ltd. (IACMHR Co., Ltd.) and supported by the IRCA-BSSA.

Drug Discoveries & Therapeutics publishes contributions in all fields of pharmaceutical and therapeutic research such as medicinal chemistry, pharmacology, pharmaceutical analysis, pharmaceuticals, pharmaceutical administration, and experimental and clinical studies of effects, mechanisms, or uses of various treatments. Studies in drug-related fields such as biology, biochemistry, physiology, microbiology, and immunology are also within the scope of this journal.

Drug Discoveries & Therapeutics publishes Original Articles, Brief Reports, Reviews, Policy Forum articles, Case Reports, Communications, Editorials, News, and Letters on all aspects of the field of pharmaceutical research. All contributions should seek to promote international collaboration in pharmaceutical science.

Editorial Board

International Field Chief Editors:

Fen-Er CHEN
Fudan University, Shanghai, China

Takashi KARAKO
National Center for Global Health and Medicine, Tokyo, Japan

Hongzhou LU
National Clinical Research Centre for Infectious Diseases, Shenzhen, Guangdong, China

Munehiro NAKATA
Tokai University, Hiratsuka, Japan

Sven SCHRÖDER
University Medical Center Hamburg Eppendorf (UKE), Hamburg, Germany

Kazuhiisa SEKIMIZU
Teikyo University, Tokyo, Japan

Corklin R. STEINHART
CAN Community Health, FL, USA

Executive Editor:

Hongzhou LU
National Clinical Research Centre for Infectious Diseases, Shenzhen, Guangdong, China

Associate Editors:

Nobuyoshi AKIMITSU
The University of Tokyo, Tokyo, Japan

Feihu CHEN
Anhui Medical University, Hefei, Anhui, China

Jianjun GAO
Qingdao University, Qingdao, Shandong, China

Hiroshi HAMAMOTO
Teikyo University, Tokyo, Japan

Chikara KAITO
Okayama University, Okayama, Japan

Gagan KAUSHAL
Jefferson College of Pharmacy, Philadelphia, PA, USA

Xiao-Kang LI
National Research Institute for Child Health and Development, Tokyo, Japan

Yasuhiko MATSUMOTO
Meiji Pharmaceutical University, Tokyo, Japan

Atsushi MIYASHITA
Teikyo University, Tokyo, Japan

Masahiro MURAKAMI
Osaka Ohtani University, Osaka, Japan

Tomofumi SANTA
The University of Tokyo, Tokyo, Japan

Tianqiang SONG
Tianjin Medical University, Tianjin, China

Sanjay K. SRIVASTAVA
Texas Tech University Health Sciences Center, Abilene, TX, USA

Hongbin SUN
China Pharmaceutical University, Nanjing, Jiangsu, China

Fengshan WANG
Shandong University, Jinan, Shandong, China.

Proofreaders:

Curtis BENTLEY
Roswell, GA, USA
Thomas R. LEBON
Los Angeles, CA, USA

Editorial and Head Office:

Pearl City Koishikawa 603,
2-4-5 Kasuga, Bunkyo-ku,
Tokyo 112-0003, Japan
E-mail: office@ddtjournal.com

Drug Discoveries & Therapeutics

Editorial and Head Office

Pearl City Koishikawa 603, 2-4-5 Kasuga, Bunkyo-ku,
Tokyo 112-0003, Japan

E-mail: office@ddtjournal.com
URL: www.ddtjournal.com

Editorial Board Members

| | | | |
|--|--|--|--|
| Alex ALMASAN (Cleveland, OH) | Youcai HU (Beijing) | Sridhar MANI (Bronx, NY) | Yong XU (Guangzhou, Guangdong) |
| John K. BUOLAMWINI (Memphis, TN) | Yu HUANG (Hong Kong) | Tohru MIZUSHIMA (Tokyo) | Bing YAN (Ji'nan, Shandong) |
| Jianping CAO (Shanghai) | Zhangjian HUANG (Nanjing, Jiangsu) | Jasmin MONPARA (Philadelphia, PA) | Chunyan YAN (Guangzhou, Guangdong) |
| Shousong CAO (Buffalo, NY) | Amrit B. KARMARKAR (Karad, Maharashtra) | Yoshinobu NAKANISHI (Kanazawa, Ishikawa) | Xiao-Long YANG (Chongqing) |
| Jang-Yang CHANG (Tainan) | Toshiaki KATADA (Tokyo) | Siriporn OKONOGLI (Chiang Mai) | Yun YEN (Duarte, CA) |
| Zhe-Sheng CHEN (Queens, NY) | Ibrahim S. KHATTAB (Kuwait) | Weisan PAN (Shenyang, Liaoning) | Yongmei YIN (Tianjin) |
| Zilin CHEN (Wuhan, Hubei) | Shiroh KISHIOKA (Wakayama, Wakayama) | Chan Hum PARK (Eumseong) | Yasuko YOKOTA (Tokyo) |
| Xiaolan CUI (Beijing) | Robert Kam-Ming KO (Hong Kong) | Rakesh P. PATEL (Mehsana, Gujarat) | Yun YOU (Beijing) |
| Saphala DHITAL (Clemson, SC) | Nobuyuki KOBAYASHI (Nagasaki, Nagasaki) | Shivanand P. PUTHLI (Mumbai, Maharashtra) | Rongmin YU (Guangzhou, Guangdong) |
| Shaofeng DUAN (Lawrence, KS) | Toshiro KONISHI (Tokyo) | Shafiqur RAHMAN (Brookings, SD) | Tao YU (Qingdao, Shandong) |
| Hao FANG (Ji'nan, Shandong) | Peixiang LAN (Wuhan, Hubei) | Gary K. SCHWARTZ (New York, NY) | Guangxi ZHAI (Ji'nan, Shandong) |
| Marcus L. FORREST (Lawrence, KS) | Chun-Guang LI (Melbourne) | Luqing SHANG (Tianjin) | Liangren ZHANG (Beijing) |
| Tomoko FUJIYUKI (Tokyo) | Minyong LI (Ji'nan, Shandong) | Yuemao SHEN (Ji'nan, Shandong) | Lining ZHANG (Ji'nan, Shandong) |
| Takeshi FUKUSHIMA (Funabashi, Chiba) | Xun LI (Ji'nan, Shandong) | Rong SHI (Shanghai) | Na ZHANG (Ji'nan, Shandong) |
| Harald HAMACHER (Tübingen, Baden-Württemberg) | Dongfei LIU (Nanjing, Jiangsu) | Chandan M. THOMAS (Bradenton, FL) | Ruiwen ZHANG (Houston, TX) |
| Kenji HAMASE (Fukuoka, Fukuoka) | Jian LIU (Hefei, Anhui) | Michihisa TOHDA (Sugitani, Toyama) | Xiu-Mei ZHANG (Ji'nan, Shandong) |
| Junqing HAN (Ji'nan, Shandong) | Jikai LIU (Wuhan, Hubei) | Li TONG (Xining, Qinghai) | Xuebo ZHANG (Baltimore, MD) |
| Xiaojiang HAO (Kunming, Yunnan) | Jing LIU (Beijing) | Murat TURKOGLU (Istanbul) | Yingjie ZHANG (Ji'nan, Shandong) |
| Kiyoshi HASEGAWA (Tokyo) | Xinyong LIU (Ji'nan, Shandong) | Hui WANG (Shanghai) | Yongxiang ZHANG (Beijing) |
| Waseem HASSAN (Rio de Janeiro) | Yuxiu LIU (Nanjing, Jiangsu) | Quanxing WANG (Shanghai) | Haibing ZHOU (Wuhan, Hubei) |
| Langchong HE (Xi'an, Shaanxi) | Hongxiang LOU (Jinan, Shandong) | Stephen G. WARD (Bath) | Jian-hua ZHU (Guangzhou, Guangdong) |
| Rodney J. Y. HO (Seattle, WA) | Hai-Bin LUO (Haikou, Hainan) | Zhun WEI (Qingdao, Shandong) | (As of October 2022) |
| Hsing-Pang HSIEH (Zhunan, Miaoli) | Xingyuan MA (Shanghai) | Tao XU (Qingdao, Shandong) | |
| Yongzhou HU (Hangzhou, Zhejiang) | Ken-ichi MAFUNE (Tokyo) | Yuhong XU (Shanghai) | |

Original Article

- 1-9 **Cyclic AMP (cAMP)-dependent proteolysis of GATA6 by proteasome: Zinc-finger domain of GATA6 has signals for nuclear export and proteolysis, both of which are responsive to cAMP.**
Tomohisa Yamamoto, Takeshi Tsuge, Makoto Araki, Masatomo Maeda
- 10-17 **Redundant roles of extra-cellular signal-regulated kinase (ERK) 1 and 2 in the G1-S transition and etoposide-induced G2/M checkpoint in HCT116 cells.**
Purev Erdenebaatar, I Ketut Gunarta, Ryusuke Suzuki, Ravdandorj Odongoo, Toshihiro Fujii, Rikiro Fukunaga, Masato T Kanemaki, Katsuji Yoshioka
- 18-25 ***Bombyx mori* as a model for *Niallia circulans* pathogenicity.**
M. Ismail Hossain, Nusrat U. A. Saleh, Al Numan, M. Mahtab Hossain, M. Aftab Uddin, Muktadir S. Hossain
- 26-36 **ENST00000438158 aids ultrasound for predicting lymph node metastasis and inhibits migration and invasion of papillary thyroid carcinoma cells.**
Hui Liu, Yixin Shi, Jia Zhan, Yingchun Liu, Jing Zhou, Biao Su, Yue Chen, Ling Wang, Lin Chen
- 37-44 **A fast RT-qPCR system significantly shortens the time for SARS-CoV-2 nucleic acid test.**
Hongjie Dong, Kundi Zhang, Junmei Zhang, Yumeng Xiao, Fengyu Zhang, Maofeng Wang, Hongwei Wang, Guihua Zhao, Shiling Xie, Xiaohong Xie, Wei Hu, Kun Yin, Lichuan Gu
- 45-51 **Factors affecting health-related quality of life among firefighters during the COVID-19 pandemic: A single-center study.**
Yukihiro Shigeno, Yukihiro Mori, Kiyoshi Hotta, Yuka Aoyama, Mamoru Tanaka, Hana Kozai, Makoto Aoike, Hatsumi Kawamura, Masato Tsurudome, Morihiro Ito
- 52-59 **Verification study on the catheterization of an upper arm vein using the new long peripheral intravenous catheter to reduce catheter failure incidence: A randomized controlled trial.**
Ryoko Murayama, Mari Abe-Doi, Yosuke Masamoto, Kosuke Kashiwabara, Chieko Komiyama, Hiromi Sanada, Mineo Kurokawa
- 60-65 **Age distribution and disease severity of COVID-19 patients continued to change in a time-dependent manner from May 2021 to April 2022 in the regional core hospital in Japan.**
Futoshi Kawaura, Takuya Kishi, Tadashi Yamamoto, Shiki Nakayama, Taku Goto, Reimi Tsurusawa, Toshio Katagiri, Kohei Yamanouchi, Ayako Matsuo, Naomi Kobayashi-Watanabe, Tomohiro Imamura, Yoshitaka Hirooka, Kuniyasu Takagi, Tsukuru Umemura, Kazuma Fujimoto, Shinichiro Hayashi, Ayako Takamori

Brief Report

- 66-69** **Continuous ingestion of sodium chloride solution promotes allergen absorption and may exacerbate allergy symptoms on ovalbumin-induced food allergy in mice.**
Mamoru Tanaka, Rui Lu, Hana Kozai

Correspondence

- 70-72** **A study of 95 infantile hemangiomas treated with propranolol: A potentially efficacious combination with laser therapy.**
Saori Yamada-Kanazawa, Shuichi Shimada, Wakana Nakayama, Soichiro Sawamura, Yuki Nishimura, Ikko Kajihara, Katsunari Makino, Jun Aoi, Shinichi Masuguchi, Fukiko Amano, Satoshi Fukushima

Cyclic AMP (cAMP)-dependent proteolysis of GATA6 by proteasome: Zinc-finger domain of GATA6 has signals for nuclear export and proteolysis, both of which are responsive to cAMP

Tomohisa Yamamoto^{1,a}, Takeshi Tsuge^{1,b}, Makoto Araki², Masatomo Maeda^{1,*}

¹Graduate School of Pharmaceutical Sciences, Osaka University, Suita, Osaka, Japan;

²Meiji Pharmaceutical University, Tokyo, Japan.

SUMMARY Transcription factor GATA6 stably expressed in Chinese hamster ovary (CHO)-K1 cells is exported from the nucleus to the cytoplasm and degraded there by proteasome upon treatment with dibutylcyclic AMP (*dbcAMP*), which is a membrane-permeable cyclic AMP (cAMP) analogue. The cAMP-dependent proteolysis of GATA6 was characterized by dissection of the GATA6 protein into a zinc-finger domain (Zf) and the surrounding region (Δ Zf). These segments were separately expressed in CHO-K1 cells stably, and followed by treatment with *dbcAMP*. The nuclear localized Zf was degraded by proteasome similarly to the full-length GATA6. Site-directed mutants of nuclear localizing signal (NLS) (³⁴⁵RKRKPK³⁵⁰ → AAAAPK and AAAAPA) and closely related GATA4 showed the same behavior. Although nuclear-localized Δ Zf was degraded by proteasome, the cytoplasmic-located Δ Zf was resistant to proteolysis in contrast to the NLS mutants. We also searched for a potential NLS and nuclear export signal (NES) with computational prediction programs and compared the results with ours. All these results suggest that the amino acid sequence(s) of the Zf of GATA6 is responsive to cAMP-dependent nuclear export and proteolysis.

Keywords Cyclic AMP-dependent protein kinase, GATA DNA-binding protein, nuclear-cytoplasmic shuttling, regulated protein degradation, stable transfection, cJun N-terminal kinase

1. Introduction

Transcription factor GATA6 is an essential gene product (1,2), and is required for the development of endoderm and mesoderm in early embryos, and differentiation of these germ layers into specific tissue cells and unique gene expression in those differentiated cells have been examined (3,4). Actually, it is well known that mutations of the *GATA6* gene often cause congenital heart disease and pancreatic agenesis (4). Furthermore, it is claimed that GATA6 participates in tumorigenesis, although controversial findings as to the tumor suppressor function of GATA6 have been also reported (5). Thus, studies on the molecular properties of GATA6 are informative to understand the cause of the disease and to develop a strategy for its treatment.

There are six GATA family DNA-binding proteins in mammals, which recognize the canonical (A/T)GATA(A/G) motif (GATA-motif) in gene regulatory regions. Each member has a highly conserved zinc-finger domain (Zf) composed of tandem zinc-finger segments separated by 29 amino acid residues (CX₂CX₁₇CX₂C)-X₂₉-

(CX₂CX₁₇CX₂C) and a following basic region, but the surrounding region (Δ Zf) shows sequence divergency (6). The carboxy (C)-terminal zinc-finger segment (C-finger) binds to the GATA-motif whereas the amino (N)-terminal zinc-finger segment (N-finger) interacts with the adjacent GATA-motif or with protein cofactors (3,4). Since the basic region following the C-finger further functions as a nuclear localization signal (NLS) (3,4), GATA proteins translated in the cytoplasm are immediately transported into the nucleus in both the native state and as exogenously expressed (7-10).

We have found that stably but not transiently expressed GATA6 is exported from the nucleus to the cytoplasm upon activation by cyclic AMP (cAMP)-dependent protein kinase (PKA) (11). Following the nuclear export mediated by Chromosome Region Maintenance 1 [CRM1, also known as Exportin-1 (XPO1)] (12), GATA6 is further degraded by proteasome (11,12). Although GATA6 remained stably in the nucleus in the presence of a proteasome inhibitor, proteasomal degradation of GATA6 is suggested to occur in the cytoplasm: activation of PKA stimulated degradation of

GATA6 when it was tethered on the cytoplasmic side of the endoplasmic reticulum membrane through the membrane anchoring domain of the sterol regulatory element-binding protein (SREBP) 2 (13). Furthermore, nuclear export and cytoplasmic degradation of GATA6 can be discriminated when stimulated on activation by cJun N-terminal kinase (JNK) since GATA6 is rapidly exported from the nucleus and then slowly degraded in the cytoplasm (12).

In this study, we focused on the Zf and Δ Zf of GATA6 separately, and characterized their degradation induced by dibutyryl-cyclic AMP (*dbcAMP*). Unveiling of the mechanism of sequestration of GATA6 from the nucleus could be helpful for manipulating the cellular localization of transcription factors from the viewpoint of therapeutics for diseases.

2. Materials and Methods

2.1. Construction of expression plasmids for human GATA6 (hGATA6) derivatives

The expression plasmid for the hGATA6 Zf (hZf) (Glu²⁴⁰-Thr³⁵⁷) (14) was constructed by the procedure shown in Figure S1 (<http://www.ddtjournal.com/action/getSupplementalData.php?ID=133>). From this plasmid, named pME-HA/FLAG-hZf, hZf was expressed as a fusion protein with amino-terminal human influenza hemagglutinin (HA) and FLAG tags.

To delete the Zf between S²³⁹ and T³⁵⁷ of S-type hGATA6 (14), *DpnI*-mediated site-directed mutagenesis (15) was carried out: the mutant DNA was amplified by means of polymerase chain reaction (PCR) with primer pair dZfa/dZfs, PrimeSTAR HS DNA polymerase (TaKaRa, Kusatsu, Shiga, Japan), and pME-hGT1SMyc (16) as a template under the following conditions: 94°C 2 min, followed by 30 cycles of denaturation (94°C, 10 sec), annealing (68°C, 6 min), and extension (68°C, 6 min), and then post-incubation (72°C, 5 min). The reaction mixture was treated with *DpnI* to degrade methylated parental DNA, and then transformed into *Escherichia coli* Top10F' (Invitrogen, Carlsbad, CA, USA). The resulting plasmid was named pME-hGT1S(Δ Zf)Myc.

To construct an expression plasmid for NLS mutant 1 with Myc-tag (NLSmut1-Myc) [pME-hGT1S(NLSmut1)Myc], the plasmid template pME-hGT1SMyc was subjected to PCR with primer pair TYmut1s/TYmut1a and Pyrobest DNA polymerase (TaKaRa) [95°C 5 min, followed by 20 cycles of denaturation (94°C, 15 sec), annealing (55°C, 30 sec), and extension (72°C, 5 min)]. The product was digested with *DpnI* and then introduced into *Escherichia coli* Top10F'. The ~400 base pair (bp) *EcoRI-SpeI* fragment with base-substitutions was inserted into the corresponding part of pME-hGT1SMyc. The expression plasmid for NLSmut2-Myc [pME-hGT1S(NLSmut2)Myc] was similarly constructed

with primer pair TYmut2s/TYmut2a using pME-hGT1S(NLSmut1)Myc as a template.

DNA fragments were size-separated by agarose gel-electrophoresis [1%~2% (w/v)], and visualized with ethidium bromide. The sequence of the cloned DNA was determined by the dideoxy chain-termination method with sequence primers for the pME18S vector (16) and a BigDyeTM terminator v3.1 Cycle Sequencing Kit (Applied Biosystems, Waltham, MA, USA), using an ABI PRISMTM 310 Genetic Analyzer (Applied Biosystems). The molecular biological methods for DNA manipulations were based on standard procedures as described in our previous study (17). The primers for PCR and sequencing are listed in Table S1 (<http://www.ddtjournal.com/action/getSupplementalData.php?ID=133>).

2.2. Cell culture and transfection of expression plasmids

Each plasmid construct was introduced into Cos-1 cells (ATCC, Manassas, VA, USA) by means of the diethylaminoethyl (DEAE)-dextran method (17) to verify expression of the recombinant protein. Cells were grown for two days in Dulbecco's modified Eagle medium (DMEM) (GIBCO BRL, Gaithersburg, MD, USA) supplemented with 7% fetal bovine serum (FBS) (GIBCO BRL) and antibiotics [100 units/mL benzylpenicillin (Wako, Osaka-city, Osaka, Japan), 100 μ g/mL streptomycin sulfate (Wako), and 2.5 μ g/mL fungison (GIBCO BRL)], and the transiently expressed proteins were detected immunologically as described in 2.3.

Chinese hamster ovary (CHO)-K1 cells (11) were grown in Ham's F12 medium (GIBCO BRL) supplemented with FBS and antibiotics as above. Each expression plasmid for GATA6 derivatives was introduced into CHO-K1 cells by means of the calcium-phosphate method (17) together with phyg (17) in the ratio of 15:1 (w/w). Resistant colonies were selected in the presence of 200 μ g/mL hygromycin (Wako). As for pME-HA/FLAG-hZf, pDsRed2-N1 (Clontech, Mountain View, CA, USA) was added in place of phyg and the transformants were selected in the presence of 100 μ g/mL G418 (Sigma, St. Louis, MO, USA), the red fluorescence of *Discosoma*-derived protein DsRed being detected under a microscope (Olympus IX70, Olympus Corporation, Shinjuku-ku, Tokyo, Japan).

2.3. Detection of GATA proteins

Cells (1×10^6 cells in Φ 10 cm dish) were cultured for 24 h, and then further incubated for 24 h in the presence or absence of 2 mM *dbcAMP* (Sigma). Proteasome inhibitor benzyloxycarbonyl-L-leucyl-L-leucyl-L-norvalinal (MG115) (Peptide Institute Inc., Ibaraki, Osaka, Japan) (10 μ M) was also added at 12 h before harvest. The postnuclear supernatant (cytoplasm) and nuclear protein

extract (nucleus) were prepared by the published method (18). Protein concentrations were determined with a Bio-Rad Protein Assay Kit (Hercules, CA, USA) (19) using bovine serum albumin (Fraction V) (Sigma) as a standard.

A protein sample (10 µg) was subjected to sodium dodecyl sulfate (SDS)-polyacrylamide gel-electrophoresis and Western blotting (17); the proteins were electro-blotted onto a Hybond-P Polyvinylidene Difluoride (PVDF) membrane (GE Healthcare, Chicago, IL, USA). The concentration of the separation gel was 7.5% (w/v) for Myc-tagged proteins, 15% (w/v) for hZf, and 10% (w/v) for others. Procedures for membrane blocking and washing were essentially the same as described previously (13,17).

The Myc-tagged human proteins and hZf were detected with peroxidase-linked mouse monoclonal antibodies; anti-c-Myc (MC045, Nacalai Tesque, Kyoto, Japan) (× 4,000 diluted) and ANTI-FLAG M2[®] (Sigma) (× 1,500 diluted), respectively. hGATA6 ΔZf (hΔZf)-Myc was further detected with rabbit site-specific polyclonal antibodies recognizing hGATA6 (Leu⁵⁹-Gln²¹⁷) (18) (× 1,000 diluted) as the first antibodies, second antibodies being horseradish peroxidase-linked donkey anti-rabbit immunoglobulin (Ig) (Amersham-Pharmacia Biotech, Burlington, MA, USA) (× 4,000 diluted). Chemiluminescence was detected with an ECL Western blotting kit (GE Healthcare) using Scientific Imaging film (KODAK, Rochester, NY, USA).

2.4. Chemicals

Restriction enzymes were obtained from New England Biolabs (Ipswich, MA, USA), Toyobo (Osaka-city, Osaka, Japan), and TaKaRa. The Klenow enzyme, T4 DNA ligase (Ligation Kit Ver.2.1) and Agarose-LE Classic Type were provided by TaKaRa. A GENECLAN III Kit was obtained from BIO101 (La Jolla, CA, USA). Oligonucleotides were purchased from Gene Design Inc. (Ibaraki, Osaka, Japan). All other chemicals used were of the highest grade commercially available.

3. Results

3.1. Effect of amino terminal deletion of GATA6 on the response to *dbcAMP*

Our previous studies demonstrated that not only full-length S-type hGATA6 (18) but also rat GATA6Δ50 (rGATA6Δ50) with deletion of the amino-terminal 50 residues (11) (hS-type and rΔ50, respectively, in Figure 1) were degraded by proteasome when CHO-K1 cells stably expressing either of these proteins were treated with *dbcAMP*. We first evaluated further deletion of the amino terminal region between residues 72 and 131 of rat GATA6 (rGATA6) as to whether it is *dbcAMP*-

sensitive or not, the deleted protein being named rat GATA6Δ(1-50, 72-131) {[rGATA6Δ(1-50, 72-131)] and rΔ(1-50, 72-131) in Figure 1}. This protein containing the Zf [Glu²³⁴-Ala³⁵¹, residue numbers of rGATA6] is localized in the nucleus and degraded by proteasome in the presence of *dbcAMP* when stably expressed in CHO-K1 cells (Figure S2, <http://www.ddtjournal.com/action/getSupplementalData.php?ID=133>), suggesting that the response to *dbcAMP* is not attributable to the deleted segments.

Since earlier studies on other GATA proteins suggested that the Zf is responsible for their nuclear localization and DNA binding (3,4), we compared the Zf and ΔZf sequences of hGATA6 as to the response to *dbcAMP*. These protein constructs (HA/FLAG-hZf, and hΔZf-Myc, respectively) are schematically shown in Figure 1 together with our previous ones (11,18).

3.2. Response of the Zf of hGATA6 to *dbcAMP*

The Zf of hGATA6 (Glu²⁴⁰-Thr³⁵⁷) (14) was stably expressed in CHO-K1 cells as a fusion protein with an N-terminal HA/FLAG-tag (Figure 1 and Figure S1, <http://www.ddtjournal.com/action/getSupplementalData.php?ID=133>). As shown in Figure 2, HA/FLAG-hZf was localized in the nucleus of two isolated clones (Zf8 and Zf20), suggesting that the nuclear localization signal is present in the Zf. The amount of nuclear HA/FLAG-

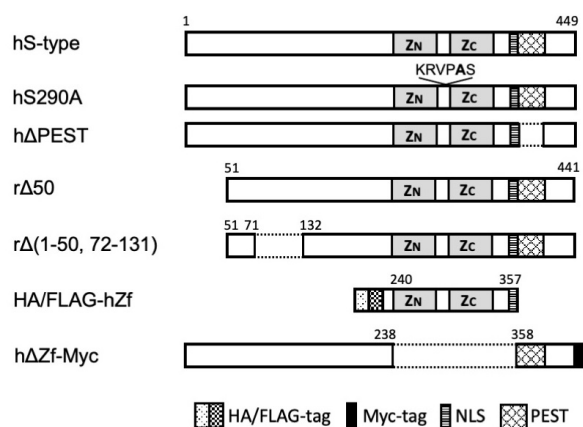


Figure 1. Schematic representation of GATA6 derivatives. The various GATA6 proteins expressed from plasmid constructs are schematically shown together with their names (left column). The sequences for rΔ50 (11) and rΔ(1-50, 72-131) (Figure S2) are of rat GATA6 origin, and those of the others human as indicated by adding a prefix "h". The expression plasmids for hS-type, hS290A and hΔPEST were described previously (18). The amino acid residue numbers of human and rat GATA6 are 449 and 441 (indicated above the boxes), respectively, based on the structure of S-type GATA6 (14). "Z_N" and "Z_C" indicating (CX₂C)_{X₁}-(CX₂C) are the N-finger and C-finger, respectively, separated by 29 amino acid residues in the Zf. The positions of epitope tags (HA/FLAG-tag and Myc-tag), and potential NLS and peptide that is rich in proline, glutamic acid, serine and threonine (PEST) sequences (18) are shown schematically. The amino acid substitution (Ser to Ala) at position 290 (18) is also indicated in hS290A in bold.

hZf decreased when stable cells (both Zf₈ and Zf₂₀) were cultured in the presence of *dbcAMP*, and this behavior was abolished in the presence of proteasome inhibitor MG115 (Figures 2A and 2B), indicating that the decrease of HA/FLAG-hZf in the cells is due to degradation by proteasome. The inhibition of its degradation would re-localize HA/FLAG-hZf into the nucleus due to the presence of NLS that functions dominantly. It was also confirmed that HA/FLAG-hZf was exclusively localized in the nucleus, *i.e.*, not found in the cytoplasm, of clone Zf₂₀ (Figure 2C, right).

3.3. Response of the Δ Zf of hGATA6 without the Zf to *dbcAMP*

To compare the results for HA/FLAG-hZf, we stably expressed h Δ Zf-Myc without the Zf. The h Δ Zf-Myc was localized in both the nucleus and cytoplasm in all four clones isolated (Figure S3A, <http://www.ddtjournal.com/action/getSupplementalData.php?ID=133>). Interestingly, nuclear h Δ Zf-Myc decreased in the presence of *dbcAMP* although that in the cytoplasm did not (Figure S3B, <http://www.ddtjournal.com/action/getSupplementalData.php?ID=133>). The behavior of one clone (Δ Zf1-1) was examined further in detail, as shown in Figure 3: the corresponding bands to h Δ Zf-Myc have both N- and C-terminal regions since not only the C-terminal Myc-tag (Figure 3A) but also antibodies recognizing upstream Leu⁵⁹-Gln²¹⁷ were reactive (Figure 3B). The decrease in the nuclear h Δ Zf-Myc was inhibited by the addition of MG115, indicating that it was degraded by proteasome.

An unexpected observation was that the cytoplasmic h Δ Zf-Myc was resistant to proteasome. A possible explanation is that association with other proteins (20,21) or the conformational state of an unusual artificial h Δ Zf-Myc, which may induce aggregation (22,23), could prevent most of the cytoplasmic h Δ Zf-Myc from gaining access to proteasome. Macromolecules smaller than ~40 kDa can passively diffuse through nuclear pores (24), and the molecular weight of h Δ Zf-Myc was calculated to be 32 k [GENETYX-MAC GENETIC INFORMATION PROCESSING SOFTWARE (GENETYX Corporation, Shibuya-ku, Tokyo, Japan)]. Thus, the monomeric h Δ Zf-Myc would freely enter the nucleus. Although some proteasome was found in the nucleus (25), we did not examine further whether the h Δ Zf-Myc is degraded in the nucleus or cytoplasm since expression of a fusion of h Δ Zf-Myc with the membrane domain of SREBP2 to fix h Δ Zf-Myc on the cytoplasmic side of the endoplasmic reticulum membrane (13) has not been successful.

3.4. Effect of substitution of the cluster of basic residues following the C-finger of hGATA6

We further examined whether the potential NLS of GATA6 affects the cAMP-dependent nuclear exit and proteolysis of GATA6. We substituted the Arg and Lys

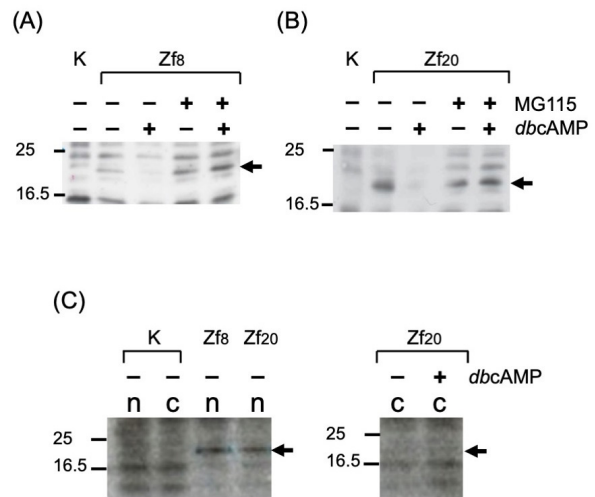


Figure 2. Behavior of HA/FLAG-hZf stably expressed in CHO-K1 cells in the presence of *dbcAMP*. The expression plasmid for HA/FLAG-hZf (Figure S1) was stably introduced into CHO-K1 cells. Among 21 G418-resistant colonies, two clones (Zf₈ and Zf₂₀) were HA/FLAG-hZf protein-positive. Cells were cultured for 24 hr in the presence (+) or absence (-) of *dbcAMP* and proteasome inhibitor MG115. The HA/FLAG-hZf protein in the nucleus was analyzed by means of Western blotting after SDS-polyacrylamide gel-electrophoresis as described under Materials and Methods (A and B). The HA/FLAG-hZf protein in the nucleus (n) (Zf₈ and Zf₂₀) and cytoplasm (c) (Zf₂₀) was analyzed in (C). Fractions prepared from CHO-K1 cells (K) were used as negative controls. The values on the left side are molecular weights ($\times 10^3$). Arrows at the right indicate the position of HA/FLAG-hZf.

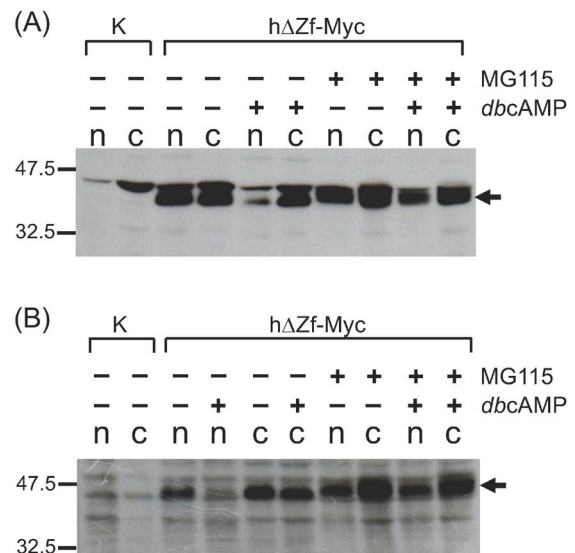


Figure 3. Behavior of h Δ Zf-Myc stably expressed in CHO-K1 cells in the presence of *dbcAMP*. A stable clone (Δ Zf1-1, see Figure S3) that expresses h Δ Zf-Myc was cultured in the presence (+) or absence (-) of *dbcAMP* and MG115. The h Δ Zf-Myc in the nucleus (n) and cytoplasm (c) was detected by Western blotting after SDS-polyacrylamide gel-electrophoresis. Fractions prepared from CHO-K1 cells (K) were used as negative controls. The values on the left side are molecular weights ($\times 10^3$). Arrows on the right indicate the position of h Δ Zf-Myc. (A) Peroxidase-linked mouse monoclonal anti-c-Myc was used. (B) Rabbit site-specific polyclonal antibodies recognizing hGATA6 (Leu⁵⁹-Gln²¹⁷) as the first antibodies, and horseradish peroxidase-linked donkey anti-rabbit Ig as the second antibodies were used.

residues, which are clustered downstream of the C-finger (3). This cluster is also predicted to be a NLS by all the prediction programs available (Table S2 [A], <http://www.ddtjournal.com/action/getSupplementalData.php?ID=133>). In the two mutants, NLSmut1-Myc and NLSmut2-Myc, the sequence ³⁴⁵RKRKPK³⁵⁰ is ³⁴⁵AAAAPK³⁵⁰ and ³⁴⁵AAAAPA³⁵⁰, respectively (Figure 4A). When these mutant proteins were stably expressed in CHO-K1 cells, they were distributed in both the nucleus and cytoplasm. Furthermore, both nuclear and cytoplasmic NLS-mutant proteins were degraded by proteasome in the presence of *dbcAMP* since MG115 inhibited their decrease (Figure 4B and 4C), in contrast to hZf-Myc.

All these results suggest that the four consecutive basic residues function as the NLS, although nuclear import of the mutant proteins was not inhibited completely. Such behavior could be ascribed to the following possibilities: (i) another NLS also participates in the nuclear import of GATA6, and/or (ii) a nuclear export signal (NES) without the RKRKPK sequence is unveiled, although such NLS and NES would have weak activity. In chicken GATA1, the RNRKVS sequence present at an identical position to GATA6 (Figure 5) is required for specific DNA-binding of GATA1 to the GATA-motif (26), suggesting that the present NLS mutants would have low affinity as to the GATA-motif and thus would be easily excreted from the nucleus in the absence of *dbcAMP*.

The results in Figure 2 and Figure 4 suggested that the Zf is important for *dbcAMP*-dependent degradation of GATA6. Consistent with this notion, we further demonstrated that nuclear GATA4, which has a highly conserved Zf [88% and 97% of the residues are identical and conservative, respectively, between rat GATA4 (rGATA4) and rGATA6 (Figure 5) (6)], similarly disappeared in the presence of *dbcAMP* (Figure S4, <http://www.ddtjournal.com/action/getSupplementalData.php?ID=133>).

4. Discussion

We have shown in this and our previous studies (11-13,18) that nuclear-localized GATA6 is exported into the cytoplasm upon *dbcAMP*-treatment. A GATA factor (GtaC) of *Dictyostelium discoideum* moves from the nucleus to the cytoplasm in response to cAMP since its NLS is neutralized upon input of the cAMP signal (27). Although the exported GtaC re-enters the nucleus, the GATA6 is degraded in the cytoplasm (13). However, conservation of the phenomena that both GATA proteins are exported from the nucleus to the cytoplasm in response to the cAMP signal is interesting, although they are evolutionally distant.

Since nuclear export of GATA6 depends on CRM1 (12), the leucine-rich NES (28) may participate in the process. The three Leu residues in

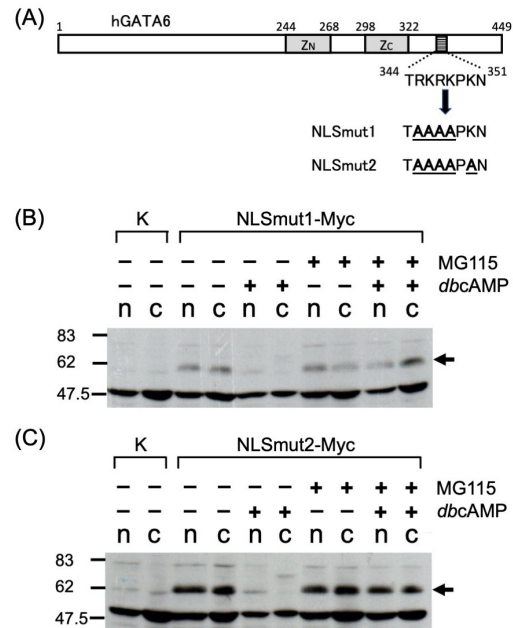


Figure 4. Effects of substitution of basic residues in the NLS. S-type hGATA6 (449 residues) is schematically shown in (A). The C-terminal Myc-tag is omitted in the figure. The N-finger and C-finger are indicated by Zn and Zc, respectively. Amino acid residue numbers are shown above the box. Basic residues (Arg and Lys) in the potential NLS of GATA6 were substituted with Ala residues in the two mutant proteins (NLSmut1 and NLSmut2), as underlined. Expression plasmids for two mutants [pME-hGT1S(NLSmut1)Myc and pME-hGT1S(NLSmut2)Myc] were constructed as described under Materials and Methods. They were introduced into CHO-K1 cells and hygromycin-resistant colonies (15 and 4, respectively) were isolated. Among them, four and one clones expressed mutant GATA6. Clones (one of the positive clones for each mutant) were cultured in the presence (+) or absence (-) of *dbcAMP* and MG115. The NLSmut1-Myc and NLSmut2-Myc in the nucleus (n) and cytoplasm (c) were detected by Western blotting after SDS-polyacrylamide gel electrophoresis [(B) and (C), respectively]. Fractions prepared from CHO-K1 cells (K) were used as negative controls. The values on the left side are molecular weights ($\times 10^{-3}$). Arrows on the right indicate the positions of NLSmut1-Myc and NLSmut2-Myc, respectively.

the sequence ⁴⁷SVLGLSYLQG⁵⁶ of mouse GATA4 (mGATA4) are crucial for its nuclear export (29). However, the corresponding sequence of hGATA6 (⁵⁰SMLPGLPYHLQG⁶¹) (14) is located outside of the Zf. When we searched for candidate NES sequences in the Zf (Table S2, <http://www.ddtjournal.com/action/getSupplementalData.php?ID=133>), the sequence between Asn³¹² and Met³³⁷ including part of the C-finger was predicted with all three tools used. Thus, this region could be the next target of mutagenesis study as to whether it participates in the *dbcAMP*-dependent nuclear export of GATA6.

The low steady-state level of tumor suppressor p53 under normal conditions is maintained through nuclear export, which results in its cytoplasmic degradation by proteasome. However, its CRM1-dependent export is complex: the mouse double minute 2 (MDM2) protein associates with p53 and the NES of

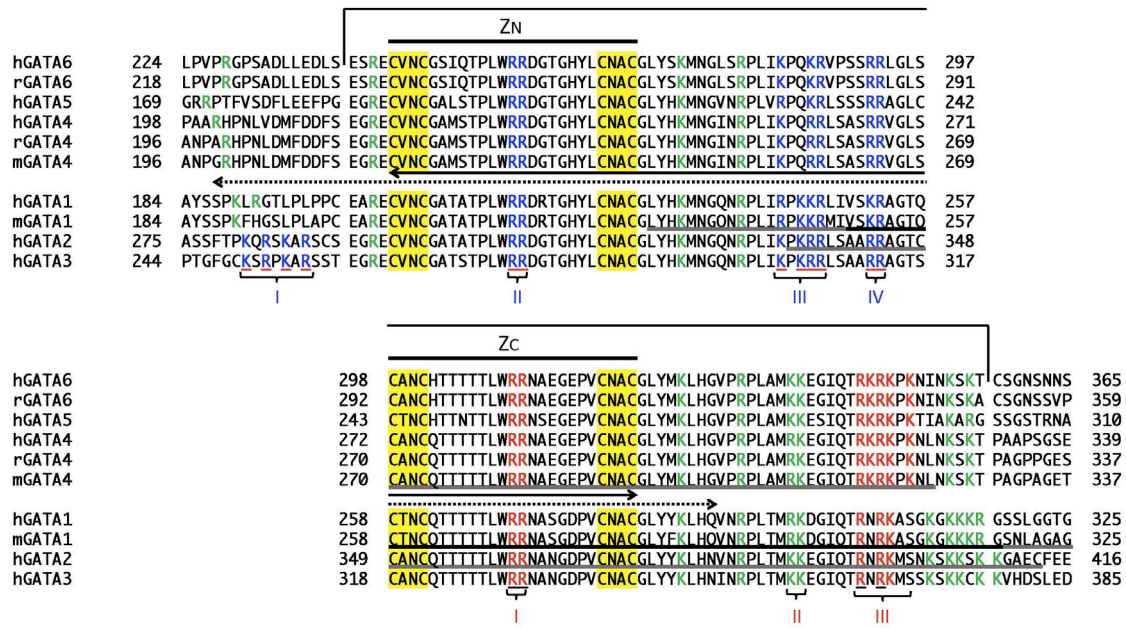


Figure 5. Sequence comparison of the Zfs of mammalian GATA proteins. Parts of the amino acid sequences of mammalian GATA proteins (h, human; r, rat; m, mouse) are aligned and shown as single letters. The Zf is indicated by a square bracket, and zinc-finger segments (CX_2C) $X_{17}(CX_2C)$ are indicated by Z_N (N-finger) and Z_C (C-finger) above, respectively. The accession numbers of the National Center for Biotechnology Information (NCBI) reference sequences are NM_005257 (hGATA6) (14), NM_019185 (rGATA6) (14), NM_080473 (hGATA5), NM_001308093 (hGATA4), NM_144730 (rGATA4) (6), NM_008092 (mGATA4), NM_002049 (hGATA1), NM_008089 (mGATA1), NM_001145661 (hGATA2), and NM_001002295 (hGATA3). Conserved basic residues (R and K) suggested to be NLS of hGATA3 (35) are indicated by blue letters, those of GATA4 (29) and GATA6 (present study) by red letters, and other conserved residues (including partially) by green letters. In mGATA4, which is more closely related to GATA6 compared to GATA1, 2, and 3, clusters I and III (indicated in red) are simultaneously required for nuclear localization of the full-length mGATA4, and R²⁸², R²⁸³, R³¹⁷ and R³¹⁹ are crucial in the clusters (29). Furthermore, the minimum sequence imported into the nucleus is fragment C²⁷⁰-L³²⁴ (underlined in grey color), although fragment C²¹⁶-C²⁹⁴ (underlined with arrowheads) and the G¹⁹⁹-G³⁰² deletion (dotted underlined with arrowheads) were not imported (9,29), which is consistent with the importance of both clusters I and III (red). In mGATA1, the construct without either the N-finger (A¹⁹⁷-H²³²) or C-finger (Q²⁵⁶-Y²⁸⁵), or deletion of K³⁰⁸-S⁴¹³ or ³¹²KGKKK³¹⁶, and fragment L²³⁰-V³³⁶ or V²⁵⁰-G³¹⁸ (underlined in grey and overlapped portions in bold black) were imported into the nucleus, suggesting that the ²⁴³RPKRR²⁴⁷ and ³¹²KGKKK³¹⁶ sequences may independently direct this nuclear localization (7,39). In hGATA2, fragment P³³⁵-C⁴¹³ (underlined in grey) was transported into the nucleus (7). In contrast to these GATA proteins, combined mutations of basic residues in all four clusters (I - IV indicated by blue) disrupt nuclear localization of full-length hGATA3 (35), although the N-finger plus its N-terminal and C-terminal flanking sequences (C²⁴⁹-A³¹¹) is enough for localization in the nucleus (8,35). However, a truncation mutation (A³¹¹→Stop) without the C-terminal sequence from cluster IV disrupts nuclear localization, suggesting that its C-terminal sequence from A³¹¹ might also affect the nuclear import mechanism (35). Furthermore, essential residues identified in mGATA4 (R²⁸², R²⁸³, R³¹⁷ and R³¹⁹) (29) could not function as the NLS in hGATA3 (R³³⁰, R³³¹, R³⁶⁵ and R³⁶⁷ located at conserved positions) (35).

MDM2 is utilized for the nuclear export of p53 (30), while the intrinsic p53 NES seems to be sufficient for its export (31). Furthermore, the Jun activation-domain binding protein 1 (Jab1), as a component of Constitutive photomorphogenesis 9 (COP9) signalosome (CSN), stimulates CSN-associated kinase, resulting in phosphorylation of p53 and its nuclear export (32). Although curcumin inhibits CSN-associated kinase and the nuclear export of p53, this inhibitor did not affect the nuclear export of GATA6 (not shown).

The A-kinase and ubiquitin participates in *dbcAMP*-induced nuclear export and degradation of GATA6 (11,18). Since GATA6 is not phosphorylated or ubiquitinated during the process, it seems likely that the escort protein, which has a NES and is subjected to phosphorylation and ubiquitination, facilitates the nuclear export and degradation of GATA6. A p27 protein designated the cyclin-dependent kinase inhibitory protein-1 (p27^{Kip1}), which has no apparent NES, is

exported from the nucleus to the cytoplasm through binding to Jab1, whose NES binds to CRM1, and then the exported p27^{Kip1} is subjected to ubiquitin-dependent degradation by cytoplasmic proteasome. However, the Jab1 binding motif (-DX₂₁LX₉N-) identified in p27^{Kip1} (33) could not be found in GATA6. Analysis of the altered genes of the mutants where GATA6 could not be exported in the presence of *dbcAMP* or stably located in the nucleus even in the presence of *dbcAMP* (34) might be helpful for identifying such escort proteins and provide their clues.

GATA6 as well as other GATA family members are localized in the nucleus after translation in the cytoplasm due to the presence of dominant NLS (3,4). The present results suggest that the classical monopartite ³⁴⁵RKRK³⁴⁸ sequence (24,28) in hGATA6 contributes significantly as an NLS. Our NLS mutants and hZf-Myc are distributed in both the nucleus and cytoplasm, which could be explained by that the weak NES or NLS in these mutant

sequences would function. Although mutant proteins were distributed in both fractions in similar experiments to identify the NLS (29,35), it must be further mentioned that the amounts of cytoplasmic protein are more than twice higher than that in the nucleus (36), indicating that the mutant proteins are mainly distributed in the cytoplasm.

To explain the nuclear localization of our mutant proteins, we examined whether there are further putative classical NLS motifs in the S-type hGATA6 sequence or not (Table S2, <http://www.ddtjournal.com/action/getSupplementalData.php?ID=133>). However, only sequences containing ³⁴⁵RKRK³⁴⁸ are predicted. Furthermore, visual examination did not reveal a classical bipartite NLS (37) or non-classical PY-NLS (38). One predicted sequence between Pro³³² and Ser³⁶² containing several basic residues together with ³⁴⁵RKRK³⁴⁸ (Table S2, <http://www.ddtjournal.com/action/getSupplementalData.php?ID=133>) may be considered in the future study as to whether it is a more active NLS or not.

For nuclear import of mGATA4, two clusters of basic residues (²⁸²RR²⁸³ and ³¹⁷RKRKPK³²²) are simultaneously required for nuclear localization of full-length mGATA4 (Figure 5) (29). However, our study demonstrated that only ³⁴⁵RKRK³⁴⁸ is enough as the NLS of full-length hGATA6. We also demonstrated that the mutant carrying the ³¹⁰AA³¹¹ and ³⁴⁵AAAAPA³⁵⁰ sequences showed essentially the same behavior as that of NLSmut1 and NLSmut2 (not shown). As for the NLSs of GATA family proteins, the basic region following each C-finger is proposed to carry the signal (3,4). However, various reports are not consistent (see legend to Figure 5), although it has been demonstrated that the highly conserved Zfs of GATA proteins (Figure 5) participate in their nuclear import (7-9,29,35,39). Such differences could be ascribed to that (i) subtle amino-acid variations in the Zf and/or the unique sequences outside of the Zf affect the mode of interaction with importins, (ii) transformed cells are used, which frequently express virus antigen (7,8,35,39), as it was demonstrated that simian virus 40 (SV40) large T-antigen having a strong NLS escorts other proteins into the nucleus (40), and/or (iii) most of the experiments were carried out with a transient expression system (7-9,29,35,39), in which excess amounts of import substrates are produced in a short time, which often induces an abnormal cellular response (41,42).

It is well known that proteolytic degradation of GATA proteins participates in normal and abnormal cell differentiation: the expression levels of GATA2 and GATA3 are regulated *via* ubiquitin-dependent degradation upon hematopoietic and T-cell differentiation, and their phosphorylation by cyclin-dependent kinase 1 and 2 (CDK1 and CDK2), respectively, is required for recognition by S-phase kinase-associated protein 1 (Skp), Cullin, and F-box (SCF)-type E3 ubiquitin ligase (43,44), although

intracellular degradation-sites of GATA2 and GATA3 have not been determined. Furthermore, GATA1 became susceptible to caspase3 upon sequestration of heat shock protein 70 (HSP70), resulting in differentiation impairment of erythropoiesis (45). However, extracellular signal-regulated kinase (ERK) [mitogen-activated protein kinase (MAPK)] rather stabilizes GATA1 and GATA3 (44,46).

In contrast, the responses of GATA6 and GATA4 to *dbcAMP* are evoked by A-kinase (11). JNK further participates between proteasomal degradation of GATA6 and activation of A-kinase by *dbcAMP* (12). Since JNK is known as a stress kinase (47), prolonged incubation with *dbcAMP* and/or successive A-kinase activation would induce a stress response as a feed-back mechanism. Elucidation of such a cellular pathway will provide a hint to cure cancers of the gastrointestinal tract and hypertrophic cardiomyopathy, in which increased expression of GATA6 and GATA4, respectively, is likely to be causative of these diseases (5,48,49). Development of specific peptides inhibiting or accelerating the binding of GATA6 and GATA4 through their NLS or NES to importin families (47) could be useful for depleting nuclear GATA proteins. Another approach to their cellular depletion would be the finding of small-molecular protein degraders (50) that glue target GATA6 and GATA4 to E3 ubiquitin ligases.

Acknowledgements

We thank Dr. Kazuaki Ohashi for construction of the expression plasmids. We also thank Mr. Ken Miura for transfection of the GATA4 expression plasmid.

Funding: This work was supported in part by the JSPS (Grant-in-Aid for Scientific Research (B), 14370744, to M.M.).

Conflict of Interest: The authors have no conflicts of interest to disclose.

References

1. Morrisey EE, Tang Z, Sigrist K, Lu MM, Jiang F, Ip HS, Parmacek MS. GATA6 regulates HNF4 and is required for differentiation of visceral endoderm in the mouse embryo. *Genes Dev.* 1998; 12:3579-3590.
2. Koutsourakis M, Langeveld A, Patient R, Beddington R, Grosfeld F. The transcription factor GATA6 is essential for early extraembryonic development. *Development.* 1999; 126:723-732.
3. Molkenin JD. The zinc finger-containing transcription factors GATA-4, -5, and -6: ubiquitously expressed regulators of tissue-specific gene expression. *J Biol Chem.* 2000; 275:38949-38952.
4. Tremblay M, Sanchez-Ferras O, Bouchard M. GATA transcription factors in development and disease. *Development.* 2018; 145:dev164384.

5. Deng X, Jiang P, Chen J, Li J, Li D, He Y, Jiang Y, Zhang Y, Xu S, Li X, Wang S, Tian F. GATA6 promotes epithelial-mesenchymal transition and metastasis through MUC1/ β -catenin pathway in cholangiocarcinoma. *Cell Death Dis.* 2020; 11:860.
6. Maeda M, Kubo K, Nishi T, Futai M. Roles of gastric GATA DNA-binding proteins. *J Exp Biol.* 1996; 199:513-520.
7. Visvader JE, Crossley M, Hill J, Orkin SH, Adams JM. The C-terminal zinc finger of GATA-1 or GATA-2 is sufficient to induce megakaryocytic differentiation of an early myeloid cell line. *Mol Cell Biol.* 1995; 15:634-641.
8. Yang Z, Gu L, Romeo P-H, Borries D, Motohashi H, Yamamoto M, Engel JD. Human GATA-3 *trans*-activation, DNA-binding, and nuclear localization activities are organized into distinct structural domains. *Mol Cell Biol.* 1994; 14:2201-2212.
9. Morrissey EE, Ip HS, Tang Z, Parmacek MS. GATA-4 activates transcription *via* two novel domains that are conserved within the GATA-4/5/6 subfamily. *J Biol Chem.* 1997; 272:8515-8524.
10. Gillio-Meina C, Hui YY, LaVoie HA. GATA-4 and GATA-6 transcription factors: expression, immunohistochemical localization, and possible function in the porcine ovary. *Biol Reprod.* 2003; 68:412-422.
11. Nakagawa R, Sato R, Futai M, Yokosawa H, Maeda M. Gastric GATA-6 DNA-binding protein: proteolysis induced by cAMP. *FEBS Lett.* 1997; 408:301-305.
12. Ushijima H, Maeda M. cAMP-dependent proteolysis of GATA-6 is linked to JNK-signaling pathway. *Biochem Biophys Res Commun.* 2012; 423:679-683.
13. Tsuge T, Uetani K, Sato R, Ohashi-Kobayashi A, Maeda M. Cyclic AMP-dependent proteolysis of GATA-6 expressed on the intracellular membrane. *Cell Biol Int.* 2008; 32:298-303.
14. Yoshida T, Sato R, Mahmood S, Kawasaki S, Futai M, Maeda M. GATA-6 DNA binding protein expressed in human gastric adenocarcinoma MKN45 cells. *FEBS Lett.* 1997; 414:333-337.
15. Fisher CL, Pei GK. Modification of a PCR-based site-directed mutagenesis method. *Biotechniques.* 1997; 23:570-574.
16. Takada K, Obayashi K, Ohashi K, Ohashi-Kobayashi A, Nakanishi-Matsui M, Maeda M. Amino-terminal extension of 146 residues of L-type GATA-6 is required for transcriptional activation but not for self-association. *Biochem Biophys Res Commun.* 2014; 452:962-966.
17. Yokura-Yamada Y, Araki A, Maeda M. Ectopic expression of Id1 or Id3 inhibits transcription of the GATA-4 gene in P19CL6 cells under differentiation condition. *Drug Discov Ther.* 2021; 15:189-196.
18. Ishida A, Iijima R, Kobayashi A, Maeda M. Characterization of cAMP-dependent proteolysis of GATA-6. *Biochem Biophys Res Commun.* 2005; 332:976-981.
19. Bradford MM. A rapid and sensitive method for the quantitation of microgram quantities of protein utilizing the principle of protein-dye binding. *Anal Biochem.* 1976; 72:248-254.
20. Hunt T. Cytoplasmic anchoring proteins and the control of nuclear localization. *Cell.* 1989; 59:949-951.
21. Pratt WB, Welsh MJ. Chaperone functions of the heat shock proteins associated with steroid receptors. *Semin Cell Biol.* 1994; 5:83-93.
22. Kaganovich D, Kopito R, Frydman J. Misfolded proteins partition between two distinct quality control compartments. *Nature.* 2008; 454:1088-1095.
23. Balchin D, Hayer-Hartl M, Hartl FU. *In vivo* aspects of protein folding and quality control. *Science.* 2016; 353: aac4354.
24. Marfori M, Mynott A, Ellis JJ, Mehdi AM, Saunders NFW, Curmi PM, Forwood JK, Bodén M, Kobe B. Molecular basis for specificity of nuclear import and prediction of nuclear localization. *Biochim Biophys Acta.* 2011; 1813:1562-1577.
25. von Mikecz A. The nuclear ubiquitin-proteasome system. *J Cell Sci.* 2006; 119:1977-1984.
26. Omichinski JG, Clore GM, Schaad O, Felsenfeld G, Trainor C, Appella E, Stahl SJ, Gronenborn AM. NMR structure of a specific DNA complex of Zn-containing DNA binding domain of GATA-1. *Science.* 1993; 261:438-446.
27. Cai H, Katoh-Kurasawa M, Muramoto T, Santhanam B, Long Y, Li L, Ueda M, Iglesias PA, Shaulsky G, Devreotes PN. Nucleocytoplasmic shuttling of a GATA transcription factor functions as a development timer. *Science.* 2014; 343:1249531.
28. Cautain B, Hill R, de Pedro N, Link W. Components and regulation of nuclear transport processes. *FEBS J.* 2015; 282:445-462.
29. Philips AS, Kwok JC, Chong BH. Analysis of the signals and mechanisms mediating nuclear trafficking of GATA-4: loss of DNA binding is associated with localization in intranuclear speckles. *J Biol Chem.* 2007; 282:24915-24927.
30. Freedman DA, Levine AJ. Nuclear export is required for degradation of endogenous p53 by MDM2 and human papillomavirus E6. *Mol Cell Biol.* 1998; 18:7288-7239.
31. Stommel JM, Marchenko ND, Jimenez GS, Moll UM, Hope TJ, Wahl GM. A leucine-rich nuclear export signal in the p53 tetramerization domain: regulation of subcellular localization and p53 activity by NES masking. *EMBO J.* 1999; 18:1660-1672.
32. Lee EW, Oh W, Song HP, Kim WK. Phosphorylation of p53 at threonine 155 is required for Jab1-mediated nuclear export of p53. *BMB Rep.* 2017; 50:373-378.
33. Tomoda K, Kubota Y, Arata Y, Mori S, Maeda M, Tanaka T, Yoshida M, Yoneda-Kato N, Kato J. The cytoplasmic shuttling and subsequent degradation of p27^{Kip1} mediated by Jab1/CNS5 and the COP9 signalosome complex. *J Biol Chem.* 2002; 277:2302-2310.
34. Maeda M, Ishida A, Ni L, Kobayashi A. Isolation of CHO-K1 clones defective in cAMP-dependent proteolysis, as determined by the stability of exogenously expressed GATA-6. *Biochem Biophys Res Commun.* 2005; 329:140-146.
35. Gaynor KU, Grigorieva IV, Allen MD, Esapa CT, Head RA, Gopinath P, Christie PT, Nesbit MA, Jones JL, Thakker RV. GATA3 mutations found in breast cancers may be associated with aberrant nuclear localization, reduced transactivation and cell invasiveness. *Horm Canc.* 2013; 4:123-139.
36. Shaiken TE, Opekun AR. Dissecting the cells to nucleus, perinucleus and cytosol. *Sci Rep.* 2014; 4:4923.
37. Kosugi S, Hasebe M, Matsumura N, Takashima H, Miyamoto-Sato E, Tomita M, Yanagawa H. Six classes of nuclear localization signals specific to different binding grooves of importin α . *J Biol Chem.* 2009; 284:478-485.
38. Lee BJ, Cansizoglu AE, Süel KE, Louis TH, Zhang Z, Chook YM. Rules for nuclear localization sequence

- recognition by karyopherin $\beta 2$. Cell. 2006; 126:543-558.
39. Shimizu R, Takahashi S, Ohneda K, Engel JD, Yamamoto M. *In vivo* requirements for GATA-1 functional domains during primitive and definitive erythropoiesis. EMBO J. 2001; 20:5250-5260.
 40. Shaulsky G, Goldfinger N, Ben-Ze'ev A, Rotter V. Nuclear accumulation of p53 protein is mediated by several nuclear localization signals and plays a role in tumorigenesis. Mol Cell Biol. 1990; 10:6565-6577.
 41. Kobayashi A, Kasano M, Maeda T, Hori S, Motojima K, Suzuki M, Fujiwara T, Takahashi E, Yabe T, Tanaka K, Kasahara M, Yamaguchi Y, Maeda M. A half-type ABC transporter TAPL is highly conserved between rodent and man, and the human gene is not responsive to interferon- γ in contrast to TAP1 and TAP2. J Biochem. 2000; 128:711-718.
 42. Kamakura A, Fujimoto Y, Motohashi Y, Ohashi K, Ohashi-Kobayashi A, Maeda M. Functional dissection of transmembrane domains of human TAP-like (ABC9). Biochem Biophys Res Commun. 2008; 377:847-851.
 43. Nakajima T, Kitagawa K, Ohhata T, Sakai S, Uchida C, Shibata K, Minegishi N, Yumimoto K, Nakayama KI, Masumoto K, Katou F, Niida H, Kitagawa M. Regulation of GATA-binding protein 2 levels *via* ubiquitin-dependent degradation by Fbw7: involvement of cyclin B-cyclin-dependent kinase 1-mediated phosphorylation of Thr¹⁷⁶ in GATA-binding protein 2. J Biol Chem. 2015; 290:10368-10381.
 44. Kitagawa K, Shibata K, Matsumoto A, Matsumoto M, Ohhata T, Nakayama KI, Niida H, Kitagawa M. Fbw7 targets GATA3 through cyclin-dependent kinase 2-dependent proteolysis and contributes to regulation of T-cell development. Mol Cell Biol. 2014; 34:2732-2744.
 45. Frisan E, Vandekerckhove J, de Thonel A, *et al.* Defective nuclear localization of Hsp70 is associated with dyserythropoiesis and GATA-1 cleavage in myelodysplastic syndromes. Blood. 2012; 119:1532-1542.
 46. Han X, Zhang J, Peng Y, Peng M, Chen X, Chen H, Song J, Hu X, Ye M, Li J, Sankaran VG, Hillyer CD, Mohandas N, An X, Liu J. Unexpected role for p19^{INK4d} in posttranscriptional regulation of GATA1 and modulation of human terminal erythropoiesis. Blood. 2017; 129:226-237.
 47. Flores K, Yadav SS, Katz AA, Seger R. The nuclear translocation of mitogen-activated protein kinases: molecular mechanisms and use as novel therapeutic target. Neuroendocrinology. 2019; 108:121-131.
 48. Kawasaki Y, Matsumura K, Miyamoto M, Tsuji S, Okuno M, Suda S, Hiyoshi M, Kitayama J, Akiyama T. REG4 is a transcriptional target of GATA6 and is essential for colorectal tumorigenesis. Sci Rep. 2015; 5:14291.
 49. Katanasaka Y, Suzuki H, Sunagawa Y, Hasegawa K, Morimoto T. Regulation of cardiac transcription factor GATA4 by post-transcriptional modification in cardiomyocyte hypertrophy and heart failure. Int Heart J. 2016; 57:672-675.
 50. Ito T, Yamaguchi Y, Handa H. Exploiting ubiquitin ligase cereblon as a target for small-molecule compounds in medicine and chemical biology. Cell Chem Biol. 2021; 28:987-999.
- Received November 25, 2022; Revised January 12, 2023; Accepted January 26, 2023.
- Present Address:* ^a Japan Tobacco Inc. Central Pharmaceutical Research Institute, ^b Corporate Communications Dept. Corporate Strategy Div. SHIONOGI & CO., LTD., Japan.
- *Address correspondence to:*
 Masatomo Maeda, Graduate School of Pharmaceutical Sciences, Osaka University, Yamada-oka, Suita, Osaka 565-0871, Japan.
 E-mail: m.maeda.d5h@osaka-u.ac.jp
- Released online in J-STAGE as advance publication February 4, 2023.

Redundant roles of extra-cellular signal-regulated kinase (ERK) 1 and 2 in the G1-S transition and etoposide-induced G2/M checkpoint in HCT116 cells

Purev Erdenebaatar¹, I Ketut Gunarta¹, Ryusuke Suzuki¹, Ravdandorj Odongoo¹, Toshihiro Fujii², Rikiro Fukunaga², Masato T Kanemaki^{3,4}, Katsuji Yoshioka^{1,*}

¹Division of Molecular Cell Signaling, Cancer Research Institute, Kanazawa University, Kanazawa, Japan;

²Department of Biochemistry, Faculty of Pharmacy, Osaka Medical and Pharmaceutical University, Takatsuki, Japan;

³Department of Chromosome Science, National Institute of Genetics, Research Organization of Information and Systems (ROIS), Mishima, Japan;

⁴Department of Genetics, The Graduate University for Advanced Studies (SOKENDAI), Mishima, Japan.

SUMMARY The extracellular signal-regulated kinase (ERK) 1 and 2 intracellular signaling pathways play key roles in a variety of cellular processes, such as proliferation and differentiation. Dysregulation of ERK1/2 signaling has been implicated in many diseases, including cancer. Although ERK1/2 signaling pathways have been extensively studied, controversy remains as to whether ERK1 and ERK2 have specific or redundant functions. In this study, we examined the functional roles of ERK1 and ERK2 in cell proliferation and cell cycle progression using an auxin-inducible degron system combined with gene knockout technology. We found that ERK1/2 double depletion, but not ERK1 or ERK2 depletion, substantially inhibited the proliferation of HCT116 cells during G1-S transition. We further demonstrated that ERK1/2-double-depleted cells were much more tolerant to etoposide-induced G2/M arrest than ERK1 or ERK2 single-knockout cells. Together, these results strongly suggest the functional redundancy of ERK1 and ERK2 in both the G1-S transition under physiological conditions and the DNA damage-induced G2/M checkpoint. Our findings substantially advance understanding of the ERK1/2 pathways, which could have strong implications for future pharmacological developments.

Keywords Cell cycle, DNA damage, mitogen-activated protein kinase

1. Introduction

Proper response to extra- and intracellular stimuli is essential for the normal development and maintenance of homeostasis in living organisms, in which intracellular signaling pathways play important roles. The mitogen-activated protein kinase (MAPK) intracellular signaling cascade, consisting of MAPK, MAPK kinase (MAPKK), and MAPKK kinase (MAP3K), is highly conserved in eukaryotes, from yeast to mammals, and transduces signals *via* sequential phosphorylation (1,2). Extracellular signal-regulated kinase (ERK) 1 and 2 are the terminal components of the MAPK cascade. In mammals, ERK MAPK signaling regulates a variety of cellular processes, including proliferation and differentiation, and its dysregulation is implicated in many diseases, including cancer (3-5). Rat sarcoma virus (RAS), a small GTPase that activates ERK *via* rapidly accelerated fibrosarcoma (RAF) MAP3K and MAPK/ERK kinase

(MEK) MAPKK, is one of the most frequently mutated oncogenes in human cancers (3,6,7).

Although ERK1 and ERK2 share over 80% amino acid sequence identity (8), the phenotypes of ERK1 and ERK2 knockout mice differ significantly. *Erk1* knockout mice are viable (9), whereas *Erk2* knockout mice are embryonic lethal (10-12). Further studies using a Cre-loxP system or short interfering RNA (siRNA) technology have shown different phenotypes of ERK1- and ERK2-deficient mice and cells (13-16), emphasizing that ERK1 and ERK2 possess specific functions. In contrast, recent studies have reported the functional redundancy of ERK1 and ERK2 (17-19). For example, Frémin *et al.* (20) showed that transgenic expression of ERK1 fully rescues mouse developmental defects associated with the loss of ERK2. However, whether ERK1 and ERK2 have specific or redundant functions remains controversial.

In this study, we investigated the functional roles

of ERK1 and ERK2 in cell proliferation and cell cycle progression using an auxin-inducible degron system combined with gene knockout technology. Our results suggest the functional redundancy of ERK1 and ERK2 in both the G1-S transition under physiological conditions and the DNA damage-induced G2/M checkpoint.

2. Materials and Methods

2.1. Cell culture and reagents

HCT116 cells either expressing or not expressing *Oryza sativa* transport inhibitor response 1 (OsTIR1) (F74G) were cultured as previously described (21,22). In some experiments, HCT116 cells were synchronized at the G1/S boundary, as described by Boulay *et al.* (23), with minor modifications. Briefly, cells were seeded at 4×10^5 cells per 35-mm dish. The following day, the medium was replaced with fresh medium containing 2 mM thymidine and incubated for 16 h. The cells were then washed three times, and the medium was replaced with fresh thymidine-free medium. After 8 h, the medium was replaced with 2 mM thymidine for 16 h, washed thrice, and replaced with thymidine-free fresh medium. Propidium iodide and 4',6-diamidino-2-phenylindole (DAPI) were obtained from Sigma-Aldrich (St. Louis, MO, USA). Blasticidin S hydrochloride and etoposide were purchased from Wako (Osaka, Japan). The Click-iT 5-ethynyl-2'-deoxyuridine (EdU) kit (C10425), 5-phenyl-1H-indole-3-acetic acid (5-Ph-IAA), puromycin, and SCH772984 were obtained from Thermo Fisher Scientific (Waltham, MA, USA), BioAcademia (Osaka, Japan), Nacalai Tesque (Kyoto, Japan), and Selleck (Houston, TX, USA), respectively.

2.2. Plasmids and viral vector preparation

The lentivirus expression plasmid for hemagglutinin (HA)-tagged protein, pCL20c-CMVΔ4-HA, has been previously described (24). The entire coding sequences of three ERK1 variants, variant 1 (accession number NM_002746), variant 2 (NM_001040056), and variant 3 (NM_001109891), and ERK2 (NM_002745) were inserted into pCL20c-CMVΔ4-HA to generate pCL20c-CMVΔ4-HA-ERK1_V1, pCL20c-CMVΔ4-HA-ERK1_V2, pCL20c-CMVΔ4-HA-ERK1_V3, and pCL20c-CMVΔ4-HA-ERK2, respectively. Lentiviral vectors were prepared as described previously (25).

The following single-guide RNA (sgRNA) target sequences were cloned into pX330-U6-Chimeric_BB-CBh-hSpCas9 (#42230; Addgene, Watertown, MA, USA): *ERK1*, 5'-GCGTAGCCACATACTCCGTC-3' and *ERK2*, 5'-GCCTACAGACCAAATATCAA-3'. The resultant plasmids, pX330-ERK1-TG12 and pX330-ERK2-TG15, together with pUREF-EX, were used to knock out *ERK1* and *ERK2*, respectively. The pUREF-

EX plasmid was constructed by introducing the simian virus 40 (SV40) promoter-driven puromycin resistance gene (*PuroR*) into the pEF-BOS-EX vector (26). The mini-auxin-inducible degron (mAID) tag (27,28) was knocked-in at the C-terminus of the endogenous *ERK2* gene through clustered regularly interspaced short palindromic repeat (CRISPR)/CRISPR-associated protein 9 (Cas9)-mediated homologous recombination with pX330-ERK2-T2 and donor DNA plasmids. The sgRNA target sequence in pX330-ERK2-T2 was 5'-CAAATTTAAGATCTGTATCC-3'. Donor plasmids were constructed using pBlueScript KS II as a backbone. The mAID tag sequence (derived from pMK381 (Addgene #140536)) and phosphoglycerate kinase (PGK)-blasticidin S deaminase (BSD) (or -*PuroR*) expression cassettes were flanked by 1.1- and 1.2-kb left and right homology arms, respectively. The left arm and mAID tag were connected with the following 30-bp linker by overlapping PCR: forward, 5'-GGCGCTGGTGCAGGCGCCGGATCCACTA GT-3' and reverse, 5'-ACTAGTGGATCCGGCGCCT GCACCAGCGCC-3'. The PGK-*PuroR* sequence was derived from pMK381, and *PuroR* was replaced with *BSD* (derived from pMK347 (Addgene #121181)) to generate the PGK-*BSD* expression cassette.

2.3. Cell line generation

To generate *ERK1* and *ERK2* single-knockout cell lines, HCT116 cells were transiently co-transfected with pUREF-EX and pX330-ERK1-TG12 (for *ERK1*) or pX330-ERK2-TG15 (for *ERK2*). Twenty-four hours after transfection, cells were cultured with 3 μg/mL puromycin for another 24 h, washed with phosphate-buffered saline (PBS), and subsequently cultured in the presence of 1 μg/mL puromycin for 24 h and in the absence of puromycin for 48 h. The cells were then subjected to limiting-dilution cloning. Gene disruption in clones was confirmed by genomic DNA PCR using the primers listed in Table S1 (<http://www.ddtjournal.com/action/getSupplementalData.php?ID=130>) and by western blot analysis.

ERK1 knockout clone cells were co-transfected with pX330-ERK2-T2 and two donor DNA plasmids containing *PuroR* and *BSD* expression cassettes, as described above. The medium was changed 24 h after transfection, and the cells were cultured for another 24 h. The transfected cells were incubated with 0.5 μg/mL puromycin and 10 μg/mL blasticidin S hydrochloride for 10 days, and then, single-cell colonies were picked and cultured for further analyses. mAID tagging at the C-terminus of the endogenous *ERK2* gene was confirmed by genomic DNA PCR using the primers listed in Table S1 (<http://www.ddtjournal.com/action/getSupplementalData.php?ID=130>) and by western blot analysis. This established cell line was named ERK1-KO/ERK2-mAID.

2.4. Western blot analysis and immunocytochemistry

Total cell lysates were prepared and analyzed by western blotting as previously described (25) using anti-actin (1:5,000; A6050; Sigma-Aldrich), anti-ERK1/2 (1:2,000; #4695; Cell Signaling Technology, Danvers, MA, USA), and anti-HA (1:2,000; 11867423001, Sigma-Aldrich) primary antibodies. Immunocytochemistry was carried out as described previously (25) using anti-HA (1:100; 11867423001, Sigma-Aldrich) primary antibody and Alexa Fluor 568-conjugated goat anti-mouse IgG (1:500; Thermo Fisher Scientific) secondary antibody. Fluorescent images were captured using an IX71 inverted microscope (Olympus, Tokyo, Japan) attached to a DP50 digital CCD camera (Olympus).

2.5. Cell proliferation and cell cycle analysis

For the cell proliferation assay, cells were seeded at 2×10^4 cells/well in a 24-well plate, grown for 1 d, and cultured in the presence or absence of SCH772984 or 5-Ph-IAA for the indicated times and concentrations, as described in the legends of the corresponding figures. The cells were fixed with 4% paraformaldehyde in PBS for 20 min and stained with DAPI. Five images were randomly captured for each well using a Keyence BZ-X800 fluorescence microscope (Keyence, Osaka, Japan), and the cell numbers were counted using ImageJ software.

The phase distribution of the cell cycle was analyzed by flow cytometry using propidium iodide, with or without EdU. Wild-type, *ERK1* single knockout, and *ERK2* single knockout clones of HCT116, as well as parental HCT116 cells, were seeded at 4×10^5 cells per 35-mm dish and grown for 1 d. The cells were labeled with 10 μ M EdU for 1 h, trypsinized, washed once with PBS containing EDTA (0.5 mM), and fixed with 70% cold ethanol for 20 min. Fixed cells were permeabilized with 0.1% Triton X-100 in PBS for 20 min, treated with

Click-iT EdU Reaction Cocktail (prepared according to the manufacturer's instructions) for 20 min, washed thrice with PBS, stained with 10 μ g/mL propidium iodide, and analyzed by flow cytometry using a BD FACSLyric Flow cytometer (BD Biosciences, Franklin Lakes, NJ, USA). HCT116 ERK1-KO/ERK2-mAID clones were seeded at 2×10^5 cells per 35-mm dish and grown for 1 d. Cells were then treated with or without 5 μ M 5-Ph-IAA for 48 h, labeled with 10 μ M EdU for 1 h, and subjected to flow cytometric analysis, as described above. For cell cycle analysis using propidium iodide, but not EdU, cells were treated with or without 20 μ M etoposide for 1 h and subjected to flow cytometry analysis as described above, except that cells were treated with 5 μ g/mL RNase A after the ethanol-fixed cells were washed with PBS.

2.6. Statistical analysis

Statistical significance was determined using two-tailed unpaired Student's *t*-test. Statistical significance was set at a *p* value of < 0.05.

3. Results

3.1. Effect of ERK1 and ERK2 inhibition on cell proliferation

First, we examined the effects of ERK inhibition on cell proliferation. The near-diploid cell line HCT116 was cultured with six different concentrations (0–256 nM) of SCH772984, an ERK1/2 inhibitor, for 3 d. As shown in Figure 1A, cell numbers decreased in a dose-dependent manner. Of the different concentrations, we chose 64 nM for the kinetic analysis, because an appropriate inhibitory effect was observed at this concentration. We treated cells with 64 nM SCH772984 and monitored cell proliferation by counting cells every day for 3 d. Compared with vehicle-treated cells, SCH772984-treated cells showed lower numbers of cells at all examined time points (Figure

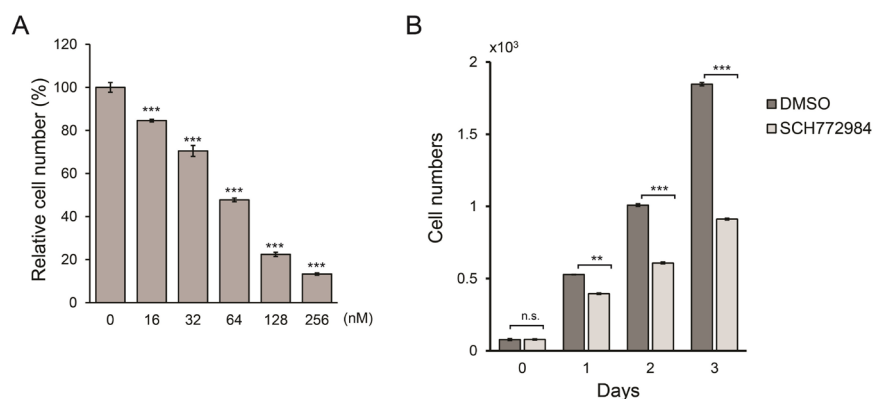


Figure 1. Inhibition of ERK1 and ERK2 prevented cell proliferation. (A) HCT116 cells were plated and grown for 1 d and treated with the ERK1/2 inhibitor SCH772984 (dissolved in dimethyl sulfoxide (DMSO)) at the indicated concentrations for 3 d. Cell numbers were normalized to those of control vehicle-treated (0 nM) cells. (B) HCT116 cells were plated and grown for 1 d (Day 0) and then cultured in the presence or absence of SCH772984 (64 nM) for the indicated days. Average cell numbers per captured image are shown. Quantitative data are expressed as mean \pm S.E.M of three independent experiments. ***p* < 0.01; ****p* < 0.001; n.s., not significant.

1B). These results suggest that ERK1 and/or ERK2 play a role in the proliferation of HCT116 cells.

3.2. Overlapping functions of ERK1 and ERK2 in cell proliferation

We examined whether ERK1 and ERK2 had redundant functions in cell proliferation. To this end, we first generated *ERK1* or *ERK2* single-knockout HCT116 cells (Figure 2A) and analyzed their proliferation. The results showed that depletion of either ERK1 or ERK2 had little effect on cell proliferation (Figure 2B), suggesting a functional redundancy of ERK1 and ERK2. To address this issue, we employed a conditional depletion system. The mAID tag was inserted at the C-terminus of endogenous *ERK2* in *ERK1* knockout HCT116 cells expressing OsTIR1(F74G). After screening with two different antibiotics (puromycin and blasticidin), we identified biallelic knock-in cell line that stably expressed the mAID-tagged ERK2 (ERK2-mAID) protein. The resulting cell line was named HCT116

ERK1-KO/ERK2-mAID. As shown in Figure 2C, the electrophoretic mobility of ERK2-mAID proteins was notably delayed, and no endogenous ERK2 proteins were detected, indicating mAID tag knock-in at both alleles. The expression levels of ERK2-mAID proteins were lower than those of endogenous ERK2 proteins, for unknown reasons. However, there were no defects in the proliferation of the HCT116 ERK1-KO/ERK2-mAID cell lines (Figure S1, <http://www.ddtjournal.com/action/getSupplementalData.php?ID=130>). Therefore, these cell lines were used for further analysis. Western blot analysis showed that the ERK2-mAID protein disappeared rapidly upon 5-Ph-IAA treatment (Figure 2D). Notably, the inhibition of proliferation was induced by depleting ERK2-mAID protein in the HCT116 ERK1-KO/ERK2-mAID cell lines (Figure 2E). Taken together, these results strongly suggest that ERK1 and ERK2 play a role in the functional redundancy of cell proliferation.

3.3. Functional evaluation of ERK1 variants in cell proliferation

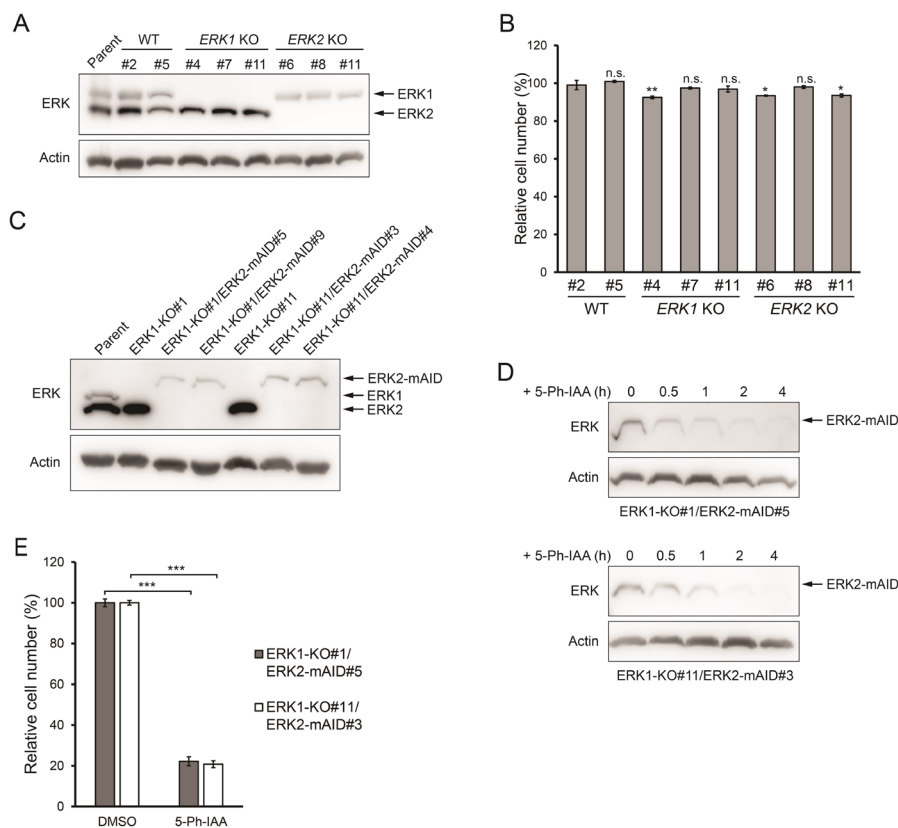


Figure 2. ERK1 and ERK2 played a redundant role in cell proliferation. (A) Parental HCT116 cells (Parent), two wild-type (WT) clones (#2 and #5), three *ERK1* knockout (KO) clones (#4, #7 and #11), and three *ERK2* KO clones (#6, #8, #11) were analyzed using western blotting with an anti-ERK1/2 antibody. (B) The WT and KO clones, as well as the parental cells, were cultured for 3 d, and cell proliferation was examined, as shown in Figure 1B. (C) ERK1-KO/ERK2-mAID cell lines were generated using ERK1-KO#1 and ERK1-KO#11. Obtained clones, ERK1-KO#1/ERK2-mAID#5, ERK1-KO#1/ERK2-mAID#9, ERK1-KO#11/ERK2-mAID#3, and ERK1-KO#11/ERK2-mAID#4, were analyzed using western blotting, as shown in (A). (D) ERK1-KO#1/ERK2-mAID#5 and ERK1-KO#11/ERK2-mAID#3 clones were treated with 5 μ M 5-phenyl-1H-indole-3-acetic acid (5-Ph-IAA). Cell lysates were collected at the indicated time points and subjected to western blotting, as shown in (A). (E) Cell proliferation was analyzed in ERK1-KO#1/ERK2-mAID#5 and ERK1-KO#11/ERK2-mAID#3 clones treated with vehicle (DMSO) or 5 μ M 5-Ph-IAA as shown in (B). Actin was utilized as the loading control. Quantitative data are expressed as mean \pm S.E.M of three independent experiments. * $p < 0.05$; ** $p < 0.01$; *** $p < 0.001$; n.s., not significant.

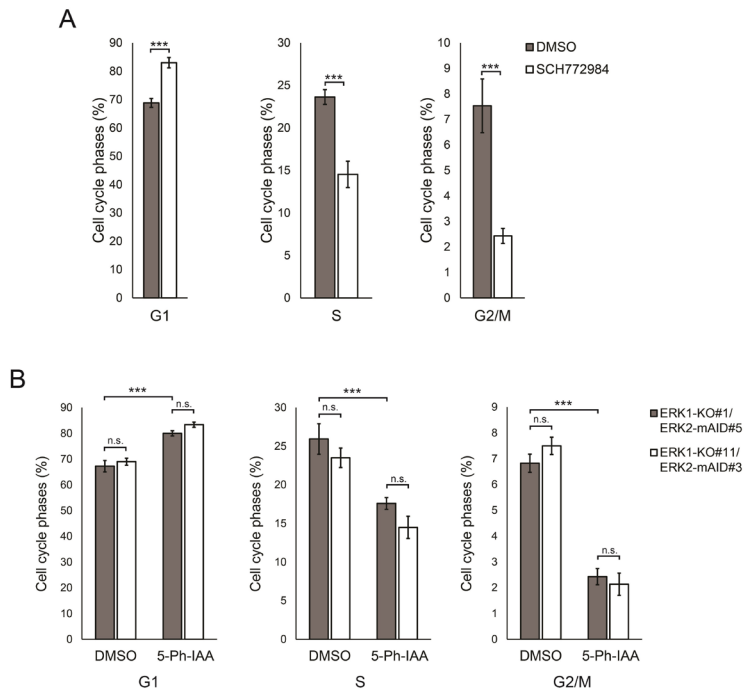


Figure 4. ERK1 and ERK2 had functional role in cell cycle progression. (A) HCT116 cells were cultured in the presence of vehicle (DMSO) or 100 nM SCH772984, and cell cycle distribution was analyzed by flow cytometry using EdU. (B) ERK1-KO#1/ERK2-mAID#5 and ERK1-KO#11/ERK2-mAID#3 clones treated with vehicle (DMSO) or 5 μ M 5-Ph-IAA were analyzed as shown in (A). Quantitative data are expressed as mean \pm S.E.M of three independent experiments. *** $p < 0.001$; n.s., not significant.

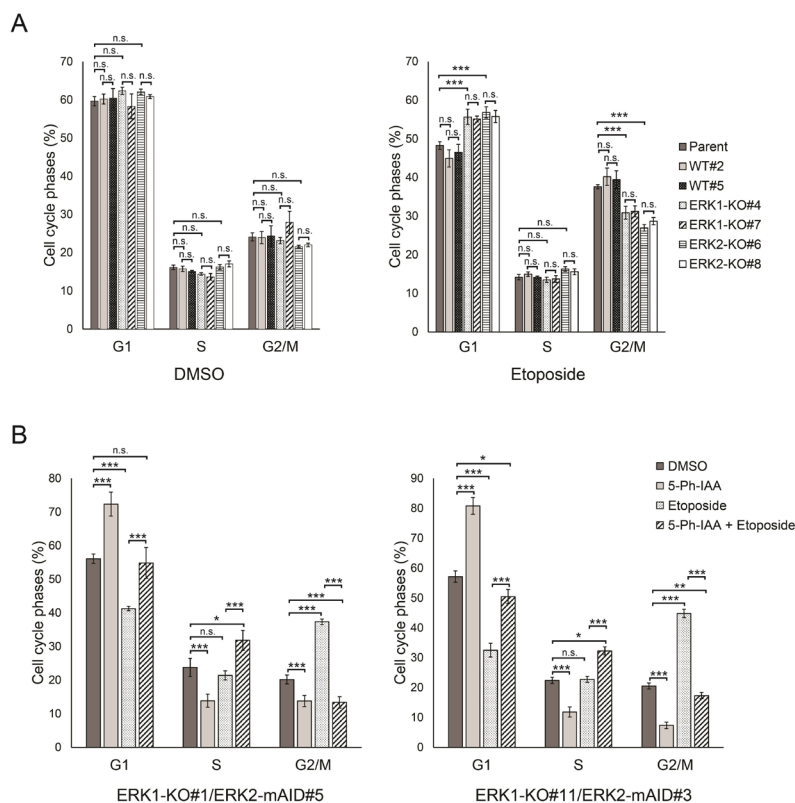


Figure 5. ERK1 and ERK2 had redundant roles in etoposide-induced G2/M accumulation. (A) The parental HCT116 cells (Parent), wild-type (WT) (#2 and #5), ERK1 knockout (KO) (#4 and #7), and ERK2 KO (#6 and #8) clones described in Figure 2A were treated with vehicle (DMSO) or 20 μ M etoposide for 1 h, and cell cycle distribution was analyzed using flow cytometry. (B) The ERK1-KO#1/ERK2-mAID#5 and ERK1-KO#11/ERK2-mAID#3 clones described in Figure 2C were synchronized at the G1/S boundary, cultured in the presence or absence of 20 μ M etoposide for 1 h with or without 5 μ M 5-Ph-IAA for 4 h, as indicated, and subjected to flow cytometry analysis. * $p < 0.05$; ** $p < 0.01$; *** $p < 0.001$; n.s., not significant.

4. Discussion

In this study, we explored the role of ERK1 and ERK2 in cell proliferation and cell cycle progression using the near-diploid cell line HCT116. At present, selective pharmacological inhibitors to distinguish between ERK1 and ERK2 are not available, and inhibition of ERK1/2 has been reported to prevent cell proliferation (3,30).

Here, we employed an auxin-inducible degron system, called AID2 (22), in combination with gene knockout technology and provided evidence that ERK1 and ERK2 play redundant roles in cell proliferation (Figure 2) and cell cycle progression during the G1-S transition (Figure 4). To date, several *in vivo* and *in vitro* studies have reported that ERK1 and ERK2 have distinct functions (13-16). However, recent studies have suggested

redundant functions for ERK1 and ERK2 (17-20). Our present study using the AID2 system supports the latter hypothesis, that is, the interchangeable functions of ERK1 and ERK2. To the best of our knowledge, this is the first study to examine the functional redundancy of ERK1/2 in a rapid protein depletion system.

Moreover, we examined the functional roles of ERK1 and ERK2 in DNA damage response using the AID2 system (Figure 5). Wei *et al.* (29) reported that ERK1 and ERK2 are involved in etoposide-induced G2/M arrest and suggested the possibility of redundant roles of ERK1/2 in the G2/M checkpoint; however, this possibility was not addressed, most likely due to technical limitations, in which the authors employed an siRNA-mediated knockdown approach. Here, we generated a conditional depletion system of ERK2 in an ERK1 knockout background and showed that ERK1/2-double-depleted cells were much more tolerant to etoposide-induced G2/M arrest than ERK1 or ERK2 single knockout cells (Figure 5A and B). These findings strongly suggest the functional redundancy of ERK1 and ERK2 in G2/M checkpoint activation in response to DNA damage. Our findings substantially advance understanding of the ERK1/2 pathways, which could have strong implications for future pharmacological developments.

Acknowledgements

This work was supported in part by JSPS KAKENHI [Grant Numbers JP21K06818 (to KY) and JP22K15378 (to RS)].

Funding: None.

Conflict of Interest: The authors have no conflicts of interest to disclose.

References

- Cano E, Mahadevan LC. Parallel signal processing among mammalian MAPKs. *Trends Biochem Sci.* 1995; 20:117-122.
- Herskowitz I. MAP kinase pathway in yeast: for mating and more. *Cell.* 1995; 80:187-197.
- Guo YJ, Pan WW, Liu SB, Shen ZF, Xu Y, Hu LL. ERK/MAPK signalling pathway and tumorigenesis. *Exp Ther Med.* 2020; 19:1997-2007.
- Lawrence MC, Jivan A, Shao C, Duan L, Goad D, Zaganjor E, Osborne J, McGlynn K, Stippee S, Earnest S, Chen W, Cobb MH. The roles of MAPKs in disease. *Cell Res.* 2008; 18:436-442.
- Kim EK, Choi EJ. Pathological roles of MAPK signaling pathways in human diseases. *Biochim Biophys Acta.* 2010; 1802:396-405.
- Prior IA, Lewis PD, Mattos C. A comprehensive survey of Ras mutations in cancer. *Cancer Res.* 2012; 72:2457-2467.
- Prior IA, Hood FE, Hartley JL. The frequency of Ras mutations in cancer. *Cancer Res.* 2020; 80:2969-2974.
- Boulton TG, Nye SH, Robbins DJ, Ip NY, Radziejewska E, Morgenbesser SD, DePinho RA, Panayotatos N, Cobb MH, Yancopoulos GD. ERKs: a family of protein-serine/threonine kinases that are activated and tyrosine phosphorylated in response to insulin and NGF. *Cell.* 1991; 65:663-675.
- Pagès G, Guérin S, Grall D, Bonino F, Smith A, Anjuere F, Auberger P, Pouyssegur J. Defective thymocyte maturation in p44 MAP kinase (Erk 1) knockout mice. *Science.* 1999; 286:1374-1377.
- Hatano N, Mori Y, Oh-hora M, Kosugi A, Fujikawa T, Nakai N, Niwa H, Miyazaki J, Hamaoka T, Ogata M. Essential role for ERK2 mitogen-activated protein kinase in placental development. *Genes Cells.* 2003; 8:847-856.
- Saba-El-Leil MK, Vella FD, Vernay B, Voisin L, Chen L, Labrecque N, Ang SL, Meloche S. An essential function of the mitogen-activated protein kinase Erk2 in mouse trophoblast development. *EMBO Rep.* 2003; 4:964-968.
- Yao Y, Li W, Wu J, Germann UA, Su MS, Kuida K, Boucher DM. Extracellular signal-regulated kinase 2 is necessary for mesoderm differentiation. *Proc Natl Acad Sci U S A.* 2003; 100:12759-12764.
- Fischer AM, Katayama CD, Pagès G, Pouyssegur J, Hedrick SM. The role of erk1 and erk2 in multiple stages of T cell development. *Immunity.* 2005; 23:431-443.
- Zeng P, Wagoner HA, Pescovitz OH, Steinmetz R. RNA interference (RNAi) for extracellular signal-regulated kinase 1 (ERK1) alone is sufficient to suppress cell viability in ovarian cancer cells. *Cancer Biol Ther.* 2005; 4:961-967.
- Vantaggiato C, Formentini I, Bondanza A, Bonini C, Naldini L, Brambilla R. ERK1 and ERK2 mitogen-activated protein kinases affect Ras-dependent cell signaling differentially. *J Biol.* 2006; 5:14.
- Frémin C, Ezan F, Boisselier P, Bessard A, Pagès G, Pouyssegur J, Baffet G. ERK2 but not ERK1 plays a key role in hepatocyte replication: an RNAi-mediated ERK2 knockdown approach in wild-type and ERK1 null hepatocytes. *Hepatology.* 2007; 45:1035-1045.
- Buscà R, Pouyssegur J, Lenormand P. ERK1 and ERK2 map kinases: Specific roles or functional redundancy? *Front Cell Dev Biol.* 2016; 4:53.
- Saba-El-Leil MK, Frémin C, Meloche S. Redundancy in the world of MAP kinases: All for one. *Front Cell Dev Biol.* 2016; 4:67.
- Cingolani F, Liu Y, Shen Y, Wen J, Farris AB, Czaja MJ. Redundant functions of ERK1 and ERK2 maintain mouse liver homeostasis through down-regulation of bile acid synthesis. *Hepato Comm.* 2022; 6:980-994.
- Frémin C, Saba-El-Leil MK, Lévesque K, Ang SL, Meloche S. Functional redundancy of ERK1 and ERK2 MAP kinases during development. *Cell Rep.* 2015; 12:913-921.
- Gunarta IK, Yuliana D, Erdenebaatar P, Kishi Y, Boldbaatar J, Suzuki R, Odongoo R, Davaakhuu G, Hohjoh H, Yoshioka K. c-Jun NH₂-terminal kinase (JNK)/stress-activated protein kinase-associated protein 1 (JSAP1) attenuates curcumin-induced cell death differently from its family member, JNK-associated leucine zipper protein (JLP). *Drug Discov Ther.* 2021; 15:66-72.
- Yesbolatova A, Saito Y, Kitamoto N, Makino-Itou H, Ajima R, Nakano R, Nakaoka H, Fukui K, Gamo K, Tominari Y, Takeuchi H, Saga Y, Hayashi KI, Kanemaki

- MT. The auxin-inducible degron 2 technology provides sharp degradation control in yeast, mammalian cells, and mice. *Nat Commun.* 2020; 11:5701.
23. Boulay K, Ghram M, Viranaicken W, Trépanier V, Mollet S, Fréchina C, DesGroseillers L. Cell cycle-dependent regulation of the RNA-binding protein Stauf1. *Nucleic Acids Res.* 2014; 42:7867-7883.
24. Boldbaatar J, Gunarta IK, Suzuki R, Erdenebaatar P, Davaakhuu G, Hohjoh H, Yoshioka K. Protective role of c-Jun NH₂-terminal kinase-associated leucine zipper protein (JLP) in curcumin-induced cancer cell death. *Biochem Biophys Res Commun.* 2020; 522:697-703.
25. Sato T, Torashima T, Sugihara K, Hirai H, Asano M, Yoshioka K. The scaffold protein JSAP1 regulates proliferation and differentiation of cerebellar granule cell precursors by modulating JNK signaling. *Mol Cell Neurosci.* 2008; 39:569-578.
26. Watanabe-Fukunaga R, Iida S, Shimizu Y, Nagata S, Fukunaga R. SEI family of nuclear factors regulates p53-dependent transcriptional activation. *Genes Cells.* 2005; 10:851-860.
27. Kubota T, Nishimura K, Kanemaki MT, Donaldson AD. The Elg1 replication factor C-like complex functions in PCNA unloading during DNA replication. *Mol Cell.* 2013; 50:273-280.
28. Natsume T, Kiyomitsu T, Saga Y, Kanemaki MT. Rapid protein depletion in human cells by auxin-inducible degron tagging with short homology donors. *Cell Rep.* 2016; 15:210-218.
29. Wei F, Xie Y, Tao L, Tang D. Both ERK1 and ERK2 kinases promote G2/M arrest in etoposide-treated MCF7 cells by facilitating ATM activation. *Cell Signal.* 2010; 22:1783-1789.
30. Mebratu Y, Tesfaijzi Y. How ERK1/2 activation controls cell proliferation and cell death: Is subcellular localization the answer? *Cell Cycle.* 2009; 8:1168-1175.

Received December 14, 2022; Revised January 2, 2023; Accepted January 7, 2023.

**Address correspondence to:*

Katsuji Yoshioka, Division of Molecular Cell Signaling, Cancer Research Institute, Kanazawa University, Kakuma-machi, Kanazawa, Ishikawa 920-1192, Japan.
E-mail: katsuji@staff.kanazawa-u.ac.jp

Released online in J-STAGE as advance publication January 14, 2023.

Bombyx mori as a model for *Niallia circulans* pathogenicity

M. Ismail Hossain¹, Nusrat U. A. Saleh¹, Al Numan¹, M. Mahtab Hossain¹, M. Aftab Uddin², Muktadir S. Hossain^{1,*}

¹Department of Biochemistry and Microbiology, School of Health and Life Sciences, North South University, Dhaka, Bangladesh;

²Bangladesh Sericulture Research and Training Institute, Rajshahi, Bangladesh.

SUMMARY Increasing incidences of resistance to antibiotics by pathogenic bacteria is a worldwide concern and isolation of antibiotic-resistant strains of *Niallia circulans* (formerly known as *Bacillus circulans*), an opportunistic human pathogen, has been reported. Due to their lack of ethical constraints as well as their cost-effective rearing, invertebrates have been commonly used to study infection by bacteria pathogenic to humans. In this study, we demonstrate that a foodborne strain of *N. circulans* kills larvae of the silkworm, *Bombyx mori* within 48 h after hemolymph injection. The infected larvae turned black with an increase in the phenoloxidase (PO) activity in the hemolymph. Midgut injection of *N. circulans* resulted in the killing of larvae within 96 h. A significant increase in bacterial load was observed in the hemolymph 12 h after infection. The viable hemocyte number decreased to 48% within 12 h of injection. RT-qPCR analysis revealed that upon hemolymph infection with *N. circulans* the expression of the antimicrobial peptide (AMP) genes, *Bmdefensin-B* and *Bmgloverin-3*, were upregulated 2.5- and 1.8-fold, respectively, whereas 1.6-fold upregulation was observed for *BmToll-2* in the larval fat body. Therapeutic effects of antibiotics like tetracycline, imipenem, ceftriaxone, ampicillin, and clindamycin were observed against *N. circulans* in the *Bombyx* larvae with varying efficacies. Results from this study suggest that larvae of *B. mori* can be used as infection models for screening therapeutics that are effective against *N. circulans*.

Keywords *Niallia circulans*, *Bombyx mori*, *Galleria mellonella*, infection model, antibiotic resistance

1. Introduction

Niallia circulans (formerly known as *Bacillus circulans*) is a Gram-positive, spore-forming, rod-shaped species (1). It is usually found in soil and the non-pathogenic *N. circulans* and other *Bacillus* spp. are used for the industrial production of enzymes, especially proteinases (2). The pathogenic *N. circulans* strains have been implicated in multiple human infections such as septicemia, and wound and abscess infections, especially in immunocompromised individuals (3-11). In some instances, *N. circulans* infection resulted in the death of the immunocompromised patient (12). A recent report has shown that *N. circulans* can also infect immunocompetent patients, which in this incident leads to spondylodiscitis (13). Since *N. circulans* is an endospore-forming bacteria, its spores can be resistant to UV radiation and certain disinfectants which makes it a source of a contaminant in operating rooms in hospitals and it can cause pseudo-epidemics in hospitals and clinic.

N. circulans strains resistant to common antibiotics pose a threat as they can lead to the formation of

more dangerous multidrug-resistant (MDR) strains. The increased rate of the appearance of antibiotic-resistant bacterial strains is a major concern worldwide. The unregulated prescriptions of antibiotics, lack of government oversight on the self-use of antibiotics, poor hygiene along with the widespread use of antibiotics in livestock farming contributed to the dramatic rise in the appearance of antibiotic-resistant strains (14-17). It is imperative to have an infection model that can be used to evaluate antibiotic susceptibility of emerging human pathogenic bacteria that are resistant to antibiotics so that the patients can be treated efficiently.

The preferred infection model for bacteria that are pathogenic to humans is the house mouse, *Mus musculus*, however, it is cost-intensive. A major disadvantage of the large-scale use of mice as an animal model is the ethical issues. The zebrafish, *Danio rerio* has been used as an alternative vertebrate model to the house mouse for bacterial pathogenesis (18) but it has limitations in quantitative experiments where accurate injections of large volumes are required. A similar disadvantage exists in invertebrate animal models like the nematode,

Caenorhabditis elegans, and the fruit fly, *Drosophila melanogaster* (19,20). In this respect, the lepidopteran larvae can be an alternative infection model due to their relatively large body size making it easier for quantitative injection for antibiotic screening. Both the silk moth, *B. mori* (commonly called silkworm), and the wax moth, *G. mellonella* have been widely used as an infection model to study bacterial pathogenicity (21,22). These larvae can be very useful for rapid initial screening of compounds with the potential to be antimicrobials followed by confirmation in the mouse model.

Insects lack adaptive immunity but they possess innate immunity and there are remarkable similarities between insects and mammals with respect to innate immunity, antimicrobial peptide (AMP) gene expression, and Toll and Imd signaling pathways (23). When infected with a pathogen, insects mount a powerful immune response mediated by hemocytes, the fat body, the midgut, the salivary glands, and other tissues. A number of structural and functional similarities to the innate immune system have been found between insects and mammals. Because of these similarities, insects have become popular choices not only for evaluating the virulence of microbial pathogens but also for evaluating the efficacy of antimicrobial agents (24). Advantages of using insect larvae as an animal model include lack of ethical constraints, cost-effective rearing procedure, accurate injection of larger volumes to hemolymph or midgut, and easy pharmacological studies with isolated organs. Other than bacterial pathogenicity, silkworm larvae have been used as an animal model for fungal pathogenicity, exotoxin identifications, etc. (25-27). Using silkworm larvae, it has been shown that the therapeutic effect of antibiotics against *Staphylococcus aureus* can be studied (28). Recently, we have reported the therapeutic effects of antibiotics against *Escherichia coli* O157:H7 and *Klebsiella pneumoniae* in the *Bombyx* larvae infection model (29,30).

Pathogenic strains of *B. cereus* and *B. anthracis* have been reported to kill *Bombyx* and *Galleria* larvae (31-34). It has been reported that both *Bombyx* and *Galleria* larvae harbor *N. circulans* in their gut under ordinary conditions (35,36). To our knowledge, there is no report on the pathogenicity of *N. circulans* in insects. In this study, we report that a food-borne *N. circulans* strain can kill *Bombyx* larvae opening up a new way of rapid screening for unknown compounds with antibacterial properties that might be effective against antibiotic-resistant strains of this pathogen.

2. Materials and Methods

2.1. *N. circulans* isolation and culture conditions

The *N. circulans* strain was isolated from street foods in Dhaka, Bangladesh. For characterization of the strain, standard biochemical tests were carried out

(Supplementary Table S1, <http://www.ddtjournal.com/action/getSupplementalData.php?ID=138>) and for examining susceptibility to antibiotics the antimicrobial resistance (AMR) profile (Supplementary Table S2, <http://www.ddtjournal.com/action/getSupplementalData.php?ID=138>) was generated. 16SrRNA gene sequencing was carried out to confirm the identity of the isolate as *N. circulans*. Tryptic Soy Agar plates (TSA) or Tryptic Soy Broth medium (TSB) was used to culture *N. circulans* at 37°C. *E. coli* DH5 α was cultured in Luria-Bertani (LB) medium at 37°C.

2.2. Insect rearing conditions

B. mori (Nistari-M) larvae were maintained and reared in the Bangladesh Sericulture Research and Training Institute (BSRTI) using fresh mulberry leaves. As reported previously (29), larvae were kept at 25°C with ~75% relative humidity at a 16/8 hour of light/dark cycle. 5th instar feeding larvae (day 2-3) were used in all experiments. 6th instar feeding *Galleria* larvae were purchased from Ispahani Agro Ltd. (Gazipur, Dhaka, Bangladesh).

2.3. Infection of insect larvae with *N. circulans*

For injection experiments, bacteria were grown overnight, washed with phosphate-buffered saline (PBS), and suspended in PBS followed by injection into the blood (hemolymph) or midgut directly using a 1-0 mL insulin syringe (30G \times 5/16"). Overnight culture of *N. circulans* was collected by centrifugation (6,000 rpm, 5 min) and washed with PBS followed by suspension at a density of 1.53×10^{10} colony forming unit (CFU)/mL in PBS. Fifty μ L of PBS or bacteria (7.65×10^8 CFU) was injected into larvae ($n = 10$). The larvae were kept on tissue papers in Tupperware boxes with the lid partially opened. Upon prodding with tips if the larvae did not show any movement we considered them dead. For *Galleria* larvae, *N. circulans* (1.53×10^8 CFU) suspended in 10 μ L of PBS or PBS only (control) were injected as described previously (30).

2.4. PO activity assay

PO activity was measured following previously published reports (37-39) with minor modifications. Hemolymph was collected from infected larvae 12 h post-infection. One hundred μ L of bleeding buffer was added to 500 μ L of the hemolymph. Enzymatic assay was carried out at 490 nm using GloMax[®] Explorer Multimode Microplate Reader (Promega, Madison, WI, USA).

2.5. Bacterial load determination and hemocyte viability in *Bombyx* hemolymph

Bacterial load and hemocyte viability in the *Bombyx*

hemolymph after infection with *N. circulans* were determined as reported previously by our group (29,30).

2.6. RT-qPCR analysis of immune response genes

RNA was isolated from the fat body of the dorsolateral region of larvae as described previously (40) using TRIzol[®] according to the manufacturer's instructions (Invitrogen, Waltham, MA, USA). cDNA was prepared using ProtoScript[®] II First Strand cDNA Synthesis Kit (New England Biolabs, Ipswich, MA, USA) following the manufacturer's instructions. RT-qPCR was performed using Luna[®] Universal qPCR Master Mix (New England Biolabs) in a Bio-Rad C1000 Touch[™] Thermal Cycler (Bio-Rad, Hercules, CA, USA). The reference gene used for the normalization of RT-qPCR results was *Bm-rp49* (41). Primers used in this study are listed in Supplementary Table S3 (<http://www.ddtjournal.com/action/getSupplementalData.php?ID=138>). Primers for *BmToll-2* were designed with Primer 3 (<https://bioinfo.ut.ee/primer3/>) based on a previously published sequence (42). Gene expressions were quantified using the $2^{-\Delta\Delta CT}$ method.

2.7. Antibiotic susceptibility tests of *N. circulans* in vitro and in vivo

AMR profile of *N. circulans* strain (Supplementary Table S1, <http://www.ddtjournal.com/action/getSupplementalData.php?ID=138>) showed that it is resistant to clindamycin (Incepta Pharmaceuticals, Dhaka, Bangladesh), moderately sensitive to tetracycline (Sigma-Aldrich, Saint Louis, MO, USA), and sensitive to imipenem (ACI Ltd., Dhaka, Bangladesh), ceftriaxone (Radiant Pharmaceuticals, Dhaka, Bangladesh), and ampicillin (Opsonin Pharma Ltd., Dhaka, Bangladesh). In accordance with Clinical and Laboratory Standards Institute (CLSI) standards, the MICs of these five antibiotics against *N. circulans* were determined through microdilution (43) in which absorbance at 600 nm was measured in a microplate reader (GloMax[®] Explorer Multimode Microplate Reader, Promega). In order to determine the therapeutic effects of antibiotics in vivo

against *N. circulans*, *Bombyx* larvae ($n = 10$) were injected with bacteria or PBS and then injected with different antibiotic doses suspended in 50 μ L of water. The viability of larvae was monitored up to 72 hours after injection. In accordance with Hamamoto *et al.* (28), the LD₅₀ value for *N. circulans* and the ED₅₀ of antibiotics were determined.

2.8. Statistical analyses

Student's *t*-test was used for statistical analyses using GraphPad Prism 9 software.

3. Results

3.1. *N. circulans* infection through hemolymph kills larvae of *B. mori*

We tested whether the food-borne *N. circulans* strain we isolated is pathogenic by injecting it into *Bombyx* larvae via hemolymph. Upon injection with 7.65×10^8 CFU of *N. circulans* ~80% of larvae died within 24 h and 100% died within 48 h and PBS- or *Escherichia coli* DH5 α -injected larvae did not die (Figure 1A). Due to melanization, the larvae that died turned black (Figures 1B and 1C). One hundred-fold reduction of injected bacterial load resulted in the survival of 40% of larvae until 72 h and more dilution of bacteria reduced larval death even more (Supplementary Figure S1, <http://www.ddtjournal.com/action/getSupplementalData.php?ID=138>). The LD₅₀ value of the *N. circulans* strain for silkworm larvae is 6.3×10^7 CFU. These results showed that the larvae of *B. mori* can be used as infection models for studying the pathogenicity of *N. circulans*. In another infection model, *Galleria mellonella*, larvae died upon injection with *N. circulans* (Supplementary Figure S2, <http://www.ddtjournal.com/action/getSupplementalData.php?ID=138>).

3.2. *N. circulans* injection into the midgut kills *Bombyx* larvae within 96 h

In order to determine whether the oral introduction of

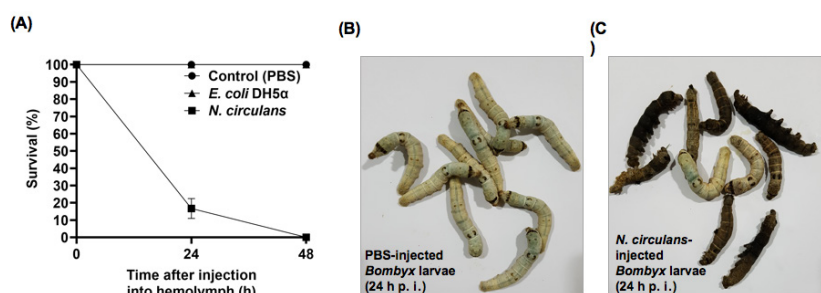


Figure 1. *N. circulans* kills larvae of *B. mori*. (A) Survival of *Bombyx* larvae ($n = 10$) upon injection with 7.65×10^8 CFU of *N. circulans* or *E. coli* DH5 α into the hemolymph. PBS was injected into the control larvae. (B, C) Images of PBS- or bacteria-injected larvae after 24 h. Increased melanization caused the blackness of the dead larval bodies. Data shown in (A) are averages of three independent experiments.

N. circulans to *Bombyx* larvae would kill them or not, bacterial suspension was spread onto mulberry leaves. However, the larvae did not show any interest in eating leaves with bacteria (data not shown). To examine whether entry of *N. circulans* through the midgut can kill larvae, we injected 7.65×10^8 CFU bacteria suspended in PBS directly into the midgut. Within 96 h post-infection, 100% of larvae were dead (Figure 2). This result further confirmed that *N. circulans* infection kills silkworm larvae.

3.3. *N. circulans* infection activates phenoloxidase (PO) activity in *Bombyx* hemolymph

In order to confirm that the blackening of the body color of *N. circulans*-infected *Bombyx* larvae was due to melanization, we measured the PO activity in the hemolymph. After *N. circulans* infection via hemolymph, the PO activity in the hemolymph was increased ~7-fold compared with that of the PBS-injected larvae (Figure 3). This result indicates that *N. circulans* infection activates PO activity in *Bombyx* hemolymph.

3.4. *N. circulans* load in *Bombyx* hemolymph increases significantly 12 h post-infection

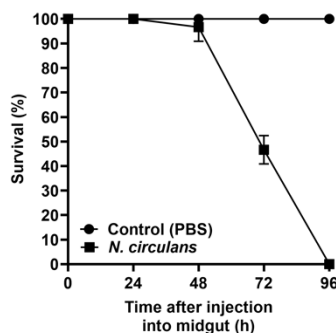


Figure 2. *N. circulans* infection through midgut kills *Bombyx* larvae. Survival of *Bombyx* larvae injected with *N. circulans* through the midgut. Larvae ($n = 10$) were injected with 7.65×10^8 CFU of *N. circulans* suspended in PBS or PBS only (control) into the midgut.

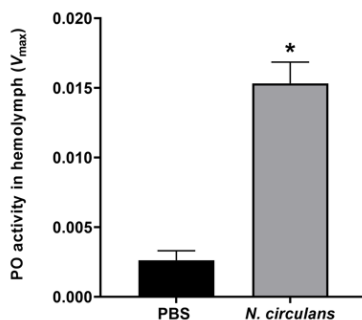


Figure 3. *N. circulans* infection of *Bombyx* larvae increases phenoloxidase (PO) activity in the hemolymph. PO activity after 12 h of injection of PBS or *N. circulans* into the hemolymph (* p -value: 0.0086).

We collected hemolymph after 6, 12, and 18 h post-injection with 7.65×10^8 CFU of *N. circulans* in order to determine bacterial load. After 6 hours of infection, the hemolymph bacterial count slightly increased, and after 12 h the increase in bacterial load was very significant (Figure 4).

3.5. Reduction of hemocyte number after *N. circulans* infection of *Bombyx* larvae

The infection of the host by bacteria leads to cell death. Hemolymph samples were collected 6 and 12 hours after *N. circulans* injection to examine hemocyte viability in silkworm larvae. After 12 h of bacterial injection, ~52% of hemocytes died (Figure 5). These results indicate that *N. circulans* induces cell death in *Bombyx* larvae.

3.6. *N. circulans* upregulates *Bmdefensin-B*, *Bmgloverin-3*, and *BmToll-2* genes in *Bombyx* fat body

AMPs play important roles in host defense to fend off invading pathogens. Among the AMP genes whose expressions were examined by RT-qPCR, we found that the expression of *Bmdefensin-B* and *Bmgloverin-3* were increased by more than two-fold in the larval fat body upon infection with *N. circulans* compared with the PBS-

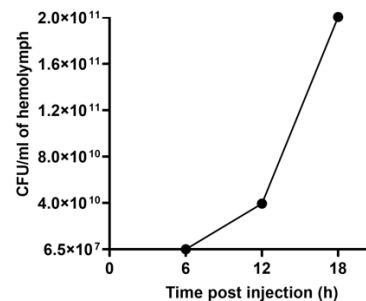


Figure 4. The proliferation of *N. circulans* in the hemolymph of *Bombyx* larvae after injection of 7.65×10^8 CFU. The data shown are averages of three independent experiments.

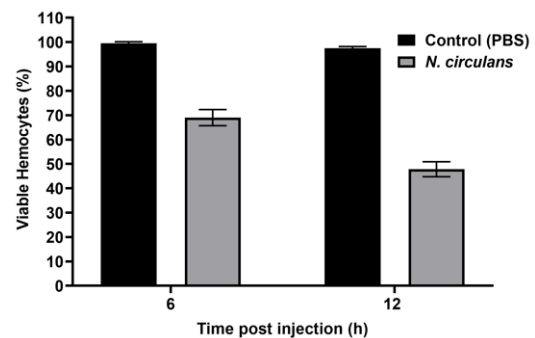


Figure 5. Reduction of hemocyte viability in the hemolymph *Bombyx* larvae upon injection with 7.65×10^8 CFU of *N. circulans*. PBS-injected larvae were used as a control. The data shown are averages of three independent experiments.

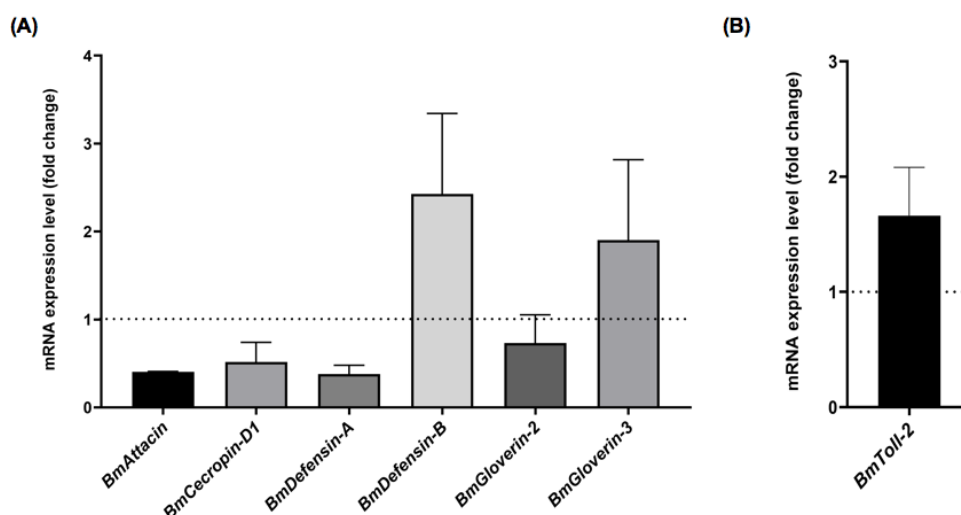


Figure 6. Upregulation of *Bmdefensin-B*, *Bmgloverin-3*, and *BmToll-2* in the *Bombyx* larval fat body. After injecting 7.65×10^8 CFU of *N. circulans* or PBS (control) fat body tissues were isolated after 6 h. The reference gene used for normalization was *Bmrp49*. The dashed line represents an expression level of 1.00. The data shown are from three independent experiments.

injected (control) larvae (Figure 6A). No upregulation was observed for *Bmattacin*, *Bmcecropin-D1*, *Bmdefensin-A*, *Bmgloverin-2*. Overexpression of *BmToll-2* in cultured *Bombyx* cells can upregulate *defensin* genes (44), and in this study, we examined *BmToll-2* expression after *N. circulans* infection. We observed ~1.6-fold upregulation in the larval fat body (Figure 6B). Our findings show that infection with *N. circulans* upregulates *Bmdefensin-B*, *Bmgloverin-3*, and *BmToll-2* in *Bombyx* larval fat body.

3.7. Antibiotics protect *Bombyx* larvae from *N. circulans*-induced death

In our next experiment, we examined the antibiotic susceptibility of the *N. circulans* strain. On the basis of the AMR profile (Supplementary Table S2, <http://www.ddtjournal.com/action/getSupplementalData.php?ID=138>) and the minimum inhibitory concentrations (MICs) of the antibiotics tested (Table 1), the *N. circulans* strain is resistant to clindamycin, moderately sensitive to tetracycline, and sensitive to imipenem, ceftriaxone, and ampicillin in accordance with the CLSI standards (43,45). To determine the efficacy of antibiotics against *N. circulans* in *Bombyx* larvae, we injected antibiotics at different doses into larvae after *N. circulans* infection. We found that all five antibiotics showed varying degrees of therapeutic effect against *N. circulans*. For 90-100% survival, 10 μ g per larva was sufficient for tetracycline and ceftriaxone whereas 100 μ g per larva was required for ampicillin and imipenem to observe 100% rescue from *N. circulans*-induced death (Figure 7A). Table 1 shows the ED₅₀ values of the antibiotics used. The antibiotics significantly reduced *N. circulans*-induced melanization of the larvae (Figure 7B). The results suggest that *Bombyx* larvae could be

Table 1. MIC of antibiotics against *N. circulans* and ED₅₀ of antibiotics in *Bombyx* larvae against *N. circulans*

| Antibiotics | MIC (μ g/mL) | ED ₅₀ (μ g per g of larva) |
|--------------|-------------------|--|
| Ampicillin | 0.781 | 1.29 |
| Ceftriaxone | 3.12 | 0.0131 |
| Tetracycline | 12.5 | 0.103 |
| Imipenem | ≤ 1.25 | 0.158 |
| Clindamycin | > 1024 | 32.8 |

used to study the therapeutic effects of antibiotics against *N. circulans*.

4. Discussion

Our study showed that both *B. mori* and *G. mellonella* larvae can be killed by *N. circulans* infection. Moreover, we have observed that antibiotics have a therapeutic effect on silk moth larvae. The results show that these larvae are an excellent animal model for studying the pathogenicity of *N. circulans* and could potentially be used for identifying novel antibiotics that are effective against strains of this bacterium that are highly resistant to known antibiotics, which can be confirmed by testing the candidate antibiotics on mice.

Our observations that an *N. circulans* strain isolated from street food can kill larvae of both silk moth and wax moth indicated that the strain is pathogenic to these insects. Similar to earlier studies about increased melanization after infection with bacteria (21), we found that the *N. circulans*-infected insect larvae also turned black (Figure 1). Our attempts to infect *Bombyx* larvae by feeding mulberry leaves with *N. circulans* failed (data not shown) whereas midgut-injection of *N. circulans* killed *Bombyx* larvae within 96 h (Figure 2). It is possible that the spreading of *N. circulans* on the mulberry

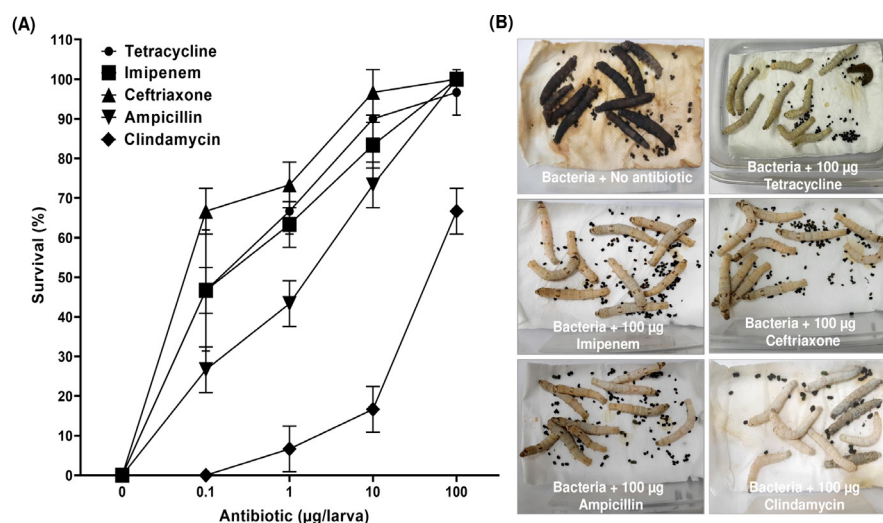


Figure 7. Antibiotics showed therapeutic effects against *N. circulans* in *Bombyx* larvae. (A) Larvae ($n = 10$) were injected with 7.65×10^8 CFU followed by injection of antibiotics at the indicated doses. Survival was counted after 48 h of injection. The data shown are averages of three independent experiments. (B) Images of bacteria-injected larvae with or without antibiotics after 48 h of injection.

leaves resulted in the production of an unpleasant smell that prevented the larvae from consuming it and we reported a similar observation for *E. coli* O157:H7 (29). It is known that larvae of Lepidoptera turned black in response to exposure to pathogens by producing melanin upon activation of hemolymph phenoloxidase to destroy it (46) and, as expected, the PO activity in *Bombyx* larvae was increased after *N. circulans* infection (Figure 3). Culture-filtrate of *S. aureus* or *P. aeruginosa* can kill silkworm larvae after hemolymph injection (27) but in this study, we found that the culture-filtrate of *N. circulans* did not kill any silkworm larvae within 24 h, although they appeared sick with very little movement upon touching (data not shown). It is possible that the food-borne *N. circulans* strain we used in this study is not a highly virulent strain or it did not produce enough exotoxins to kill larvae.

Our data showed that the number of circulating *N. circulans* in *Bombyx* hemolymph continued to increase until 18 h post-infection (Figure 4). It would be interesting to know whether there are any preferred silkworm organs that are infected by *N. circulans* which would shed light on its mechanism of action. Localization of a GFP-expressing *N. circulans* strain inside the larval body would be very useful. Similar to *Serratia marcescens*-induced hemocyte death in *Bombyx* larvae (47), we have also observed a reduction of viable hemocytes upon *N. circulans* infection (Figure 5), although it remains to be examined whether the cell death is due to apoptosis or not.

AMP genes are upregulated during bacterial infection to destroy the invader without affecting the host cells (48). Infection with *Bacillus bombysepticus* resulted in the upregulation of a number of AMPs including gloverin, attacin, moricin *etc.* (49). After *N. circulans* infection of *Bombyx* larvae, we have observed upregulation of *Bmdefensin-B* and *Bmgloverin-3* among the AMP

genes whose expressions were examined, although no increase of gene expression was observed for *Bmattacin*, *Bmcecropin-D1*, *Bmdefensin-A*, and *Bmgloverin-2* (Figure 6A). *BmToll-2* has been shown to upregulate AMP genes in *Bombyx* cultured cells *in vitro* (44) and we also found upregulation of *BmToll-2* after *N. circulans* infection of *Bombyx* larvae (Figure 6B). Loss-of-function mutant of *BmToll-2* would be useful to examine whether *N. circulans*-induced upregulation of *Bmdefensin-B* and *Bmgloverin-2* is *BmToll-2* dependent or not.

Therapeutic effects of antibiotics in *Bombyx* larvae against pathogenic bacteria like *S. aureus* have been reported (28). Recently, we have also reported such effects against *E. coli* O157:H7 and *K. pneumoniae* (29,30). Our data revealed that *Bombyx* larvae can also be used to examine the therapeutic effect of antibiotics against *N. circulans*. *In vitro*, *N. circulans* showed susceptibility to ampicillin, ceftriaxone, and imipenem, moderate sensitivity to tetracycline, and resistance to clindamycin (Table 1, Supplementary Table S2, <http://www.ddtjournal.com/action/getSupplementalData.php?ID=138>). However, *in vivo* experiments revealed that all these five antibiotics protected silkworm larvae from *N. circulans*-induced death with varying efficacies (Figure 7). Interestingly, clindamycin, against which *N. circulans* showed resistance *in vitro*, rescued ~70% of larvae *in vivo*. Such a lack of correlation between *in vitro* and *in vivo* antibiotic susceptibility data of bacteria are common (50) and recently, we have also reported such discrepancies with *E. coli* O157:H7 and *K. pneumoniae* using *Bombyx* larvae infection model (29,30). These findings strengthen the notion that for testing antibiotic susceptibility tests of pathogenic bacteria appropriate infection models should be used rather than relying solely on *in vitro* data. The antimicrobial effect of medicinal plant extracts in silkworm larvae against *N. circulans* is currently under investigation. By rapidly

screening chemicals with antimicrobial properties against pathogens using *Bombyx* larvae as an animal model, we will be better equipped to combat the ever-increasing number of multidrug-resistant bacteria.

Funding: This work was supported by a North South University grant, NSU-RP-18-044 to MSH.

Conflict of Interest: The authors have no conflicts of interest to disclose.

References

- Gupta RS, Patel S, Saini N, Chen S. Robust demarcation of 17 distinct *Bacillus* species clades, proposed as novel Bacillaceae genera, by phylogenomics and comparative genomic analyses: description of *Robertmurraya kyonggiensis* sp. nov. and proposal for an emended genus *Bacillus* limiting it only to the members of the Subtilis and Cereus clades of species. *Int J Syst Evol Microbiol.* 2020; 70:5753-5798.
- Danilova I, Sharipova M. The practical potential of Bacilli and their enzymes for industrial production. *Front Microbiol.* 2020; 11:1782.
- Boyett DP, Rights FL. Heretofore undescribed aerobic spore forming *Bacillus* in child with meningitis. *J Am Med Assoc.* 1952; 148:1223-1224.
- Logan NA, Old DC, Dick HM. Isolation of *Bacillus circulans* from a wound infection. *J Clin Pathol.* 1985; 38:838-839.
- Wilde AH, Ruth JT. Two-stage reimplantation in infected total knee arthroplasty. *Clin Orthop Relat Res.* 1988; 236:23-35.
- Gatermann S, Mitusch R, Djonlagic H, Hollandt H, Marre R. Endocarditis caused by *Bacillus circulans*. *Infection.* 199; 19:445.
- Castagnola E, Conte M, Venzano P, Garaventa A, Viscoli C, Barretta MA, Pescetto L, Tasso L, Nantron M, Milanaccio C, Giacchino R. Broviac catheter-related bacteraemias due to unusual pathogens in children with cancer: Case reports with literature review. 1997; 34:215-218.
- Krause A, Gould FK, Forty J. Prosthetic heart valve endocarditis caused by *Bacillus circulans*. *J Infect.* 1999; 39:160-162.
- Tandon A, Tay-Kearney ML, Metcalf C, McAllister L. *Bacillus circulans* endophthalmitis. *Clin Exp Ophthalmol.* 2001; 29:92-93.
- Berry N, Hassan I, Majumdar S, Vardhan A, McEwen A, Gokal R. *Bacillus circulans* peritonitis in a patient treated with CAPD. *Perit Dial Int.* 2004; 24:488-489.
- Sanyal SK, Karmaker M, Sultana M, Hossain MA. Association of *Bacillus circulans* with non-diabetic foot infection in Bangladeshi patient. *Indian J Med Microbiol.* 2015; 33:606-608.
- Alebouyeh M, Gooran OP, Azimi-Rad M, Tajbaksh M, Tajeddin E, Sherafat SJ, Mojarad EN, Zali Mr. Fatal sepsis by *Bacillus circulans* in an immunocompromised patient. *Iran J Microbiol.* 2011; 3:156-158.
- Russo A, Tarantino U, d'Ettore G, Rocca CD, Ceccarelli G, Gasbarra E, Vendetti M, Iundusi R. First report of spondylodiscitis caused by *Bacillus circulans* in an immunocompetent patient: Clinical case and review of the literature. *IDCases.* 2021; 23:e01058.
- Van Boeckel TP, Pires J, Silvester R, Zhao C, Song J, Criscuolo NG, Gilbert M, Bonhoeffer S, Laxminarayan R. Global trends in antimicrobial resistance in animals in low- And middle-income countries. *Science.* 2019; 365:eaaw1944.
- Duval RE, Grare M, Demoré B. Fight against antimicrobial resistance: We always need new antibacterials but for right bacteria. *Molecules.* 2019; 24:3152.
- WHO. Antimicrobial resistance. Global report on surveillance. 2014.
- da Cunha BR, Fonseca LP, Calado CRC. Antibiotic discovery: Where have we come from, where do we go? *Antibiotics.* 2019; 8:45.
- van der Sar AM, Appelmelk BJ, Vandenbroucke-Grauls CMJE, Bitter W. A star with stripes: Zebrafish as an infection model. *Trends Microbiol.* 2004; 12:451-457.
- Ermolaeva MA, Schumacher B. Insights from the worm: The *C. elegans* model for innate immunity. *Semin Immunol.* 2014; 26:303-309.
- Bergman P, Seyedoleslami Esfahani S, Engström Y. *Drosophila* as a model for human diseases-Focus on innate immunity in barrier epithelia. *Curr Top Dev Biol.* 2017; 121:29-81.
- Kaito C, Sekimizu K. A silkworm model of pathogenic bacterial infection. *Drug Discov Ther.* 2007; 1:89-93.
- Menard G, Roullion A, Cattoir V, Donnio PY. *Galleria mellonella* as a suitable model of bacterial infection: Past, present and future. *Front Cell Infect Microbiol.* 2021; 11:782733.
- Sheehan G, Garvey A, Croke M, Kavanagh K. Innate humoral immune defences in mammals and insects: The same, with differences? *Virulence.* 2018; 9:1625-1639.
- Panthee S, Paudel A, Hamamoto H, Sekimizu K. Advantages of the silkworm as an animal model for developing novel antimicrobial agents. *Front Microbiol.* 2017; 8:373.
- Kaito C, Akimitsu N, Watanabe H, Sekimizu K. Silkworm larvae as an animal model of bacterial infection pathogenic to humans. *Microb Pathog.* 2002; 32:183-190.
- Matsumoto Y, Sekimizu K. Silkworm as an experimental animal for research on fungal infections. *Microbiol Immunol.* 2019; 63:41-50.
- Hossain MS, Hamamoto H, Matsumoto Y, Razanajatovo IM, Larranaga J, Kaito C, Kasuga H, Sekimizu K. Use of silkworm larvae to study pathogenic bacterial toxins. *J Biochem.* 2006; 140:439-444.
- Hamamoto H, Kurokawa K, Kaito C, Kamura K, Razanajatovo IM, Kusuhara H, Santa T, Sekimizu K. Quantitative evaluation of the therapeutic effects of antibiotics using silkworms infected with human pathogenic microorganisms. *Antimicrob Agents Chemother.* 2004; 48:774-779.
- Ahad II, Hossain MM, Uddin MA, Bari ML, Hossain MS. Therapeutic effect of antibiotics against *Escherichia coli* O157:H7 in silk moth larvae animal model. *Curr Microbiol.* 2020; 77:2172-2180.
- Tuba T, Chowdhury FR, Hossain T, Farzana M, Ahad II, Hossain MM, Hossain MI, Saleh NUA, Nawaar N, Uddin MA, Bari ML, Hossain MS. *Klebsiella pneumoniae* pathogenicity in silk moth larvae infection model. *FEMS Microbiol Lett.* 2022; 368:fnab159.
- Dong X, Lü P, Cao W, Zhang C, Zhu F, Meng X, Nie Z, Lu S, Chen K. Study of the toxicity of *Bacillus cereus*

- on silkworm (*Bombyx mori*) and the relevant proteome. *Invert Surv J*. 2017; 14:129-139.
32. Doll VM, Ehling-Schulz M, Vogelmann R. Concerted action of sphingomyelinase and non-hemolytic enterotoxin in pathogenic *Bacillus cereus*. *PLoS One*. 2013; 8:e61404.
 33. Paudel A, Furuta Y, Higashi H. Silkworm model for *Bacillus anthracis* infection and virulence determination. *Virulence*. 2021; 12:2285-2295.
 34. Malmquist JA, Rogan MR, McGillivray SM. *Galleria mellonella* as an infection model for *Bacillus anthracis* Sterne. *Front Cell Infect Microbiol*. 2019; 9:360.
 35. Anand AAP, Vennison SJ, Sankar SW, Prabhu DIG, Vasanth PT, Raghuraman T, Geoffrey CJ, Vendan SE. Isolation and characterization of bacteria from the gut of *Bombyx mori* that degrade cellulose, xylan, pectin and starch and their impact on digestion. *J Insect Sci*. 2010; 10:107.
 36. Saikia SS, Borah BK, Baruah G, Rokozeno, Deka MK. Characterization of the gut microbes of greater wax moth (*Galleria mellonella* Linnaeus) shows presence of potential polymer degraders. *Folia Microbiol (Praha)*. 2022; 67:133-141.
 37. Sadd B, Holman L, Armitage H, Lock F, Marland R, Siva-Jothy MT. Modulation of sexual signalling by immune challenged male mealworm beetles (*Tenebrio molitor*, L.): evidence for terminal investment and dishonesty. *J Evol Biol*. 2006; 19:321-325.
 38. Tabunoki H, Dittmer NT, Gorman MJ, Kanost MR. Development of a new method for collecting hemolymph and measuring phenoloxidase activity in *Tribolium castaneum*. *BMC Res Notes*. 2019; 12:7.
 39. Ramirez JL, Muturi EJ, Dunlap C, Rooney AP. Strain-specific pathogenicity and subversion of phenoloxidase activity in the mosquito *Aedes aegypti* by members of the fungal entomopathogenic genus *Isaria*. *Sci Rep*. 2018; 8:9896.
 40. Hossain MS, Li Y, Zhou S, Li K, Tian L, Li S. 20-Hydroxyecdysone-induced transcriptional activity of FoxO upregulates *brummer* and *acid lipase-1* and promotes lipolysis in *Bombyx* fat body. *Insect Biochem Mol Biol*. 2013; 43:829-838.
 41. Tsubota T, Uchino K, Suzuki TK, Tanaka H, Kayukawa T, Shinoda T, Sezutsu H. Identification of a novel strong and ubiquitous promoter/enhancer in the silkworm *Bombyx mori*. *G3 (Bethesda)*. 2014; 4:1347-1357.
 42. Cheng TC, Zhang YL, Liu C, Xu PZ, Gao ZH, Xia QY, Xiang ZH. Identification and analysis of Toll-related genes in the domesticated silkworm, *Bombyx mori*. *Dev Comp Immunol*. 2008; 32:464-475.
 43. CLSI. Methods for dilution antimicrobial susceptibility tests for bacteria that grow aerobically. 11th ed. CLSI standards M07. Wayne, PA Clin Lab Stand Inst 2018.
 44. Wang XY, Li T, Johannes M, Xu JP, Sun X, Qin S, Xu PZ, Li MW, Wu YC. The regulation of *cecropin-A* and *gloverin 2* by the silkworm Toll-like gene 18 wheeler in immune response. *J Invertebr Pathol*. 2019; 164:49-58.
 45. CLSI. M45. Methods for antimicrobial dilution and disk susceptibility testing of infrequently isolated or fastidious bacteria ; Proposed Guideline. 2015.
 46. Cerenius L, Lee BL, Soderhall K. The pro-PO system: pros and cons of its role in invertebrate immunity. *Trends Immunol*. 2008; 29:263-271.
 47. Ishii K, Adachi T, Imamura K, Takano S, Usui K, Suzuki K, Hamamoto H, Watanabe T, Sekimizu K. *Serratia marcescens* induces apoptotic cell death in host immune cells via a lipopolysaccharide- and flagella-dependent mechanism. *J Biol Chem*. 2012; 287:36582-36592.
 48. Nesa J, Sadat A, Buccini DF, Kati A, Mandal AK, Franco OL. Antimicrobial peptides from *Bombyx mori*: a splendid immune defense response in silkworms. *RSC Adv*. 2020; 10:512-523.
 49. Huang L, Cheng T, Xu P, Cheng D, Fang T, Xia Q. A genome-wide survey for host-response of silkworm, *Bombyx mori* during pathogen *Bacillus bombysepticus* infection. *PLoS One*. 2009; 4:e8098.
 50. Zak O, Tosch W, Sande MA. Correlation of antibacterial activities of antibiotics *in vitro* and in animal models of infection. *J Antimicrob Chemotherap*. 1982; 15:273-282.
 51. Tanaka H, Furukawa S, Nakazawa H, Sagisaka A, Yamakawa M. Regulation of gene expression of attacin, an antimicrobial protein in the silkworm, *Bombyx mori*. *J Insect Biotechnol Sericol*. 2005; 74:45-56.
 52. Kaneko Y, Tanaka H, Ishibashi J, Iwasaki T, Yamakawa M. Gene expression of a novel *defensin* antimicrobial peptide in the silkworm, *Bombyx mori*. *Biosci Biotechnol Biochem*. 2008; 72:2353-2361.
 53. Zhang J, Yang W, Xu J, Yang W, Li Q, Zhong Y, Cao Y, Yu XQ, Deng X. Regulation of antimicrobial peptide genes via insulin-like signaling pathway in the silkworm *Bombyx mori*. *Insect Biochem Mol Biol*. 2018; 103:12-21.
 54. Geng T, Huang Y, Hou C, Qin G, Lv D, Guo X. Inductive expression patterns of genes related to Toll signaling pathway in silkworm (*Bombyx mori*) upon *Beauveria bassiana* infection. *J Asia Pac Entomol*. 2016; 19:861-868.
 55. Ma L, Zhou L, Lin J, Ji J, Wang Y, Jiang H, Shen X, Lu Z. Manipulation of the silkworm immune system by a metalloprotease from the pathogenic bacterium *Pseudomonas aeruginosa*. *Dev Comp Immunol*. 2019; 90:176-185.
- Received December 3, 2022; Revised February 17, 2023; Accepted February 25, 2023.
- *Address correspondence to: Muktadir S. Hossain, Department of Biochemistry and Microbiology, North South University, Plot 15, Block B, Bashundhara, Dhaka 1229, Bangladesh.
- Released online in J-STAGE as advance publication February 27, 2023.

ENST00000438158 aids ultrasound for predicting lymph node metastasis and inhibits migration and invasion of papillary thyroid carcinoma cells

Hui Liu^{1,§}, Yixin Shi^{1,§}, Jia Zhan¹, Yingchun Liu¹, Jing Zhou^{2,3,4}, Biao Su¹, Yue Chen¹, Ling Wang^{2,3,4,*}, Lin Chen^{1,*}

¹Department of Ultrasound, Huadong Hospital, Fudan University, Shanghai, China;

²Laboratory for Reproductive Immunology, Obstetrics and Gynecology Hospital of Fudan University, Shanghai, China;

³The Academy of Integrative Medicine of Fudan University, Shanghai, China;

⁴Shanghai Key Laboratory of Female Reproductive Endocrine-related Diseases, Shanghai, China.

SUMMARY Cervical lymph node metastasis (CLNM) of papillary thyroid carcinoma (PTC) is directly associated with clinical management and prognosis. In this study, we aimed to evaluate the value of conventional ultrasound (US) combined with ENST00000438158 in predicting CLNM of PTC. Forty-nine PTC patients underwent US examination and US-guided fine needle aspiration (FNA). ENST00000438158 expression in FNA cytological specimens and PTC cell lines was detected using real-time reverse transcription polymerase chain reaction (qRT-PCR). The role of ENST00000438158 expression in the proliferation, migration, invasion, apoptosis, and cell cycle of PTC cells was investigated by Cell Counting Kit-8 (CCK8) and clone formation experiments, transwell assay, and flow cytometry, respectively. Calcification, capsule contact, and low ENST00000438158 expression were independently associated with PTC with CLNM (all $p < 0.05$). The combination of multiple US features was more valuable than a single US feature in predicting CLNM in PTC. Adding ENST00000438158 to US greatly improved the value of differentiation of PTC with or without CLNM. In conclusion, ENST00000438158 is a potential molecular marker for predicting CLNM in PTC. ENST00000438158 combined with US features is highly valuable for predicting CLNM in PTC.

Keywords Ultrasound, papillary thyroid carcinoma, ENST00000438158, cervical lymph node metastasis

1. Introduction

Thyroid cancer is the most frequent endocrine gland malignancy, and its incidence has been increasing substantially over the past few decades. It is predicted to become the fourth most malignant tumor by 2030 in the United States (1,2). In most thyroid cancers, papillary thyroid carcinoma (PTC) has less distant metastasis and a good prognosis (3-6). However, there are still a few PTC that develop rapidly, with high invasion, local recurrence, and early distant metastasis (7,8). Clinical studies have shown that the incidence of cervical lymph node metastasis (CLNM) in the central and lateral cervical compartment was 12-81% and 3.1-65.4%, respectively. Follow-up results after surgery showed that recurrence and metastasis rates were more than 30%. Therefore, CLNM in PTC is directly related to its management and prognosis (9,10).

In recent years, preventive lymph node dissection has not reduced the local recurrence rate of PTC but has increased the size of the surgical wound, probability of parathyroid injury, recurrent laryngeal nerve injury, and other complications. Therefore, many studies have recommended preventive central lymph node dissection only for PTC with CLNM confirmed before surgery (11). Thus, there is an urgent need to develop an accurate and efficient method for predicting CLNM of PTC. Ultrasound (US) is convenient, radiation-free, and inexpensive, making it the preferred method for the detection of CLNM in PTC. Metastatic lymph nodes are commonly characterized by a round shape, absence of an echogenic hilum, hyperechogenicity, microcalcifications, cystic changes, and peripheral vascularity (11). A previous meta-analysis reported that the sensitivity of US for central CLNM was only 33%, of which approximately 70% refer to lateral CLNM (12).

Previous studies indicated that US missed 33-90% of CLNM in PTC patients (13,14). Therefore, in order to improve the level of scientific decision-making for PTC surgery, instead of directly detecting cervical lymph nodes, we focused on the US features of PTC to predict CLNM.

In recent years, molecular markers have become a hot topic in cancer research (15,16). Among them, long noncoding RNA (lncRNAs) *i.e.*, noncoding RNA of more than 200 nucleotides in length are considered key regulators of the occurrence and inhibition of many cancers (17-19). lncRNAs play a role in cell biological processes, such as cell differentiation, migration, and invasion, especially in cancers (20-22). For example, upregulation of the expression level of lncRNA NONHSAT129183 promoted proliferation, migration, and invasion in PTC cell lines (23). High expression of ENST00000606790.1 was strongly correlated with aggressive clinicopathological characteristics of PTC (24). On the other hand, lncRNA expression was negatively associated with poor prognosis of thyroid cancer, such as lncRNA GAS5 and lncRNA MEG3 (25,26).

The lncRNA ENST0000438158 is located on the antisense strand of chromosome 1, with a length of 562 bp, and contains three gene exons, playing the role of enhancer to affect gene expression nearby. Studies have reported that the expression of lncRNA ENST0000438158 is significantly higher in colon cancer tissues than in normal tissues, and its dysregulation is involved in the complicated process of colon cancer development (27). Xie *et al.* (28) indicated that ENST0000438158 was the target of miR-223-5p, and that miR-223-5p/ENST0000438158 was differentially expressed in osteosarcoma lung metastasis by constructing a competitive endogenous RNA network related to lung metastasis. However, the role of ENST0000438158 in PTC remains unclear. Therefore, ENST0000438158 was selected as the research object in this study to investigate its use as an auxiliary molecular marker to predict CLNM in PTC together with US.

2. Materials and Methods

2.1. Patients

The Ethics Committee of Huadong Hospital authorized this study. The ethical considerations for the study followed the principles of the Declaration of Helsinki. A total of 49 thyroid nodules from 49 consecutive patients (35 women and 14 men) were included in this study from June 2018 to December 2019. All patients were well-informed, and informed consent was obtained before the examination. The inclusion criteria were as follows: (a) patients who underwent US examination and US-guided fine-needle aspiration

(FNA) before subtotal or total thyroidectomy; (b) nodules pathologically confirmed as PTC; and (c) patients who underwent lymph node resection. Nodules with the following criteria were excluded: (a) unclear US images, (b) insufficient puncture specimens to obtain adequate RNA, and (c) preoperative radiotherapy or chemotherapy.

2.2. Image examination

An Aplio 500 (Canon Medical Systems, Otawara, Japan) equipped with a linear array probe (14L5 probe, 5-14 MHz) was used. US imaging was performed by two radiologists with extensive experience in thyroid US diagnosis, both blinded to all histologic information and clinical history. Thyroid tumors were evaluated for internal architecture (mostly solid, solid), echogenicity (isoechoic, hypoechoic, marked hypoechoic), margin (regular, irregular), shape (wider than tall, taller than wide), calcification (none or macro, micro), peripheral halo (absent, present), capsular invasion (absent, present), and blood flow (none, low, high). In US findings, capsular invasion was defined as greater than 25% of capsule contact between thyroid nodule and capsule, obvious loss of the echogenic capsule line, or invasion of the surrounding soft tissue (29,30).

2.3. Specimen collection

All patients underwent US-guided FNA with a 22-gauge needle by the same radiologists who had performed the US examination previously. Aspiration was performed at least three times. Cytological tissue from the first two aspiration samples was smeared on glass slides, immediately placed in 95% alcohol, and stained for hematoxylin-eosin staining. Cytological tissue from the last aspiration was eluted with normal saline and immediately frozen in -80°C liquid nitrogen.

2.4. Cell culture and transfection

The human PTC cell lines (B-CPAP and KTC-1) were obtained from the Chinese Academy of Sciences Committee on Type Culture Collection Cell Bank (Shanghai, China). Two cell lines were cultured in RPMI-1640 medium (Gibco, Australia) supplemented with 10% of fetal bovine serum (FBS) (Gibco, Australia) and incubated at 37°C in a constant temperature incubator.

ENST00000438158 overexpression plasmid was used to upregulate ENST00000438158 expression. Small interfering RNAs (siRNAs) were obtained from GenePharma Co., Ltd. (Shanghai, China) to downregulate ENST00000438158 expression. Transfection was conducted using Lipofectamine 2000 test agent (Invitrogen, Carlsbad, CA, USA), according to the manufacturer's instructions.

2.5. Real-time quantitative PCR assays

TRIzol reagent (Invitrogen, Carlsbad, CA, USA) was used to extract total RNA from clinical tissue samples and transfected cells, according to the manufacturer's instructions. Quantitative reverse transcription polymerase chain reaction (qRT-PCR) was performed using the ChamQ Universal SYBR qPCR Master Mix (Vazyme, Nanjing, China). The relative expression levels of ENST00000438158 were calculated using the $2^{-\Delta\Delta Ct}$ method which was normalized to GAPDH.

2.6. CCK8 assay and plate clone formation assay

Cell Counting Kit-8 (CCK8; Beyotime Biotechnology, Jiangsu, China) was used to analyze the proliferation capacity of the cells. Absorbance of different time points at 450 nm was measured using a microplate reader according to which the proliferation ability curve of B-CPAP and KTC-1 cells was generated.

The effect of ENST00000438158 on PTC cell proliferation was further confirmed using a plate clone formation assay. The cells were seeded into six-well plates at a density of 500 cells/well. The medium was replaced every two days. On the tenth day, the medium was discarded. The cells were stained with crystal violet at room temperature and photographed.

2.7. Transwell assay

Transwell chambers (Corning, NY, USA) were used to determine cell migration and invasion. Matrigel was placed at the bottom of the upper chamber for invasion assay. Complete medium (500 μ L) was added to the lower chamber, and 5×10^4 cells resuspended in a suitable medium with free serum were added to the upper chamber. After 24 h incubation, the cells from the upper chamber were removed. Cells that migrated or invaded the bottom surface of the membrane were stained with crystal violet, observed under a light microscope, and photographed.

2.8. Flow cytometry

The cell apoptosis assay was conducted using the Annexin V Apoptosis Detection Kit FITC (Invitrogen, NY, USA). Cell cycle analysis was performed using a Cell Cycle and Apoptosis Analysis Kit (Beyotime Biotechnology, Jiangsu, China). Cell apoptosis assay and cell cycle analysis were performed according to the manufacturer's protocol. Cell apoptosis and the cell cycle were analyzed using a Gallios Flow Cytometer (Beckman Coulter, USA) and FlowJo software.

2.9. Statistical analysis

Continuous variables are presented as mean values \pm

standard deviation (SD), and were compared using an independent two-sample *t*-test. Categorical variables were described as rate or frequency and compared the χ^2 -test. Multivariate logistic analysis was used to analyze the significant variables in the univariate analysis. Based on pathological diagnosis, a receiver operating characteristic (ROC) curve was drawn to obtain the area under the curve (AUC), sensitivity, and specificity. The diagnostic effectiveness of the different methods was analyzed using the *z*-test.

All statistical analyses were performed using Statistical Product and Service Solutions (SPSS) 25.0 software and GraphPad Prism software (version 8.0). Differences were considered statistically significant at $p < 0.05$.

3. Results

3.1. Clinical and US Characteristics of patients

According to the pathological results, 18 and 31 patients were in the CLNM+ (PTC with CLNM) and CLNM- (PTC without CLNM) group. As shown in Table 1, sex, size, calcification, and capsule contact were significantly related to CLNM in PTC (all $p < 0.05$) (Figures 1A-1D). However, no significant differences were found in age, location, multifocality, diffuse lesions, extra-thyroid extension, internal architecture, echogenicity, margin, shape, halo, and blood between the two groups (all $p > 0.05$). Calcification (OR = 7.398) and capsule contact (OR = 6.749) were independent predictors of CLNM of PTC in the multivariate logistic regression analysis (both $p < 0.05$) (Table 2).

3.2. The expression of ENST0000438158 in FNA cytological specimen and PTC cell lines

The expression of ENST00000438158 differed significantly between the CLNM- and CLNM+ groups, with lower ENST00000438158 expression in the CLNM+ group ($p = 0.035$) (Figure 2A). In the PTC cell line, the expression of ENST00000438158 was significantly higher than that of KTC-1 in B-CPAP cells (Figure 2B). Therefore, KTC-1 was selected for the overexpression experiment, and B-CPAP was selected for the low expression test (Figures 2C-2D). To investigate the significance of ENST0000438158 expression in PTC with CLNM, receiver operator characteristic (ROC) was used to calculate the cutoff value of ENST0000438158 expression (Figure 2E). According to the best cut-off value of $\Delta Ct = 43.71$, 29 and 20 patients were in the low ($\Delta Ct < 43.71$) and high expression group ($\Delta Ct > 43.71$), respectively. ENST0000438158 expression was correlated with PTC accompanied by CLNM ($p = 0.009$) (Figures 1A-1D). However, ENST0000438158 expression was not associated with sex, age, location, size, multifocality, diffuse lesion, extrathyroidal

Table 1. Clinicopathological characteristics and ultrasound characteristics of CLNM in PTC

| Variable | n | CLNM+, n (%) | CLNM-, n (%) | p value |
|-------------------------|-----------|--------------|--------------|---------|
| Sex | | | | 0.001 |
| Male | 14 (28.6) | 10 (55.6) | 4 (12.9) | |
| Female | 35 (71.4) | 8 (44.4) | 27 (87.1) | |
| Age | | | | 0.095 |
| > 45 | 24 (49.0) | 6 (33.3) | 18 (58.1) | |
| ≤ 45 | 25 (51.0) | 12 (66.7) | 13 (41.9) | |
| Tumor location | | | | 0.108 |
| Left | 20 (40.8) | 4 (22.2) | 16 (51.6) | |
| Right | 26 (53.1) | 12 (66.7) | 14 (45.2) | |
| Isthmus | 3 (6.1) | 2 (11.1) | 1 (3.2) | |
| Tumor size (mm) | | | | 0.048 |
| ≤ 10 | 33 (67.3) | 9 (50.0) | 24 (77.4) | |
| > 10 | 16 (32.4) | 9 (50.0) | 7 (22.6) | |
| Multifocality | | | | 0.925 |
| Unifocal | 35 (71.4) | 13 (72.2) | 22 (71.0) | |
| Multifocal | 14 (28.6) | 5 (27.8) | 9 (29.0) | |
| Diffuse lesion | | | | 0.743 |
| Absent | 34 (69.4) | 13 (72.2) | 21 (67.7) | |
| Present | 15 (30.6) | 5 (27.8) | 10 (32.3) | |
| Extra-thyroid extension | | | | 1.000 |
| Absent | 38 (77.6) | 14 (77.8) | 24 (77.4) | |
| Present | 11 (22.4) | 4 (22.2) | 7 (22.6) | |
| Internal architecture | | | | 0.367 |
| Mostly solid | 1 (2.0) | 1 (5.6) | 0 (0) | |
| Solid | 48 (98.0) | 17 (94.4) | 31 (100) | |
| Echogenicity | | | | 0.505 |
| Isoechoic | 1 (2.0) | 0 (0) | 1 (3.2) | |
| Hypoechoic | 41 (83.7) | 14 (77.8) | 27 (87.1) | |
| Markedly hypoechoic | 7 (14.3) | 4 (22.2) | 3 (9.7) | |
| Margin | | | | 0.069 |
| Regular | 16 (32.7) | 3 (16.7) | 13 (41.9) | |
| Irregular | 33 (67.3) | 15 (83.3) | 18 (58.1) | |
| Shape | | | | 0.417 |
| Wider than tall | 20 (40.8) | 6 (33.3) | 14 (45.2) | |
| Taller than wide | 29 (50.2) | 12 (66.7) | 17 (54.8) | |
| Calcification | | | | 0.009 |
| None or Macro | 20 (40.8) | 3 (16.7) | 17 (54.8) | |
| Micro | 29 (59.2) | 15 (83.3) | 14 (45.2) | |
| Halo | | | | 1.000 |
| Absent | 36 (73.5) | 13 (72.2) | 23 (74.2) | |
| Present | 13 (26.5) | 5 (27.8) | 8 (25.8) | |
| Capsular invasion | | | | 0.007 |
| Absent | 31 (63.3) | 7 (38.9) | 24 (77.4) | |
| Present | 18 (36.7) | 11 (61.1) | 7 (22.6) | |
| CLNM on US | | | | 0.084 |
| Absent | 46 (93.9) | 15 (83.3) | 21 (100) | |
| Present | 3 (6.1) | 3 (16.7) | 0 (0) | |
| Blood flow | | | | 0.837 |
| None | 18 (36.7) | 6 (33.3) | 12 (38.7) | |
| Low | 25 (51.0) | 9 (50.0) | 16 (51.6) | |
| High | 6 (12.3) | 3 (16.7) | 3 (9.7) | |

CLNM, cervical lymph node metastasis; PTC, papillary thyroid carcinoma; CLNM+, papillary thyroid carcinoma with cervical lymph node metastasis; CLNM-, papillary thyroid carcinoma without cervical lymph node metastasis; US, ultrasound.

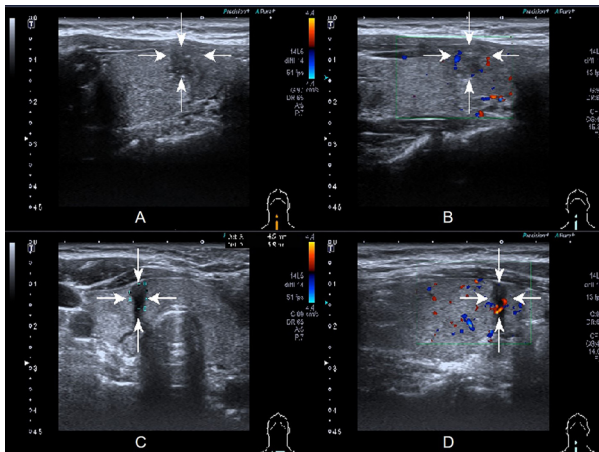


Figure 1. Examples of ultrasound features and the expression of ENST0000438158. (A) A 27-year-old female with CLNM in PTC showing low expression of ENST0000438158. US images presented with taller than wide and microcalcification; **(B)** A 30-year-old female with CLNM in PTC showing low expression of ENST0000438158. US images presented with microcalcification, 25% - 50% contact capsule and low blood supply on. **(C)** A 59-year-old female without CLNM in PTC showing high expression of ENST0000438158. US images presented with taller than wide and < 25% contact capsule. **(D)** A 53-year-old male without CLNM in PTC showing high expression of ENST0000438158. US images presented with taller than wide, < 25% contact capsule and high blood supply on.

Table 2. Multivariate logistic regression analysis to identify predictors of CLNM in PTC

| Parameter | B | SE | OR | 95% CI | p value |
|---------------------------------------|--------|-------|-------|----------------|---------|
| Size (> 10 mm) | 0.768 | 0.741 | 2.155 | 0.504 - 9.212 | 0.300 |
| Calcification(microcalcification) | 2.001 | 0.846 | 7.398 | 1.409 - 38.845 | 0.018 |
| Capsular invasion (Capsular invasion) | 1.909 | 0.771 | 6.749 | 1.491 - 30.556 | 0.013 |
| Constant | -2.913 | 0.872 | 0.054 | | |

CLNM, cervical lymph node metastasis; PTC, papillary thyroid carcinoma; 95% CI, 95% confidence interval.

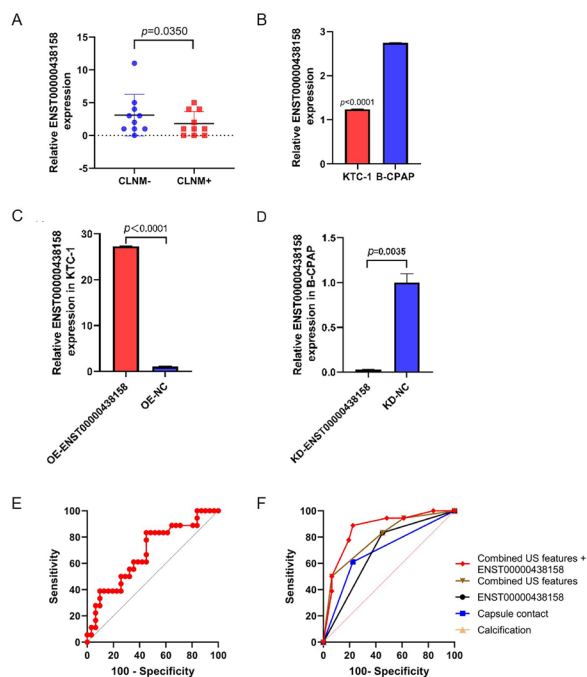


Figure 2. The expression of ENST0000438158 in PTC patients' cytological specimen and PTC cell lines. (A) The expression of ENST0000438158 in PTC tissues was detected by qRT-PCR according to CLNM in PTC. (B) The expression of ENST0000438158 in KTC-1 and B-CPAP cells was detected by qRT-PCR. (C) Overexpression of ENST0000438158 in KTC-1 cells. (D) Knockdown of ENST0000438158 in B-CPAP cells. (E) The cut-off value of ENST0000438158 expression was determined by ROC curve. (F) The ROC curves of US features and ENST0000438158 predicted cervical lymph node metastasis of PTC.

extension, internal architecture, echogenicity, margin, shape, calcification, halo, capsular invasion, or blood (all $p > 0.05$) (Table 3). Compared with the single US characteristics, the multiple US features were more valuable in predicting the CLNM of PTC (AUC = 0.794, 95% confidence interval (CI) = 0.654 - 0.896). The AUC of ENST0000438158 in predicting the CLNM in PTC was 0.691 (95% CI = 0.543 - 0.815). Adding ENST0000438158 to US can increase the value of predicting CLNM in PTC (AUC = 0.861, 95% CI = 0.732 - 0.943) ($p < 0.05$) (Figure 2F) (Table 4).

3.3. Effect of ENST0000438158 expression in migration and invasiveness of PTC cell lines

In transwell migration experiments, the migratory

capability of KTC-1 cells was lower than that of the negative control group when ENST0000438158 expression was upregulated. In addition, the high migratory abilities of B-CPAP cells were statistically induced by downregulating ENST0000438158 compared with the negative control group (Figures 3A-3B). Transwell invasion experiments showed that overexpression of ENST0000438158 could inhibit the ability of invasion of KTC-1 cells, conversely, knockdown of ENST0000438158 could promote the invasion of B-CPAP cells (Figures 3C-3D). In summary, the expression of ENST0000438158 was closely related to the migration and invasion of PTC cells.

3.4. Role of ENST0000438158 expression on cell proliferation, apoptosis, and cell cycle in PTC

In the CCK8 assay, upregulating ENST0000438158 expression inhibited KTC-1 proliferation (Figure 4A), whereas the proliferation of B-CPAP cells was increased when the expression of ENST0000438158 was knocked down (Figure 4B). In addition, the colony formation assay showed similar results (Figures 4C-4D).

As shown in Figures 5A-5B, the percentage of apoptotic cells remarkably decreased when ENST0000438158 was knocked down. ENST0000438158 overexpression increased the proportion of apoptotic cells. Compared with the negative control group, there was no significant difference in the proportion of G1, S, and G2/M phase cells in both B-CPAP and KTC-1 cells when ENST0000438158 was knocked down or overexpressed (Figures 6A-6B).

Collectively, knockdown of ENST0000438158 expression promoted PTC cell proliferation and reduced cell apoptosis.

4. Discussion

Although PTC is an indolent cancer, it is frequently accompanied by CLNM (5,6). One study found that the recurrence and mortality rates of thyroid cancer with CLNM were 30 times higher than those of thyroid cancer without CLNM (31). Hence, CLNM is considered a high-risk factor for local recurrence and a poor prognosis, which may influence the selection of surgical procedures (11,32). US is the preferred method for the preoperative diagnosis of PTC and evaluation of cervical lymph nodes. In our study, only three PTC

Table 3. Correlations between ENST0000438158 expression, clinicopathological characteristics and ultrasound characteristics of PTC

| Variable | <i>n</i> | Low expression, <i>n</i> (%) | High expression, <i>n</i> (%) | <i>p</i> value |
|-------------------------|-----------|------------------------------|-------------------------------|----------------|
| Sex | | | | 0.646 |
| Male | 14 (28.6) | 9 (31.0) | 5 (25.0) | |
| Female | 35 (71.4) | 20 (69.0) | 15 (75.0) | |
| Age | | | | 0.200 |
| > 45 | 24 (49.0) | 12 (41.4) | 12 (60.0) | |
| ≤ 45 | 25 (51.0) | 17 (58.6) | 8 (40.0) | |
| Tumor location | | | | 0.897 |
| Left | 20 (40.8) | 11 (37.9) | 9 (45.0) | |
| Right | 26 (53.1) | 16 (55.2) | 10 (50.0) | |
| Isthmus | 3 (6.1) | 2 (6.9) | 1 (5.0) | |
| Tumor size (mm) | | | | 0.343 |
| ≤ 10 | 33 (67.3) | 18 (62.1) | 15 (75.0) | |
| > 10 | 16 (32.4) | 11 (37.9) | 5 (25.0) | |
| Multifocality | | | | 0.141 |
| Unifocal | 35 (71.4) | 23 (79.3) | 12 (60.0) | |
| Multifocal | 14 (28.6) | 6 (20.7) | 8 (40.0) | |
| Diffuse lesion | | | | 0.479 |
| Absent | 34 (69.4) | 19 (65.5) | 15 (75.0) | |
| Present | 15 (30.6) | 10 (34.5) | 5 (25.0) | |
| Extra-thyroid extension | | | | 0.740 |
| Absent | 38 (77.6) | 23 (79.3) | 15 (75.0) | |
| Present | 11 (22.4) | 6 (20.7) | 5 (25.0) | |
| Internal architecture | | | | 1.000 |
| Mostly solid | 1 (2.0) | 1 (3.4) | 0 (0.0) | |
| Solid | 48 (98.0) | 28 (96.6) | 20 (100.0) | |
| Echogenicity | | | | 0.662 |
| Isoechoic | 1 (2.0) | 1 (3.4) | 0 (0.0) | |
| Hypoechoic | 41 (83.7) | 25 (86.2) | 16 (80.0) | |
| Markedly hypoechoic | 7 (14.3) | 3 (10.4) | 4 (20.0) | |
| Margin | | | | 0.771 |
| Regular | 16 (32.7) | 9 (31.0) | 7 (35.0) | |
| Irregular | 33 (67.3) | 20 (69.0) | 13 (65.0) | |
| Shape | | | | 0.491 |
| Wider than tall | 20 (40.8) | 13 (44.8) | 7 (35.0) | |
| Taller than wide | 29 (50.2) | 16 (55.2) | 13 (65.0) | |
| Calcification | | | | 0.621 |
| None or Macro | 20 (40.8) | 11 (37.9) | 9 (45.0) | |
| Micro | 29 (59.2) | 18 (62.1) | 11 (55.0) | |
| Halo | | | | 0.840 |
| Absent | 36 (73.5) | 21 (72.4) | 15 (75.0) | |
| Present | 13 (26.5) | 8 (27.6) | 5 (25.0) | |
| Capsular invasion | | | | 0.417 |
| Absent | 31 (63.3) | 17 (58.6) | 14 (70.0) | |
| Present | 18 (36.7) | 12 (41.4) | 6 (30.0) | |
| Blood flow | | | | 0.124 |
| None | 18 (36.7) | 7 (24.1) | 11 (55.0) | |
| Low | 25 (51.0) | 18 (62.1) | 7 (35.0) | |
| High | 6 (12.3) | 4 (13.8) | 2 (10.0) | |
| CLNM | | | | 0.009 |
| CLNM- | 31 (63.3) | 14 (48.3) | 17 (85.0) | |
| CLNM+ | 18 (36.7) | 15 (51.7) | 3 (15.0) | |

CLNM, cervical lymph node metastasis; PTC, papillary thyroid carcinoma; CLNM+, papillary thyroid carcinoma with cervical lymph node metastasis; CLNM-, papillary thyroid carcinoma without cervical lymph node metastasis.

Table 4. Combined diagnostic value of ENST0000438158 with ultrasound of CLNM in PTC

| Variable | Critical value | AUC (95% CI) | Sensitivity (%) | Specificity (%) |
|---------------------------------------|---------------------------------------|-----------------------|-----------------|-----------------|
| ENST0000438158 | Low expression | 0.691 (0.543 - 0.815) | 83.3 | 54.8 |
| Capsule contact | ≥25% | 0.693 (0.545 - 0.816) | 61.11 | 77.42 |
| Calcification | Microcalcification | 0.691 (0.543 - 0.815) | 83.33 | 54.84 |
| Combined US features | Combined US features | 0.794 (0.654 - 0.896) | 50.00 | 93.55 |
| Combined US features + ENST0000438158 | Combined US features + ENST0000438158 | 0.861 (0.732 - 0.943) | 88.89 | 77.42 |

CLNM, cervical lymph node metastasis; PTC, papillary thyroid carcinoma. 95% CI, 95% confidence interval.

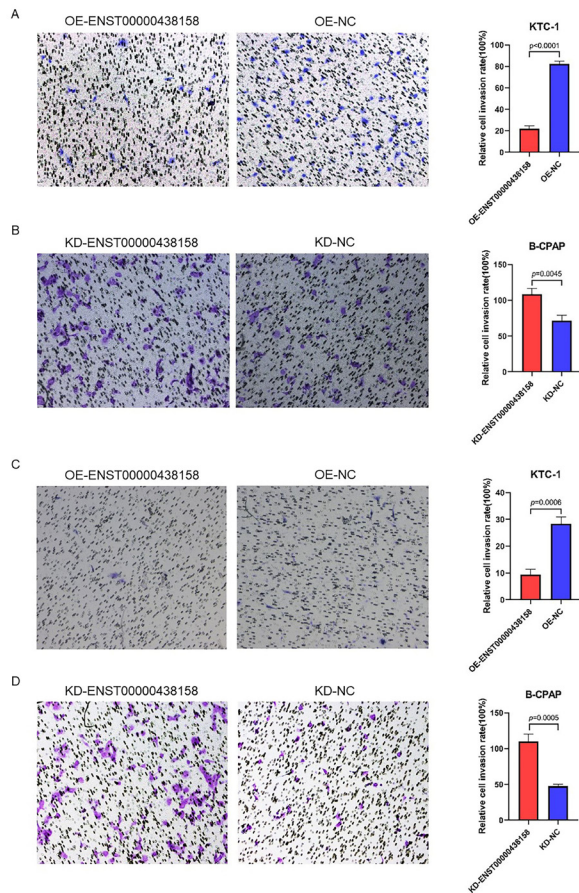


Figure 3. Effect of ENST00000438158 on the migration and invasiveness of PTC cell lines. A Transwell assay was performed to determine the migration ability of (A) KTC-1 cells and (B) B-CPAP cells. A Transwell assay was performed to determine the invasion ability of (C) KTC-1 cells and (D) B-CPAP cells. Representative images show migrated cells and invasive cells stained with crystal violet. The quantification of cell migration and invasion is presented as number of migrating and invading cells. All experiments were performed independently in triplicate.

patients with CLNM were detected by US, with 16.7% sensitivity. A similar result has been reported in other studies (12-14). Considering the higher prevalence of CLNM and the poor performance of US in preoperative detection of CLNM, it is necessary to predict CLNM with US features of primary PTC. Some scholars have found that greater than 25% of capsule contact with thyroid nodules is a useful index to predict the CLNM of PTC, with 74.3-86.2% sensitivity and 55.3-66.1% specificity (33,34), which is consistent with the findings of our study. This is because the thyroid gland is surrounded by a capsule with abundant lymphatic vessels. The closer the lesion is to the capsule, the greater the risk of contact between the cancer tissue and lymphatic vessels, and the probability of lymphatic metastasis to lymph nodes increases. The mechanism of microcalcification in thyroid cancer may be caused by excessive hyperplasia of fibrous tissue and blood vessels in the nodules. However, Das *et al.* (35) proposed that the sand precursor in the pericarp was released into

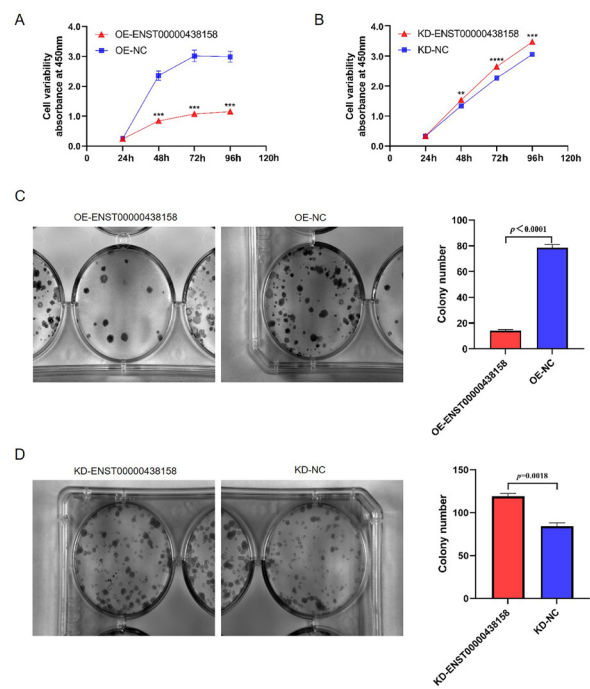


Figure 4. Effect of ENST00000438158 on the proliferation of PTC cell lines. A CCK-8 assay was performed to determine the proliferation of (A) KTC-1 cells and (B) B-CPAP cells. A colony formation assay was performed to determine the proliferation of (C) KTC-1 cells and (D) B-CPAP cells. The colonies were captured and counted and the results were presented in the histogram. All experiments were performed independently in triplicate.

local tissues by intact tumor cells and then calcified; therefore, the sand precursor (microcalcification on imaging) represented an active biological process rather than dystrophic calcification or tumor cell death. The current study also indicated that microcalcification was associated with CLNM, which is in accordance with results of previous studies (36,37). Furthermore, we performed an analysis of single US features and multiple US features combined to predict PTC with CLNM. The results showed that the value of combining multiple US features to predict PTC with CLNM was higher than that of a single US feature, but its sensitivity was still low. Xia *et al.* (38) also analyzed the value of US features in diagnosing CLNM of PTC and presented high specificity but low sensitivity, which was consistent with our results.

FNA is an effective method to predict CLNM in PTC, with 73-94% sensitivity. The main reason for this is that FNA largely depends on the experience and ability of the operators and cell pathologists (39,40). In addition, the small size of lymph nodes and the interference of lymphocyte infiltration and internal necrosis also affect FNA results (40,41). To overcome the limitations of imaging and cytology, the detection of molecular markers has become the focus of current research. Diaz *et al.* (42) compared the diagnostic value of FNA alone and FNA combined with detection of

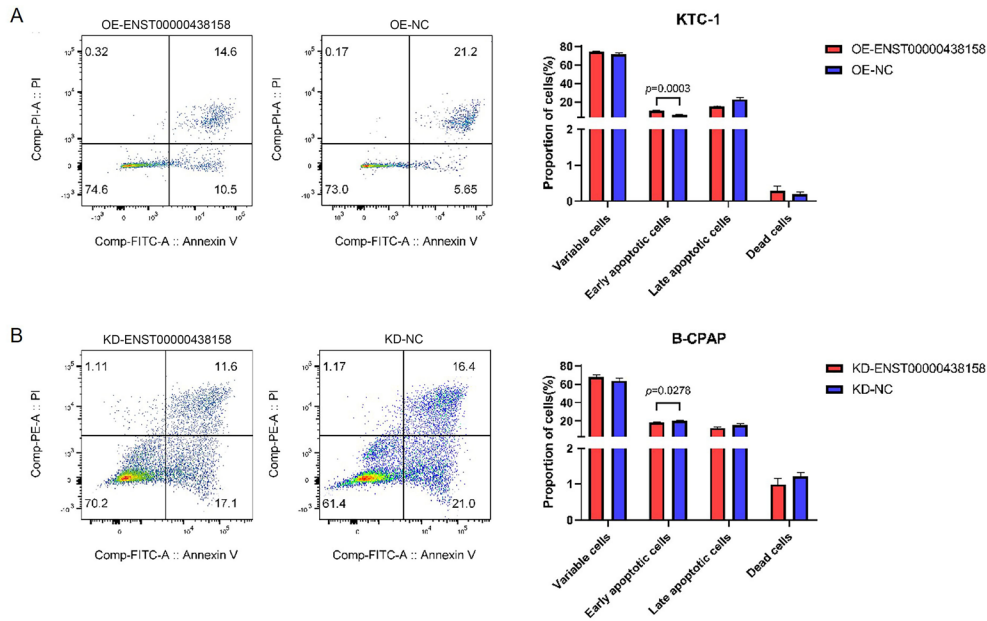


Figure 5. Effect of ENST00000438158 on the apoptosis of PTC cell lines. Flow cytometric analysis of apoptosis in (A) KTC-1 cells and (B) B-APAP cells. The percentage of apoptotic cells was presented in the histogram. Data were expressed as the means ± SD of three independent experiments.

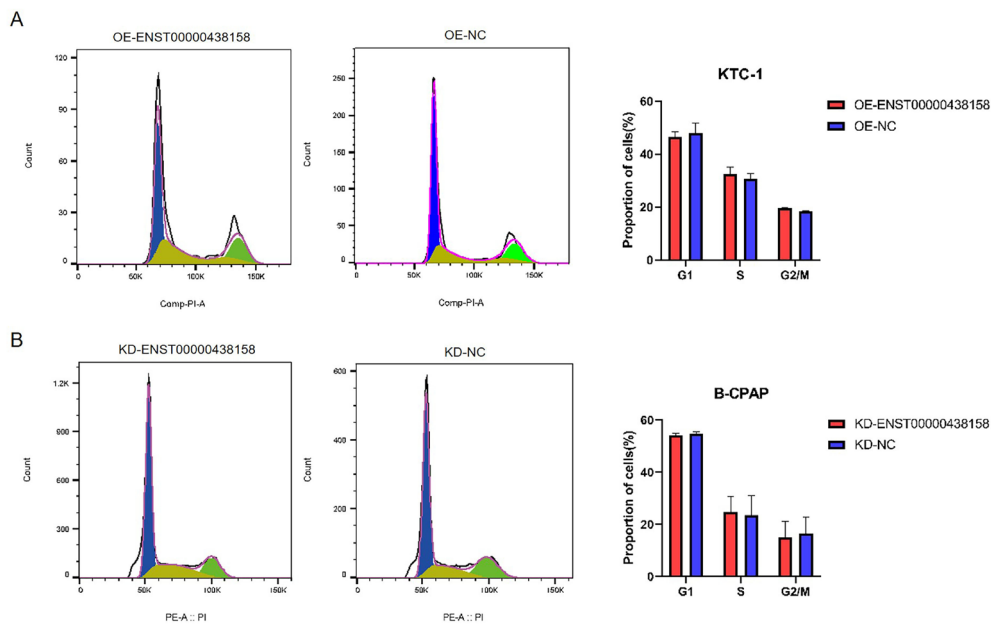


Figure 6. Effect of ENST00000438158 on the cell cycle status of PTC cell lines. Flow cytometric analysis of the cell cycle in (A) KTC-1 cells and (B) B-APAP cells. Results quantified in the cell cycle analysis were shown as a percentage of the total number of cells. Data were expressed as the means ± SD of three independent experiments.

KI-67 in pancreatic endocrine tumors, and the results showed that the latter method had a higher diagnostic value. Li *et al.* (43) evaluated the value of lymph node FNA alone and combined with thyroglobulin detection in PTC with CLNM, and the results also showed that the combined detection had higher accuracy. Therefore, FNA combined with the detection of molecular markers can not only obtain cytology samples but also carry

out molecular diagnostic information at the same time, which has a certain guiding significance for clinical use. In our study, PTC primary lesions were punctured rather than cervical lymph nodes, with the advantage of avoiding injury to the cervical blood vessels and nerve sheath to reduce operational risk.

At present, some researchers have found that lncRNAs have certain clinical guiding potential

in various tumors, and it may become an effective biomarker (44,45). Some studies, such as HOTAIR (46) and ANRIL (47), have shown that lncRNAs can effectively predict CLNM in PTC. Xia *et al.* (38) indicated that the expression level of NONHSAT076754 was positively correlated with CLNM in PTC and clinical stage. Zheng *et al.* (48) showed that an increase in BANCR expression is associated with poor prognosis, CLNM, and distant metastasis by regulating the expression of TSHR and its downstream cyclin D1. Previous studies have confirmed that ENST0000438158 is associated with the occurrence, development, and lung metastasis of osteosarcoma (28). It has been reported that lncRNAs may act as endogenous "sponges," which downregulate a series of miRNA activities, affecting the occurrence and development of thyroid cancer (49,50). We assume that ENST0000438158 may function as a "sponge," competitively binding to miRNAs, and regulating the occurrence and development of PTC. In our study, we confirmed that ENST0000438158 is negatively associated with CLNM in PTC. Furthermore, an *in vitro* functional study demonstrated that knockdown or upregulation of ENST0000438158 expression promotes or inhibits the proliferation, migration, and invasion of PTC cells. Because of the low sensitivity of US in predicting CLNM, we adopted a combination of US features and the expression of ENST0000438158 to improve diagnostic sensitivity. When ENST0000438158 was added to the US, the value of differentiating PTC from CLNM was greatly improved, and the AUC, sensitivity, and specificity of combined ENST0000438158 and US were 0.861, 88.89%, and 77.42%, respectively. Therefore, preoperative detection of ENST0000438158 expression is of great importance. The rate of missed diagnoses can be reduced by combining the US and ENST0000438158.

However, this study has some limitations. First, a small number of PTC cases were recruited in this study, which can be further studied by expanding the number of specimens over the long term. Second, the mechanism by which ENST0000438158 regulates CLNM in PTC was not elucidated in our study. Therefore, further studies on this mechanism are needed to provide guidance for clinical practice.

In conclusion, the low expression of ENST0000438158 was related to CLNM in PTC, which can promote cell proliferation, metastasis, and invasion, while inhibiting apoptosis. Adding ENST0000438158 to US can increase the diagnostic value of predicting PTC with CLNM. Therefore, ENST0000438158 may be a promising auxiliary diagnostic biomarker to be combined with US for the prediction of CLNM in PTC.

Acknowledgements

The authors wish to sincerely thank Peng Li and Suna Tian for their assistance in preparing the figures in this

manuscript.

Funding: This work was supported by the Shanghai Municipal Health and Family Planning Commission of China (grant number 201640285 to L Chen), a project under the Scientific and Technological Innovation Action Plan of the Shanghai Natural Science Fund (grant no. 20ZR1409100 to L Wang), and a project of the Chinese Association of Integration of Traditional and Western Medicine Special Foundation for Obstetrics and Gynecology-PuZheng Pharmaceutical Foundation (grant no. FCK-PZ-08 to L Wang), a project for hospital management of the Shanghai Hospital Association (grant no. X2021046 to L Wang), and a clinical trial project of the Special Foundation for Healthcare Research of the Shanghai Municipal Health Commission (Grant No. 202150042 to L Wang).

Conflict of Interest: The authors have no conflicts of interest to disclose.

References

1. Siegel RL, Miller KD, Jemal A. Cancer statistics, 2020. *CA Cancer J Clin.* 2020; 70:7-30.
2. Rahib L, Smith BD, Aizenberg R, Rosenzweig AB, Fleshman JM, Matrisian LM. Projecting cancer incidence and deaths to 2030: The unexpected burden of thyroid, liver, and pancreas cancers in the United States. *Cancer Res.* 2014; 74:2913-2921.
3. Lim H, Devesa SS, Sosa JA, Check D, Kitahara CM. Trends in thyroid cancer incidence and mortality in the United States, 1974-2013. *JAMA.* 2017; 317:1338-1348.
4. Kitahara CM, Sosa JA. The changing incidence of thyroid cancer. *Nat Rev Endocrinol.* 2016; 12:646-653.
5. Al-Brahim N, Asa SL. Papillary thyroid carcinoma: An overview. *Arch Pathol Lab Med.* 2006; 130:1057-1062.
6. Ito Y, Kihara M, Takamura Y, Kobayashi K, Miya A, Hirokawa M, Miyauchi A. Prognosis and prognostic factors of papillary thyroid carcinoma in patients under 20 years. *Endocr J.* 2012; 59:539-545.
7. Viola D, Agate L, Molinaro E, Bottici V, Lorusso L, Latrofa F, Torregrossa L, Boldrini L, Ramone T, Vitti P, Elisei R. Lung recurrence of papillary thyroid cancer diagnosed with antithyroglobulin antibodies after 10 years from initial treatment. *Front Endocrinol (Lausanne).* 2018; 9:590.
8. Mazzaferri EL, Jhiang SM. Long-term impact of initial surgical and medical therapy on papillary and follicular thyroid cancer. *Am J Med.* 1994; 97:418-428.
9. So YK, Kim MJ, Kim S, Son YI. Lateral lymph node metastasis in papillary thyroid carcinoma: A systematic review and meta-analysis for prevalence, risk factors, and location. *Int J Surg.* 2018; 50:94-103.
10. Sturgeon C, Yang A, Elaraj D. Surgical management of lymph node compartments in papillary thyroid cancer. *Surg Oncol Clin N Am.* 2016; 25:17-40.
11. Haugen BR, Alexander EK, Bible KC, *et al.* 2015 American thyroid association management guidelines for adult patients with thyroid nodules and differentiated thyroid cancer: The American thyroid association guidelines task force on thyroid nodules and differentiated

- thyroid cancer. *Thyroid*. 2016; 26:1-133.
12. Zhao H, Li H. Meta-analysis of ultrasound for cervical lymph nodes in papillary thyroid cancer: Diagnosis of central and lateral compartment nodal metastases. *Eur J Radiol*. 2019; 112:14-21.
 13. Baek SK, Jung KY, Kang SM, Kwon SY, Woo JS, Cho SH, Chung EJ. Clinical risk factors associated with cervical lymph node recurrence in papillary thyroid carcinoma. *Thyroid*. 2010; 20:147-152.
 14. Moo TA, McGill J, Allendorf J, Lee J, Fahey T, Zarnegar R. Impact of prophylactic central neck lymph node dissection on early recurrence in papillary thyroid carcinoma. *World J Surg*. 2010; 34:1187-1191.
 15. Xu Y, Yang X, Si T, Yu H, Li Y, Xing W, Guo Z. MCM4 in human hepatocellular carcinoma: A potent prognostic factor associated with cell proliferation. *Biosci Trends*. 2021; 15:100-106.
 16. Zhu J, Zhao R, Xu W, Ma J, Ning X, Ma R, Meng F. Correlation between reticulon ribosome-binding protein 1 (RRBP1) overexpression and prognosis in cervical squamous cell carcinoma. *Biosci Trends*. 2020; 14:279-284.
 17. Flynn RA, Chang HY. Long noncoding RNAs in cell-fate programming and reprogramming. *Cell Stem Cell*. 2014; 14:752-761.
 18. Mercer TR, Dinger ME, Mattick JS. Long non-coding RNAs: Insights into functions. *Nat Rev Genet*. 2009; 10:155-159.
 19. Lin X, Qiu J, Hua K. Long non-coding RNAs as emerging regulators of epithelial to mesenchymal transition in gynecologic cancers. *Biosci Trends*. 2018; 12:342-353.
 20. Gu Y, Xiao X, Yang S. LncRNA MALAT1 acts as an oncogene in multiple myeloma through sponging miR-509-5p to modulate FOXP1 expression. *Oncotarget*. 2017; 8:101984-101993.
 21. Zuo Y, Li Y, Zhou Z, Ma M, Fu K. Long non-coding RNA MALAT1 promotes proliferation and invasion *via* targeting miR-129-5p in triple-negative breast cancer. *Biomed Pharmacother*. 2017; 95:922-928.
 22. Hu Y, Deng C, Zhang H, Zhang J, Peng B, Hu C. Long non-coding RNA XIST promotes cell growth and metastasis through regulating miR-139-5p mediated Wnt/ β -catenin signaling pathway in bladder cancer. *Oncotarget*. 2017; 8:94554-94568.
 23. Ding J, Wang F, Xiang T, Qiao M. Expression and function of long noncoding RNA NONHSAT129183 in papillary thyroid cancer. *Oncol Res*. 2018; 26:1047-1053.
 24. Zuo Z, Liu L, Song B, Tan J, Ding D, Lu Y. Silencing of long non-coding RNA ENST00000606790.1 inhibits the malignant behaviors of papillary thyroid carcinoma through the PI3K/AKT pathway. *Endocr Res*. 2021; 46:1-9.
 25. Guo LJ, Zhang S, Gao B, Jiang Y, Zhang XH, Tian WG, Hao S, Zhao JJ, Zhang G, Hu CY, Yan J, Luo DL. Low expression of long non-coding RNA GAS5 is associated with poor prognosis of patients with thyroid cancer. *Exp Mol Pathol*. 2017; 102:500-504.
 26. Wang C, Yan G, Zhang Y, Jia X, Bu P. Long noncoding RNA MEG3 suppresses migration and invasion of thyroid carcinoma by targeting of Rac1. *Neoplasma*. 2015; 62:541-549.
 27. Luo J, Xu L, Jiang Y, Zhuo D, Zhang S, Wu L, Xu H, Huang Y. Expression profile of long non-coding RNAs in colorectal cancer: A microarray analysis. *Oncol Rep*. 2016; 35:2035-2044.
 28. Xie L, Yao Z, Zhang Y, Li D, Hu F, Liao Y, Zhou L, Zhou Y, Huang Z, He Z, Han L, Yang Y, Yang Z. Deep RNA sequencing reveals the dynamic regulation of miRNA, lncRNAs, and mRNAs in osteosarcoma tumorigenesis and pulmonary metastasis. *Cell Death Dis*. 2018; 9:772.
 29. Kim H, Kim JA, Son EJ, Youk JH, Chung TS, Park CS, Chang HS. Preoperative prediction of the extrathyroidal extension of papillary thyroid carcinoma with ultrasonography versus MRI: A retrospective cohort study. *Int J Surg*. 2014; 12:544-548.
 30. Kim H, Kim JA, Son EJ, Youk JH. Quantitative assessment of shear-wave ultrasound elastography in thyroid nodules: Diagnostic performance for predicting malignancy. *Eur Radiol*. 2013; 23:2532-2537.
 31. Noguchi M, Kumaki T, Taniya T, Miyazaki I. Bilateral cervical lymph node metastases in well-differentiated thyroid cancer. *Arch Surg*. 1990; 125:804-806.
 32. Pisanu A, Reccia I, Nardello O, Uccheddu A. Risk factors for nodal metastasis and recurrence among patients with papillary thyroid microcarcinoma: Differences in clinical relevance between nonincidental and incidental tumors. *World J Surg*. 2009; 33:460-468.
 33. Moon HJ, Sung JM, Kim EK, Yoon JH, Youk JH, Kwak JY. Diagnostic performance of gray-scale US and elastography in solid thyroid nodules. *Radiology*. 2012; 262:1002-1013.
 34. Choi JS, Kim J, Kwak JY, Kim MJ, Chang HS, Kim EK. Preoperative staging of papillary thyroid carcinoma: Comparison of ultrasound imaging and CT. *AJR Am J Roentgenol*. 2009; 193:871-878.
 35. Das DK. Psammoma body: A product of dystrophic calcification or of a biologically active process that aims at limiting the growth and spread of tumor? *Diagn Cytopathol*. 2009; 37:534-541.
 36. Li F, Pan D, He Y, Wu Y, Peng J, Li J, Wang Y, Yang H, Chen J. Using ultrasound features and radiomics analysis to predict lymph node metastasis in patients with thyroid cancer. *BMC Surg*. 2020; 20:315.
 37. Liu J, Zheng D, Li Q, Tang X, Luo Z, Yuan Z, Gao L, Zhao J. A predictive model of thyroid malignancy using clinical, biochemical and sonographic parameters for patients in a multi-center setting. *BMC Endocr Disord*. 2018; 18:17.
 38. Xia S, Wang C, Ni X, Ni Z, Dong Y, Zhan W. NONHSAT076754 aids ultrasonography in predicting lymph node metastasis and promotes migration and invasion of papillary thyroid cancer cells. *Oncotarget*. 2017; 8:2293-2306.
 39. Frasoldati A, Toschi E, Zini M, Flora M, Caroggio A, Dotti C, Valcavi R. Role of thyroglobulin measurement in fine-needle aspiration biopsies of cervical lymph nodes in patients with differentiated thyroid cancer. *Thyroid*. 1999; 9:105-111.
 40. Frasoldati A, Valcavi R. Challenges in neck ultrasonography: Lymphadenopathy and parathyroid glands. *Endocr Pract*. 2004; 10:261-268.
 41. Hall TL, Layfield LJ, Philippe A, Rosenthal DL. Sources of diagnostic error in fine needle aspiration of the thyroid. *Cancer*. 1989; 63:718-725.
 42. Diaz Del Arco C, Diaz Perez JA, Ortega Medina L, Sastre Valera J, Fernandez Acenero MJ. Reliability of Ki-67 determination in FNA samples for grading pancreatic neuroendocrine tumors. *Endocr Pathol*. 2016; 27:276-283.
 43. Li J, Zhang K, Liu X, Hao F, Liu Z, Wang Z. Cervical lymph node thyroglobulin measurement in washout of

- fine-needle aspirates for diagnosis of papillary thyroid cancer metastases. *Br J Biomed Sci.* 2016; 73:79-83.
44. Nagasawa M, Tomimatsu K, Terada K, Kondo K, Miyazaki K, Miyazaki M, Motooka D, Okuzaki D, Yoshida T, Kageyama S, Kawamoto H, Kawauchi A, Agata Y. Long non-coding RNA MANCR is a target of BET bromodomain protein BRD4 and plays a critical role in cellular migration and invasion abilities of prostate cancer. *Biochem Biophys Res Commun.* 2020; 526:128-134.
45. Shen S, Li K, Liu Y, Liu X, Liu B, Ba Y, Xing W. Silencing lncRNA AGAP2-AS1 upregulates miR-195-5p to repress migration and invasion of EC cells *via* the decrease of FOSL1 expression. *Mol Ther Nucleic Acids.* 2020; 20:331-344.
46. Di W, Li Q, Shen W, Guo H, Zhao S. The long non-coding RNA HOTAIR promotes thyroid cancer cell growth, invasion and migration through the miR-1-CCND2 axis. *Am J Cancer Res.* 2017; 7:1298-1309.
47. Zhao JJ, Hao S, Wang LL, Hu CY, Zhang S, Guo LJ, Zhang G, Gao B, Jiang Y, Tian WG, Luo DL. Long non-coding RNA ANRIL promotes the invasion and metastasis of thyroid cancer cells through TGF- β /Smad signaling pathway. *Oncotarget.* 2016; 7:57903-57918.
48. Zheng H, Xu J, Hao S, Liu X, Ning J, Song X, Jiang L, Liu Z. Expression of BANCR promotes papillary thyroid cancer by targeting thyroid stimulating hormone receptor. *Oncol Lett.* 2018; 16:2009-2015.
49. Liang L, Xu J, Wang M, Xu G, Zhang N, Wang G, Zhao Y. LncRNA HCP5 promotes follicular thyroid carcinoma progression via miRNAs sponge. *Cell Death Dis.* 2018; 9:372.
50. Lin Y, Jiang J. Long non-coding RNA LINC00704 promotes cell proliferation, migration, and invasion in papillary thyroid carcinoma via miR-204-5p/HMGB1 axis. *Open Life Sci.* 2020; 15:561-571.

Received August 8, 2022; Revised October 10, 2022; Accepted October 12, 2022.

[§]These authors contributed equally to this work.

*Address correspondence to:

Ling Wang, Laboratory for Reproductive Immunology, Obstetrics and Gynecology Hospital of Fudan University, 419 Fangxie Road, Shanghai, China 200011.
E-mail: Dr.wangling@fudan.edu.cn

Lin Chen, Department of Ultrasound, Huadong Hospital of Fudan University, 211 West Yan'an Rd, Shanghai, China 200040.

E-mail: linchen11@fudan.edu.cn

Released online in J-STAGE as advance publication October 19, 2022.

A fast RT-qPCR system significantly shortens the time for SARS-CoV-2 nucleic acid test

Hongjie Dong^{1,2,§}, Kundi Zhang^{1,§}, Junmei Zhang², Yumeng Xiao¹, Fengyu Zhang¹, Maofeng Wang¹, Hongwei Wang¹, Guihua Zhao², Shiling Xie³, Xiaohong Xie³, Wei Hu¹, Kun Yin^{2,*}, Lichuan Gu^{1,*}

¹ State Key Laboratory of Microbial Technology, Shandong University, Qingdao, Shandong, China;

² Shandong Institute of Parasitic Diseases, Shandong First Medical University & Shandong Academy of Medical Sciences, Jining, Shandong, China;

³ Shandong Shtars Medical Technology Co. Ltd, Jinan, Shandong, China.

SUMMARY Severe acute respiratory syndrome coronavirus 2 (SARS-CoV-2) is a serious threat to global development. Rapid and accurate diagnosis is critical for containing the pandemic and treating patients in time. As the gold standard for SARS-CoV-2 diagnosis, the qualitative reverse transcription-PCR (RT-qPCR) test has long been criticized for its long detection time. In this study, we optimized the primers and probes targeting SARS-CoV-2 *ORF1ab* and *N* gene designed by the Chinese Center for Disease Control and Preventions (CDC) to increase their T_m values to meet the optimal elongation temperature of Taq DNA polymerase, thus greatly shortened the elongation time. The higher elongation temperature in turn narrowed the temperature range of the reaction and saved more time. In addition, by shortening the distance between the fluorophore at the 5' end and the quencher in the middle we got a probe with higher signal-to-noise ratio. Finally, by using all these measures and optimized RT-qPCR program we successfully reduced the time (nucleic acid extraction step is not included) for nucleic acid test from 74 min to 26 min.

Keywords SARS-CoV-2, detection time, T_m value, elongation temperature, probe

1. Introduction

The coronavirus disease 2019 (COVID-19), caused by severe acute respiratory syndrome coronavirus 2 (SARS-CoV-2) (1), is still spreading globally since the first case was reported in Wuhan, China, in December 2019 (2). As of December 18, 2022, an estimated 647.97 million people had been infected and more than 6.64 million have died (3). Although several kinds of vaccines and therapeutics have been developed and come into use (4), rapid and accurate diagnosis is always critical for containing the pandemic and treating patients in time (5,6). In China, due to the dynamic zero-out policy, large-scale screening of millions of people in an entire local region is occasionally needed to identify the latent infected persons in the population (7). Higher efficient detection means faster containment of the spread of SARS-CoV-2 and less economic loss.

Currently, nucleic acid test (NAS) and antigen tests are the two main methods for COVID-19 diagnosis and of which NAS is the main diagnostic method due to its

higher sensitivity (8,9). Based on technical principle, NAS can be divided into two categories: one is targeted nucleic acid amplification testing (TNAAT), mainly including qualitative reverse transcription-PCR (RT-qPCR) and isothermal amplification (10); the other is direct nucleic acid testing without targeted amplification, such as nucleic acid hybridization, gene chip (11). Among all these nucleic acid test methods, RT-qPCR technology has the highest sensitivity, reliability and accuracy, thus become the gold standard for SARS-CoV-2 diagnosis (12).

RT-qPCR reaction includes two steps: reverse transcription and PCR cycle amplification (13). The routine program combines annealing and elongation into one step and adopts two-step cycle amplification to reduce the frequency of temperature rise and cooling, which requires a compromise between the annealing temperature of primers and the elongation temperature of Taq DNA polymerase. Generally, this process takes more than 70 min making a bottleneck of the diagnosis (14). In previous studies, rapid PCR was achieved

mainly through the improvement of DNA polymerase, reaction buffer and temperature control instruments. At present, the performance of Taq DNA polymerase used in RT-PCR detection has been quite excellent. And due to the popularity of RT-PCR technology, it would cost a lot to replace detection instruments in the majority of detection institutions. In this research, by optimizing the primer and probe design as well as the whole procedure we shortened the whole RT-qPCR time (nucleic acid extraction step is not included) 74 min to 26 min without sacrificing the sensitivity and accuracy. Our method provides a new way to shorten the PCR time.

2. Materials and Methods

2.1. Preparation of RT-qPCR template

225 μL SARS-CoV-2 *ORF1ab-N* pseudovirus (Sangon Biotech Co., Ltd, Shanghai, China) with the initial concentration of 10^8 copies/mL was added to a throat swab and placed into 3 mL preservative solution (25 mM Tris-HCl pH 7.6, 1 mM EDTA, 20 mM Guanidine thiocyanate) to simulate clinically positive samples. Then 200 μL preservation solution was taken out for RNA extraction using MiniBEST Viral RNA Extraction Kit (Takara Biomedical Technology Co., Ltd, Beijing, China) and the target nucleic acid was eluted from the purification column with 30 μL enzyme-free water. Finally, 4 μL of RNA solution was used in the final reaction volume of 20 μL . According to the conversion, the pseudovirus concentration was 10^7 copies/mL in the RT-PCR system. The target nucleic acid was diluted with enzyme-free water, and the pseudovirus concentrations in the RT-PCR system were 10^6 copies/mL, 10^5 copies/mL, 10^4 copies/mL, 10^3 copies/mL, 700 copies/mL, 500 copies/mL, 300 copies/mL, and 100 copies/mL, respectively.

2.2. Determination of T_m value of primers and probes

The primers, probes to be tested and the single-stranded DNA fragments (template strand) to which they bind were synthesized by Sangon Biotech Co., Ltd. and purified by high performance liquid chromatography (HPLC). The volume of system for test was 20 μL , including 2.5 μM oligonucleotide, 2.5 μM template strand and $1\times$ SYBR green1 dye (Beijing Solarbio Science & Technology Co., Ltd., Beijing, China). The reaction was carried out on the SLAN-96P RT-qPCR instrument (Hongshi Medical Technology Co., Ltd., Shanghai, China) according to the following procedures: 95°C for 10 min, 30°C for 2 min, 65 cycles, each cycle increased by 1°C, and fluorescence was collected in each cycle. The standard melting curve of DNA fragments was measured and the reciprocal curve was obtained. Take the temperature corresponding to the peak of the reciprocal curve as the T_m value of the primers.

2.3. Comparison of quenching efficiency of probes

The probe to be tested and the corresponding probe labeled only with 5'-fluorophore were synthesized by Sangon Biotech Co., Ltd. and diluted to 10 μM . The fluorescence of the probe at 250 nM (the common concentration of probes in RT-qPCR reaction) was measured on a microplate spectrophotometer (Tecan Trading AG, Mannedorf, Switzerland), and the quenching efficiency of the probe was evaluated by comparing the fluorescence intensity with that of the corresponding probe labeled only with 5'-fluorophore.

2.4. RT-qPCR assay

The reaction system consisted of 10 μL $2\times$ TaqMan Fast Master Mix, 1 μL Taq DNA polymerase (Vazyme Biotech Co., Ltd, Nanjing, China), 0.5 μL forward primer (10 μM), 0.5 μL reverse primer (10 μM), 0.5 μL probe (10 μM), 3.5 μL nuclease-free water and 4 μL nucleic acid sample. RT-qPCR assay was performed on qTOWER3 (Analytik Jena AG, Jena, Germany). The procedure settings of four detection schemes were as follows. Scheme 1: reverse transcription at 55°C for 15 min, pre-denaturation at 95°C for 30 s, denaturation at 95°C for 10 s, annealing and elongation at 60°C for 30 s, 45 cycles. Scheme 2: reverse transcription at 55°C for 15 min, pre-denaturation at 95°C for 30 s, denaturation at 95°C for 10 s, annealing and elongation at 70°C for 30 s, 45 cycles. Scheme 3: reverse transcription at 55°C for 15 min, pre-denaturation at 95°C for 30 s, denaturation at 95°C for 10 s, annealing and elongation at 70°C for 2 s, 45 cycles. Scheme 4: reverse transcription at 55°C for 2 min, pre-denaturation at 95°C for 2 s, denaturation at 95°C for 1 s, annealing and elongation at 70°C for 2 s, 41 cycles.

2.5. Determination of the limit of detection

A scheme was performed with 5 template concentrations of 10^3 copies/mL, 700 copies/mL, 500 copies/mL, 300 copies/mL and 100 copies/mL, and each concentration was repeated 20 times. The template concentration with a positive rate greater than 95% (19 times) was defined as the limit of detection of the detection scheme. The criteria for judging the results were as follows. Positive results: cycle threshold (CT) values of FAM and VIC channels were both less than or equal to 38. Negative results: CT values of FAM and VIC channels were both greater than 38. Suspicious results: The CT value of one detection channel was less than or equal to 38, and the CT value of the other channel was greater than 38. Repeated testing was required for the suspicious results. And if the results were still consistent with the previous results, the samples were judged as negative.

2.6. Determination of the detection specificity

The long primers and long probe we designed were improved on the basis of the primers and probe targeting SARS-CoV-2 *ORF1ab* and *N* gene designed by China CDC, and the data of various detection institutions in China have proved the excellent specificity of these primers. In the evolution analysis of SARS-CoV-2, the viruses genetically similar to the SARS-CoV-2 genome sequence are the other six human coronaviruses. Therefore, we cloned the corresponding detection genes of various human coronaviruses into plasmids as RT-qPCR templates for detection specificity analysis. The data was obtained from triplet experiments.

2.7. Determination of the detection repeatability

To assess the repeatability of the three-channel fast RT-qPCR system, five replicates were executed within and between groups with three pseudovirus concentrations (10^6 copies/mL, 10^5 copies/mL and 10^4 copies/mL). The coefficient of variation (CV) was calculated according to the Ct value of the test results, and the calculation method was: $CV = \text{standard deviation}/\text{mean} \times 100\%$.

2.8. Statistics analysis

All experiments were repeated independently three times in order to minimize the effect of random initialisation, and we reported the mean and standard deviation (SD) of the experiments. The Student's *t*-test by SPSS 15 was used to perform data analysis. Statistical significance was assessed based on the *p*-value: * $p < 0.05$, ** $p < 0.01$, and *** $p < 0.001$.

3. Results

3.1. Primers and probe designed by China CDC cannot work at the optimal elongation temperature of Taq DNA polymerase

The T_m values of CDC-*ORF1ab* PF, CDC-*ORF1ab* PR, CDC-*ORF1ab* Probe, CDC-*N* PF, CDC-*N* PR and CDC-*N* Probe were $68.49 \pm 0.04^\circ\text{C}$, $65.29 \pm 0.06^\circ\text{C}$, $71.85 \pm 0.02^\circ\text{C}$, $64.66 \pm 0.05^\circ\text{C}$, $66.52 \pm 0.09^\circ\text{C}$, and $71.81 \pm 0.02^\circ\text{C}$, respectively (Figure 1). This implied that PCR system containing these primers and probes will not work well at the optimal elongation temperature (70-74°C) of Taq DNA polymerase. This speculation was then confirmed by the lack of amplification curve after 45 cycles of PCR with an elongation temperature of 70°C. This result suggested that in order to make Taq DNA polymerase work at the optimal elongation temperature of about 70°C the primers and probe must be modified.

3.2. Primers and probe modification

In order to get primers and probes that can be used at the optimum elongation temperature of Taq DNA polymerase, an array of derivatives of the China CDC primers targeting SARS-CoV-2 *ORF1ab* and *N* gene were designed and tested. The best pair of primers and probes were named as long-*ORF1ab* PF, long-*ORF1ab* PR, long-*ORF1ab* Probe, long-*N* PF, long-*N* PR and long-*N* Probe, respectively (Table 1). Their T_m values measured $72.49 \pm 0.03^\circ\text{C}$, $73.91 \pm 0.01^\circ\text{C}$, $78.82 \pm$

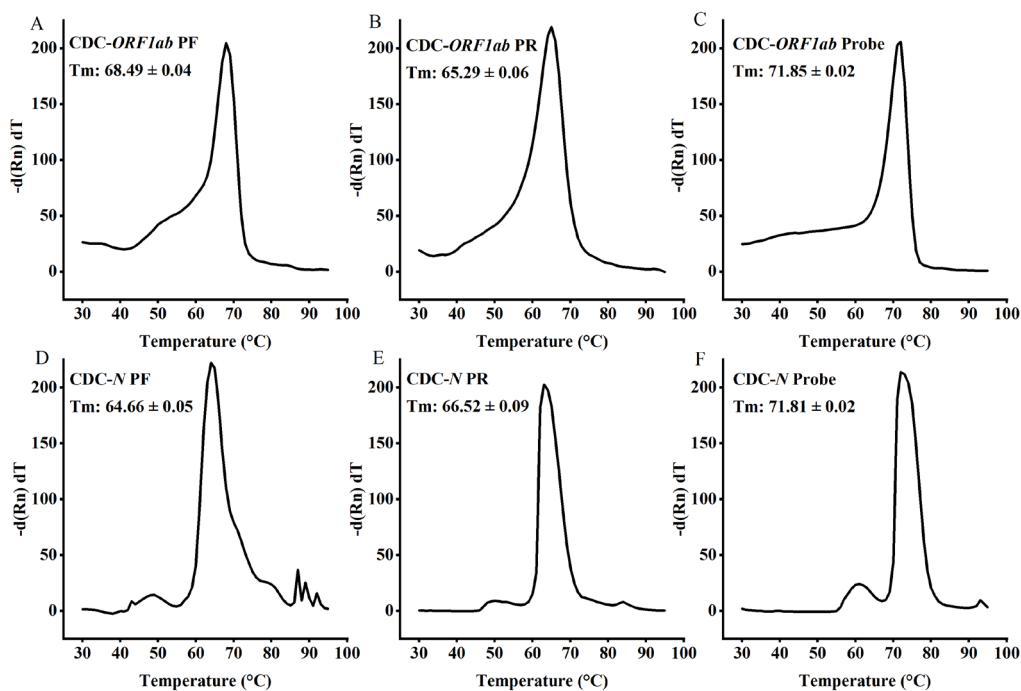


Figure 1. The melting curves of primers and probes designed by China CDC.

0.06°C, $73.22 \pm 0.07^\circ\text{C}$, $73.77 \pm 0.03^\circ\text{C}$ and $77.63 \pm 0.04^\circ\text{C}$, respectively (Figure 2). To monitor the sampling step of nucleic acid detection, we designed detection primers and probe targeting human ribonuclease P (*RP*) gene based on the same principle, named long-*RP* PF, long-*RP* PR and long-*RP* Probe. And their T_m values were $71.33 \pm 0.02^\circ\text{C}$, $73.49 \pm 0.08^\circ\text{C}$ and $79.56 \pm 0.05^\circ\text{C}$, respectively. Experiments indicated that these pairs of primers worked well at the elongation temperature of 70°C .

The commonly used Taqman probe has a 5'-fluorophore and 3'-quencher, named FQ probe. The probes (long-*ORF1ab* Probe, long-*N* Probe and long-*RP* Probe) with higher T_m value means longer distance

between the fluorophore and the quencher. This would greatly reduce the quenching efficiency and thus the signal-to-noise ratio (15). In order to solve this problem, the design of the probe must be changed. Taking long-*ORF1ab* Probe as research object, we then designed two kinds of probes for test: both probes have a fluorophore at 5' end and a quencher (BHQ1) at thymine 10 bases from the 5' end with the 3'-OH of probes sealed with another BHQ1 (for FQQ Probe) or Spacer C3 (for FQS Probe) to prevent elongation (Table 1). Experiment showed that both probes have a fluorescent background of 1% indicating a quenching efficiency of 99% for both (Figure 3). Under the same reaction conditions, the background signal of FQS Probe and FQQ Probe

Table 1. The sequences of primers and probes used in RT-qPCR test

| Primers | Sequence |
|-------------------------------|---|
| CDC- <i>ORF1ab</i> PF | 5'-CCCTGTGGGTTTTACTTAA-3' |
| CDC- <i>ORF1ab</i> PR | 5'-ACGATTGTGCATCAGCTGA-3' |
| CDC- <i>ORF1ab</i> Probe | 5'-VIC-CCGTCTGCGGTATGTGGAAAGTTATGG-BHQ1-3' |
| CDC- <i>N</i> PF | 5'-GGGGAAGTCTCTCTGCTAGAAT-3' |
| CDC- <i>N</i> PR | 5'-CAGACATTTTGTCTCAAGCTG-3' |
| CDC- <i>N</i> Probe | 5'-FAM-TTGTCTGCTGTGACAGATT-BHQ1-3' |
| long- <i>ORF1ab</i> PF | 5'-GACCCTGTGGGTTTTACTTAAAAACACAGTCTGT-3' |
| long- <i>ORF1ab</i> PR | 5'-AACGATTGTGCATCAGCTGACTGAAGCATGGGT-3' |
| long- <i>ORF1ab</i> Probe | 5'-VIC-CCGTCTGCGGTATGTGGAAAGTTATGGCTGTAGTTGTGATCAACTCCGC-BHQ1-3' |
| long- <i>ORF1ab</i> FQQ Probe | 5'-VIC-CCGTCTGCGGT-BHQ1-ATGTGGAAAGTTATGGCTGTAGTTGTGATCAACTCCGC-BHQ1-3' |
| long- <i>ORF1ab</i> FQS Probe | 5'-VIC-CCGTCTGCGGT-BHQ1-ATGTGGAAAGTTATGGCTGTAGTTGTGATCAACTCCGC-Spacer C3-3' |
| long- <i>N</i> PF | 5'-CCAGGCAGCAGTAGGGGAAGTCTCTCTGCTAGAATGGC-3' |
| long- <i>N</i> PR | 5'-GGCCTTGTGTTGTTGGCCTTTACCAGACATTTGCTCTCAAGCTG-3' |
| long- <i>N</i> Probe | 5'-FAM-TGGCGGTGATGCTGCTCTTGTCTTGTGCTGCTGCTTGACAG-BHQ1-3' |
| long- <i>N</i> FQS Probe | 5'-FAM-TGGCGGTGAT-BHQ1-GCTGCTCTGCTTGTGCTGCTGCTTGACAG-Spacer C3-3' |
| long- <i>RP</i> PF | 5'-CCTCGGCCATCAGAAGGAGATGAAGATTGTCTCCAGCTTCCA-3' |
| long- <i>RP</i> PR | 5'-GAGCCCAAGAGGCAAAGTTGCAGTGAGCCGAGATTG-3' |
| long- <i>RP</i> FQS Probe | 5'-ROX-TGGTCTCACT-BHQ2-CTGTACCCAGGCTGGAGTGCAGTGGC-Spacer C3-3' |

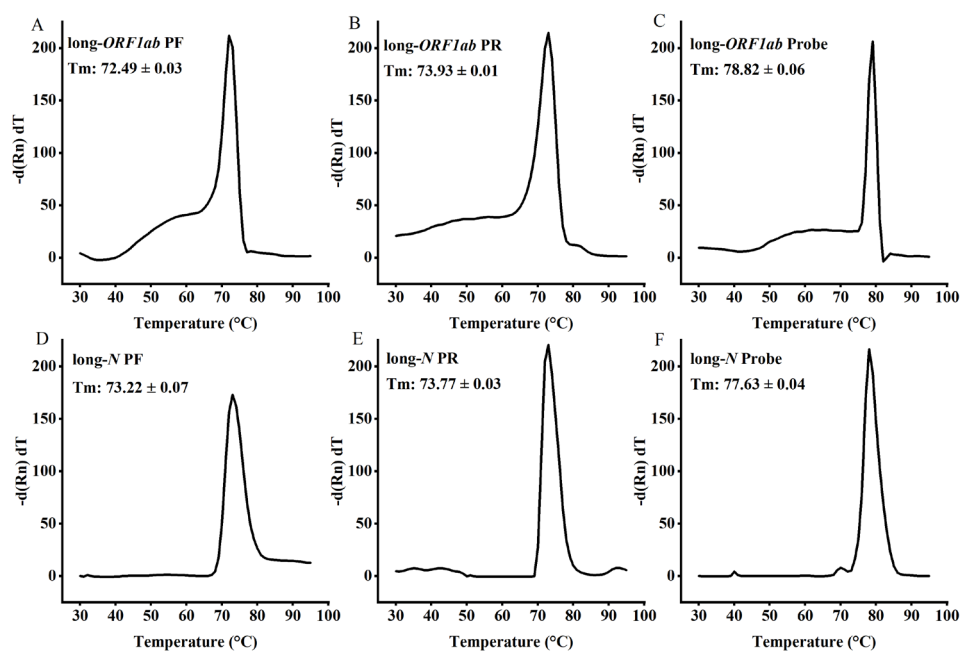


Figure 2. The melting curves of primers and probes that can work at the optimal elongation temperature of Taq DNA polymerase.

was about 1/6 of that of FQ Probe (Figure 4). Since the Spacer C3 group was cheaper than BHQ1 group, the FQS Probe was more cost-effective. And We designed the long-*N* FQS Probe and the long-*RP* FQS Probe according to the same principle.

3.3. The detection performance of the optimized primers and probe is excellent

The detection program of China CDC was taken as scheme 1 (CDC-*ORF1ab* PF, CDC-*ORF1ab* PR, CDC-*ORF1ab* Probe, CDC-*N* PF, CDC-*N* PR, CDC-*N* Probe, reaction program: reverse transcription in 55°C for 15 min followed by denaturation in 95°C for 30 s prior to undergoing 45 cycles of 95°C for 10 s and 60°C for 30 s). The primers and probe in scheme 1 were replaced with the optimized primers and probe, and the elongation temperature was changed from 60°C to 70°C, thus generating scheme 2 (long-*ORF1ab* PF, long-*ORF1ab* PR and long-*ORF1ab* FQS Probe, long-*N* PF, long-*N* PR and long-*N* FQS Probe, reaction program: reverse transcription in 55°C for 15 min followed by denaturation in 95°C for 30 s prior to undergoing 45 cycles of 95°C for 10 s and 70°C for 30 s). The limit of detection of scheme 2 was 500 copies/ml, which was consistent with that of scheme 1 (Table 2). Then a serial of PCR was carried out to reduce the elongation time at the elongation temperature of 70°C. Under four template concentrations, the Ct value of detection target remained unchanged when the elongation time was reduced from 30 s to 2 s. The Ct value increased when the elongation time was shorter than 2 s (Figure 5), indicating that the limit had been reached. In this case (Scheme 3), the limit

of detection can still reach 500 copies/mL.

In terms of specificity, when the template concentration was 10⁷ copies/mL, the Ct values of FAM channel and VIC channel were 23.29 and 23.37, respectively. When SARS-CoV, MERS-CoV, HCoV-

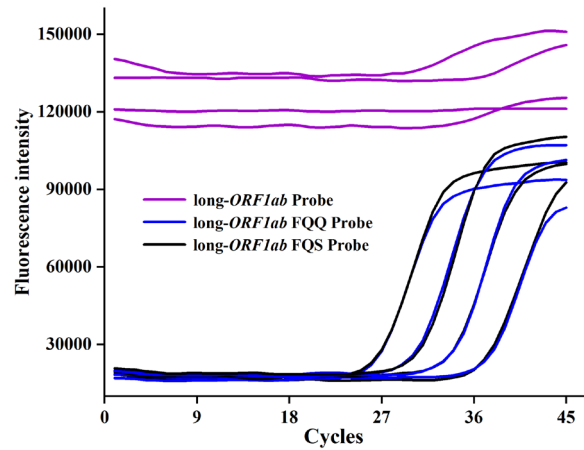


Figure 4. The raw data of RT-qPCR under four template concentrations using FQ, FQQ and FQS probes, respectively.

Table 2. Positive rate for schemes at different template concentrations

| Schemes | Sample concentrations (copies/ml) | | | | |
|----------|-----------------------------------|------|-----|-----|-----|
| | 1000 | 700 | 500 | 400 | 300 |
| Scheme 1 | 100% | 100% | 95% | 85% | 75% |
| Scheme 2 | 100% | 100% | 95% | 80% | 75% |
| Scheme 3 | 100% | 100% | 95% | 85% | 70% |
| Scheme 4 | 100% | 100% | 95% | 75% | 65% |

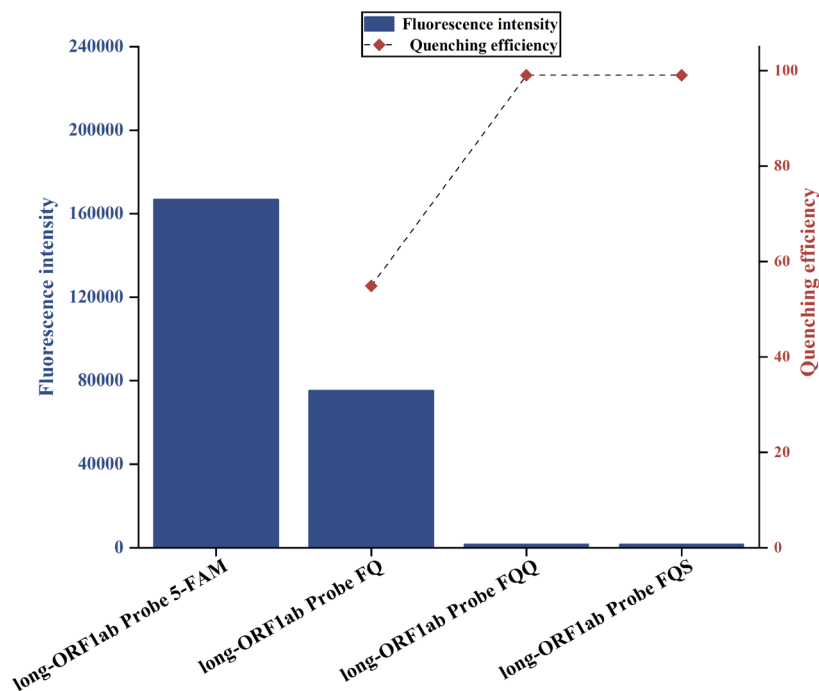


Figure 3. Fluorescence intensity of probes with different labeling types.

229E, HCoV-OC43, HCoV-NL63 and HCoV-HKU1 were used as templates, only SARS-CoV was amplified by the two detection channels, and the Ct values of FAM channel and VIC channel were 26.76 and 25.69, respectively. Amplification does not occur for other five HCoVs. Since the SARS virus has not been identified in the world since 2003, we thought that the specificity of scheme 3 was excellent.

These data indicated that Taq DNA polymerase do have a faster extension rate at 70°C in RT-qPCR reaction, and the time consumption was shortened from 74 min (Scheme 1) to 48 min (Scheme 3), which was 35.14% shorter than the China CDC standard procedure (Figure 6).

3.4. Optimization of reverse transcription and denaturation time to further reduced the time consumption

In order to further reduce the total time consumption,

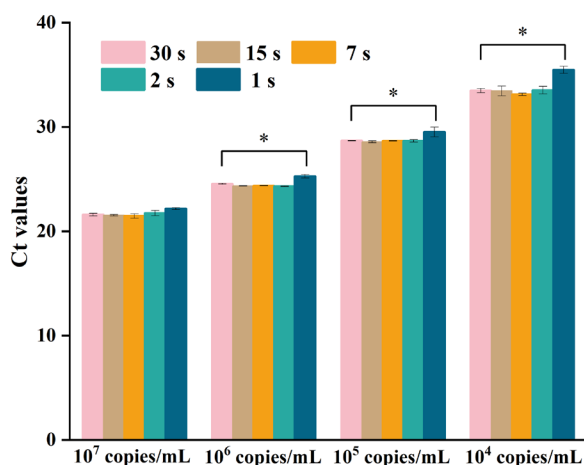


Figure 5. The RT-qPCR results under four template concentrations amplifying at 70°C for 30 s, 70°C for 15 s, 70°C for 7 s, 70°C for 2 s, 70°C for 1 s, respectively.

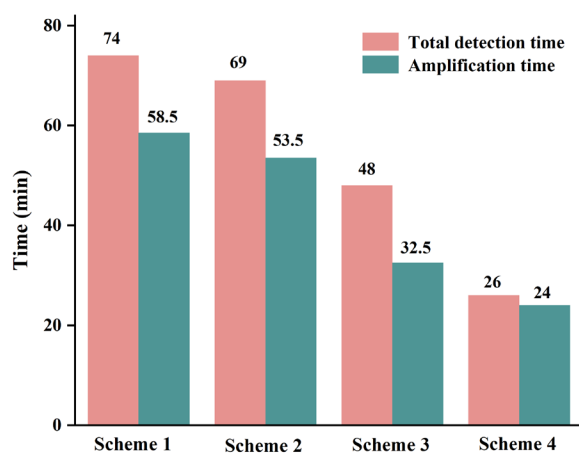


Figure 6. The total detection time and PCR amplification time of four schemes.

reverse transcription and denaturation time were also optimized based on scheme 3. Surprisingly, the limit of detection was still 500 copies/mL when the reverse transcription time was reduced from 15 min to 2 min and the denaturation time was reduced from 10 s to 1 s (scheme 4). The intra-group and inter-group coefficients of variation of the two detection channels were both less than 2.0%, indicating that scheme 4 had good repeatability (Table 3). In terms of detection time, the PCR amplification time and the total detection time of scheme 4 were 24 min and 26 min, respectively, which were 58.97% and 64.86% shorter than scheme 1 (Figure 6).

4. Discussion

RT-qPCR has long been used to detect a variety of pathogens and viruses (16-18). Rapid, accurate and low cost virus detection methods are critical for pandemic containment (19). On the one hand, rapid virus detection enables rapid tracking of primary contacts, prolongs therapeutic window and supports targeted treatment (20). On the other hand, it helps to interrupt the spread of the disease in the shortest time and at the lowest cost (21). In order to reduce time consumption, scientists have done a lot of work to improve the Taq DNA polymerase used in RT-qPCR: improving its reverse transcription activity for one-step detection (22,23); simplifying the Taq DNA polymerase by deleting unnecessary regions; improving the binding rate of Taq DNA polymerase to primer or template by combining Taq DNA polymerase with protein functional domain (Sso7d or Topo V) which can interact with DNA chain in the form of fusion protein (24,25); performing site-directed mutations and modifications to increase its elongation rate (26). There are also ways to increase the rate of temperature change by using special instruments and smaller reaction systems, such as droplet digital PCR (ddPCR), but this reduces the detection stability and throughput (27). Isothermal amplification has been viewed as a very successful method of diagnosis with high speed and sensitivity and no need for precise temperature control instruments (28,29), but most of the isothermal amplification systems include a complex enzyme system and special primers and probe, so have a high technical requirement (11,30).

In this research, by improving the T_m values of primers and probe, Taq DNA polymerase can be made to work at its optimal elongation temperature. This improvement combines with the optimization of the reverse transcription and denaturation time, finally reducing the detection time to 26 min on the premise that the limit of detection remained unchanged. The most important advantage of our strategy is this method can be implemented on a common RT-PCR instrument which has been popularized all over the world. Other methods, however, require updating instruments and thus may

Table 3. Repeatability analysis of primer pairs under different template concentrations

| | Template concentration (copies/mL) | Intra-group experiments | | Inter-group experiments | |
|-------------|------------------------------------|-------------------------|-------|-------------------------|-------|
| | | Ct Value (mean ± SD) | CV | Ct Value (mean ± SD) | CV |
| FAM channel | 10 ⁶ | 27.89 ± 0.17 | 0.61% | 27.92 ± 0.19 | 0.68% |
| | 10 ⁵ | 31.73 ± 0.21 | 0.66% | 31.81 ± 0.25 | 0.97% |
| | 10 ⁴ | 35.39 ± 0.36 | 1.02% | 35.50 ± 0.34 | 0.96% |
| VIC channel | 10 ⁶ | 27.71 ± 0.12 | 0.43% | 27.93 ± 0.37 | 1.32% |
| | 10 ⁵ | 31.83 ± 0.23 | 0.72% | 31.93 ± 0.22 | 0.69% |
| | 10 ⁴ | 35.25 ± 0.33 | 0.94% | 35.58 ± 0.36 | 1.01% |

cause heavy financial burden. A critical preanalytical step for real-time PCR assays, as well as any assay in which nucleic acid is analyzed, is nucleic acid extraction. Currently, in order to conserve human resources, all testing institutions utilize automatic nucleic acid extractors. And the extraction time is about 20-30 min. The optimized fast RT-qPCR system and nucleic acid extraction time can complete the detection within about an hour, greatly improving the detection efficiency.

Acknowledgements

We thank Zhifeng Li, Jing Zhu and Jinyao Qu at Analysis & Testing Center of SKLMT (State Key laboratory of Microbial Technology, Shandong University) for assistance in use of qTOWER3 instrument for RT-qPCR assays.

Funding: This work was supported by the Shandong Provincial Youth Innovation Team Development Plan of Universities (No. 2022KJ194), Jining Key Research and Development Program (No. 2022YXNS158), Shandong Provincial Key Research and Development Program (No. 2020CXGC011305), Health Science and Technology Development Program of Shandong Province (No. 202201050463), Taishan Scholars Project of Shandong Province (No. tsqn202103186) and the Innovation Project of Shandong Academy of Medical Sciences.

Conflict of Interest: We have filed a patent application on the design and use of the primers.

References

1. Coronaviridae Study Group of the International Committee on Taxonomy of V. The species severe acute respiratory syndrome-related coronavirus: Classifying 2019-nCoV and naming it SARS-CoV-2. *Nat Microbiol.* 2020; 5:536-544.
2. Huston NC, Wan H, Strine MS, de Cesaris Araujo Tavares R, Wilen CB, Pyle AM. Comprehensive *in vivo* secondary structure of the SARS-CoV-2 genome reveals novel regulatory motifs and mechanisms. *Mol Cell.* 2021; 81:584-598 e585.
3. Worldwide number of confirmed COVID-19 cases and deaths. <https://www.who.int/emergencies/diseases/novel-coronavirus-2019> (accessed December 18, 2022).
4. Lazarus JV, Ratzan SC, Palayew A, Gostin LO, Larson HJ, Rabin K, Kimball S, El-Mohandes A. A global survey of potential acceptance of a COVID-19 vaccine. *Nat Med.* 2021; 27:225-228.
5. Wang R, Hozumi Y, Yin C, Wei GW. Mutations on COVID-19 diagnostic targets. *Genomics.* 2020; 112:5204-5213.
6. Islam KU, Iqbal J. An update on molecular diagnostics for COVID-19. *Front Cell Infect Microbiol.* 2020; 10:560616.
7. Luo L, Liu D, Liao X, *et al.* Contact settings and risk for transmission in 3410 close contacts of patients with COVID-19 in Guangzhou, China : A prospective cohort study. *Ann Intern Med.* 2020; 173:879-887.
8. Yamayoshi S, Sakai-Tagawa Y, Koga M, *et al.* Comparison of rapid antigen tests for COVID-19. *Viruses.* 2020; 12:1420.
9. Ravi N, Cortade DL, Ng E, Wang SX. Diagnostics for SARS-CoV-2 detection: A comprehensive review of the FDA-EUA COVID-19 testing landscape. *Biosens Bioelectron.* 2020; 165:112454.
10. Esbin MN, Whitney ON, Chong S, Maurer A, Darzacq X, Tjian R. Overcoming the bottleneck to widespread testing: A rapid review of nucleic acid testing approaches for COVID-19 detection. *RNA.* 2020; 26:771-783.
11. Chen Y, Qian C, Liu C, Shen H, Wang Z, Ping J, Wu J, Chen H. Nucleic acid amplification free biosensors for pathogen detection. *Biosens Bioelectron.* 2020; 153:112049.
12. Zhou Y, Pei F, Ji M, Wang L, Zhao H, Li H, Yang W, Wang Q, Zhao Q, Wang Y. Sensitivity evaluation of 2019 novel coronavirus (SARS-CoV-2) RT-PCR detection kits and strategy to reduce false negative. *PLoS One.* 2020; 15:e0241469.
13. Nakura Y, Wu HN, Okamoto Y, Takeuchi M, Suzuki K, Tamura Y, Oba Y, Nishiumi F, Hatori N, Fujiwara S, Yasukawa K, Ida S, Yanagihara I. Development of an efficient one-step real-time reverse transcription polymerase chain reaction method for severe acute respiratory syndrome-coronavirus-2 detection. *PLoS One.* 2021; 16:e0252789.
14. Wu H, Zhang S, Chen Y, Qian C, Liu Y, Shen H, Wang Z, Ping J, Wu J, Zhang Y, Chen H. Progress in molecular detection with high-speed nucleic acids thermocyclers. *J Pharm Biomed Anal.* 2020; 190:113489.
15. Demuth J, Kantor M, Kucera R, Miletin M, Novakova V. Comparison of quenching efficiencies in long triple-labeled and double-labeled TaqMan oligodeoxynucleotide probes. *Bioconjug Chem.* 2022; 33:788-794.
16. Huang X, Chen J, Yao G, Guo Q, Wang J, Liu G. A TaqMan-probe-based multiplex real-time RT-qPCR for simultaneous detection of porcine enteric coronaviruses.

- Appl Microbiol Biotechnol. 2019; 103:4943-4952.
17. Vanneste K, Garland L, Broeders S, Van Gucht S, Roosens NH. Application of whole genome data for *in silico* evaluation of primers and probes routinely employed for the detection of viral species by RT-qPCR using dengue virus as a case study. BMC Bioinformatics. 2018; 19:312.
 18. Nagy A, Jirinec T, Jirincova H, Cernikova L, Havlickova M. *In silico* re-assessment of a diagnostic RT-qPCR assay for universal detection of Influenza A viruses. Sci Rep. 2019; 9:1630.
 19. Diao B, Wen K, Zhang J, Chen J, Han C, Chen Y, Wang S, Deng G, Zhou H, Wu Y. Accuracy of a nucleocapsid protein antigen rapid test in the diagnosis of SARS-CoV-2 infection. Clin Microbiol Infect. 2021; 27:289 e281-289 e284.
 20. Dinnes J, Deeks JJ, Berhane S, *et al.* Rapid, point-of-care antigen and molecular-based tests for diagnosis of SARS-CoV-2 infection. Cochrane Database Syst Rev. 2021; 3:CD013705.
 21. Taleghani N, Taghipour F. Diagnosis of COVID-19 for controlling the pandemic: A review of the state-of-the-art. Biosens Bioelectron. 2021; 174:112830.
 22. Bhadra S, Maranhao AC, Paik I, Ellington AD. One-enzyme reverse transcription qPCR using Taq DNA polymerase. Biochemistry. 2020; 59:4638-4645.
 23. Kranaster R, Drum M, Engel N, Weidmann M, Hufert FT, Marx A. One-step RNA pathogen detection with reverse transcriptase activity of a mutated thermostable *Thermus aquaticus* DNA polymerase. Biotechnol J. 2010; 5:224-231.
 24. Wang Y, Prosen DE, Mei L, Sullivan JC, Finney M, Vander Horn PB. A novel strategy to engineer DNA polymerases for enhanced processivity and improved performance *in vitro*. Nucleic Acids Res. 2004; 32:1197-1207.
 25. Pavlov AR, Belova GI, Kozyavkin SA, Slesarev AI. Helix-hairpin-helix motifs confer salt resistance and processivity on chimeric DNA polymerases. Proc Natl Acad Sci U S A. 2002; 99:13510-13515.
 26. Kim KP, Cho SS, Lee KK, Youn MH, Kwon ST. Improved thermostability and PCR efficiency of *Thermococcus celericrescens* DNA polymerase *via* site-directed mutagenesis. J Biotechnol. 2011; 155:156-163.
 27. Li H, Bai R, Zhao Z, Tao L, Ma M, Ji Z, Jian M, Ding Z, Dai X, Bao F, Liu A. Application of droplet digital PCR to detect the pathogens of infectious diseases. Biosci Rep. 2018; 38.
 28. Qi H, Yue S, Bi S, Ding C, Song W. Isothermal exponential amplification techniques: From basic principles to applications in electrochemical biosensors. Biosens Bioelectron. 2018; 110:207-217.
 29. Mattioli IA, Hassan A, Oliveira ON, Jr., Crespilho FN. On the challenges for the diagnosis of SARS-CoV-2 based on a review of current methodologies. ACS Sens. 2020; 5:3655-3677.
 30. Vermisoglou E, Panacek D, Jayaramulu K, Pykal M, Frebort I, Kolar M, Hajduch M, Zboril R, Otyepka M. Human virus detection with graphene-based materials. Biosens Bioelectron. 2020; 166:112436.
- Received October 24, 2022; Revised December 18, 2022; Accepted February 18, 2023.
- [§]These authors contributed equally to this work.
- *Address correspondence to:
Lichuan Gu, State Key Laboratory of Microbial Technology, Shandong University, 72 Binhai Road, Qingdao 266237, P.R. China.
E-mail: lcgu@sdu.edu.cn
- Kun Yin, Shandong Institute of Parasitic Diseases, Shandong First Medical University & Shandong Academy of Medical Sciences, 11 Taibaizhong Road, Jining 272033, P.R. China.
E-mail: Kyin@sdfmu.edu.cn
- Released online in J-STAGE as advance publication February 25, 2023.

Factors affecting health-related quality of life among firefighters during the COVID-19 pandemic: A single-center study

Yukihiro Shigeno^{1,2,§}, Yukihiro Mori^{3,4,§}, Kiyoshi Hotta⁴, Yuka Aoyama^{3,5}, Mamoru Tanaka⁶, Hana Kozai⁶, Makoto Aoike³, Hatsumi Kawamura³, Masato Tsurudome^{3,7}, Morihito Ito^{3,7,*}

¹ Center for Emergency Medical Technician Practicum Support, Chubu University, Aichi, Japan;

² The Fire Department Headquarters in Kasugai-City, Aichi, Japan;

³ Graduate School of Life and Health Sciences, Chubu University, Aichi, Japan;

⁴ Center for Nursing Practicum Support, Chubu University, Aichi, Japan;

⁵ Department of Clinical Engineering, College of Life and Health Sciences, Chubu University, Aichi, Japan;

⁶ Department of Food and Nutritional Sciences, College of Bioscience and Biotechnology, Chubu University, Aichi, Japan;

⁷ Department of Biomedical Sciences, College of Life and Health Science, Chubu University, Aichi, Japan.

SUMMARY During the coronavirus disease 2019 (COVID-19) outbreak, firefighters have been working in an environment that is both physically and mentally taxing. This study aimed to investigate factors affecting health-related quality of life (HRQOL) among firefighters in Japan during the COVID-19 pandemic. A total of 227 firefighters from a single firefighting organization were surveyed in June 2021, during the fourth infection spread period of COVID-19 in Japan. Regression analysis was performed to examine factors affecting HRQOL of firefighters measured with the SF-8. In the present study, factors affecting HRQOL among firefighters during the COVID-19 pandemic were lack of sleep, physical abnormalities due to infection control measures, exercise habits, living with family members, and history of suspected COVID-19 infection. The present findings may help develop support services for first responders, including firefighters during the COVID-19 pandemic.

Keywords COVID-19 pandemic, firefighters, health-related quality of life

1. Introduction

Severe acute respiratory syndrome coronavirus 2 (SARS-CoV-2), which causes the novel coronavirus disease 2019 (COVID-19), was first reported in Wuhan, China, in December 2019 (1). Shortly thereafter, the outbreak developed into a pandemic. As of September 2022, the total number of infected people in Japan is more than 20 million. A national lockdown introduced in Italy during the COVID-19 pandemic has had negative effects on mental health, anxiety, and sleep (2). In Japan, on April 7, 2020, the state of emergency was declared in seven prefectures, including Tokyo and Kanagawa; subsequently, from April 16 to May 31, 2020, the state of emergency was extended nationwide to prevent the spread of SARS-CoV-2. In October 2021, the state of emergency was declared for the fourth time in areas with high rates of infection spread. The state of emergency shortened restaurant operating hours and imposed a curfew and social distancing measures, including remote working, to help reduce the pressure on medical systems. During periods when the state of emergency was not

declared, the government continued to encourage social distancing and discouraged large indoor gatherings. Overall, the pandemic has affected lifestyle choices and socioeconomic conditions worldwide.

Since the outbreak, firefighters have been responding to emergency calls from confirmed and suspected COVID-19 patients and supporting treatment and transport activities. Fear of infection and the resulting anxiety increase the levels of emotional and physical strain that affect the ways in which duties are performed in the field. Additional concerns include worries about transmitting infection acquired at work to one's family or other cohabiting individuals. In South Florida, United States, the rate of infection among firefighters has been estimated at 8.9% (3), resulting in frequent leave of absence requests (4). Firefighters, as first responders, have a particularly high risk of contracting COVID-19; in addition, like their colleagues in the clinic, firefighters are susceptible to the psychological effects of the pandemic and require appropriate care and support (5). Early evidence from studies conducted in Germany has shown psychological effects of the pandemic on

frontline workers, including increased rates of anxiety and depression (6).

In Japan, the strain of the pandemic on doctors and nurses has received some public scrutiny, including discussions on the need for care and support. Meanwhile, the risks faced by firefighters and other emergency personnel have received little attention. Despite government guidance on infection control and health management among firefighters, leadership may only respond to individual cases. In addition, the evidence on health-related quality of life (HRQOL) among firefighters during the pandemic is scarce, making intervention design and implementation challenging.

The present study aimed to conduct a survey of firefighters working for a single organization to elucidate the impact of the pandemic on emergency responders' levels of HRQOL. We hypothesized that the factors listed in this study related to life, work, COVID-19, *etc.* would affect the HRQOL of firefighters during a COVID-19 pandemic. HRQOL was measured with the SF-8™ questionnaire (Japanese version), which is a shortened version of the SF-36 health survey, both of which have been previously used for HRQOL assessments (7). The SF-8 was used due to its brevity, helping make assessments straightforward.

2. Materials and Methods

2.1. Participants

The participants were firefighters who work for a firefighting team, rescue team, and ambulance services at a single front-line organization providing pre-hospital care. In the years studied, each team had 113, 24, and 92 placements, for a total of 229 people. This organization covers a population of approximately 310,000 people in the study area and receives approximately 13,000 emergency calls per year. During the COVID-19 pandemic, many of the participating firefighters were engaged in 24-hour workdays to account for the additional infection prevention and control protocols and equipment introduced since the start of the outbreak. In addition, the participants remained on duty during their shifts and responded to emergency calls.

This survey was conducted in mid-June 2021, in the middle of the fourth infection spread period of COVID-19 in Japan. During this period, lockdowns were introduced elsewhere in the world but not in Japan. However, some restrictions were introduced in the study area. In June 2021, the month in which the study was conducted, 160 COVID-19 patients (1 in June of the previous year) were reported for the month in the targeted city. The number of emergency calls in the city during the surveyed month was approximately 1,100 (previous year: approximately 990), of which 260 (previous year: approximately 200) were dispatched by the firefighting teams at the same time. The Fire and Disaster

Management Agency notified the fire department of the following points to keep in mind for the continuation of fire department operations in preparation for the spread of COVID-19: securing infection-prevention equipment and materials, thorough infection-prevention measures within the fire department, and quarantine for emergency personnel who were engaged in responding to infectious diseases.

This aims, objectives, and protocols of this study were presented to the fire department manager to obtain their consent for collaboration. The questionnaires were distributed through facility administrators and were filled out anonymously and individually before being sealed in submission envelopes and returned to the site administrators.

2.2. Survey

The participants' HRQOL was assessed with the SF-8™ Japanese version. The SF-8 consists of eight items: physical functioning (PF), role physical (RP), bodily pain (BP), general health (GH), vitality (VT), social functioning (SF), role emotional (RE), and mental health (MH), and reflects on health status over the past month. Each item is rated on a 5- or 6-point Likert scale; the scores are standardized, using 50 points as the national average score indicating normal health and functioning. Physical summary scores (PCS) and mental summary scores (MCS) were calculated by weighting the individual SF-8 item scores. For each factor, higher scores indicate better health. The Japanese version of the SF-8 is based on the 2017 nationwide survey of 3,286 Japanese residents and meets the standard criteria for content and construct validity (8,9). Cronbach's coefficient alpha was 0.841 in this study as well, confirming its reliability.

Data on the following demographic and clinical characteristics were collected: division affiliation, age, sex, living with family, sleep quality (lack of sleep), and exercise habits (1-2 times/week, 3-4 times/week, and 5-6 times/week). In addition, the participants were asked "yes" or "no" questions on their previous confirmed or suspected COVID-19 infection, vaccine uptake, Experience of transporting COVID-19 patients, and any physical abnormalities due to the infection control measures. Infection control measures here include wearing masks, face shields, gowns, and using disinfectant solutions.

2.3. Statistical analysis

The mean score for each SF-8 item was calculated and compared with the national standard value in Japan. Inter-group comparisons were performed using the Mann-Whitney *U* Test or Kruskal-Wallis test. The variables that were found to be significantly associated with each of the SF-8 items by this analysis were used

as independent variables, and regression analysis by the forced injection method was conducted with each of the SF-8 items as the dependent variables. In the regression analysis, variance inflation factor (VIF) was calculated to determine multicollinearity. The following variables were transformed into dummy variables (1, 0) and included in the model: living with a family member, lack of sleep, exercise habits, suspected COVID-19 infection status, experience of transporting COVID-19 patients, SARS-CoV-2 vaccination, and physical abnormalities due to infection control measures. In all statistical analyses, a significance level of $< 5\%$ was set. All analyses were performed in SPSS for windows (IBM Corp Armonk, NY, USA).

2.4. Ethics

The study was conducted in accordance with the principles of the Declaration of Helsinki and conducted with the approval of the Ethical Review Committee of Chubu University (Approval No.: 20200042). Written informed consent was obtained from the all participants of this study after they were provided a detailed explanation of the purpose of the study, methods involved, process of sample collection, and management of personal information.

3. Results

3.1. Participants

A total of 227 (99.1%) people were enrolled in this study. The response rate for each department was 90.2% for the

firefighting team, 91.7% for the rescue team, and 98.9% for ambulance services. Responses were obtained from a total of 222 (98.0%) respondents, with 215 (94%) valid responses. The sample was stratified by age, including 2 (1.0%), 79 (36.7%), 77 (35.8%), 49 (22.8%), 5 (2.3%), and 3 (1.4%) participants aged < 20 years, 20-29 years, 30-39 years, 40-49 years, 50-59 years, and > 60 years, respectively. This study included 208 (96.7%) males and 7 (3.3%) females.

3.2. Comparison with SF-8 standard values in Japan

The mean SF-8 item scores for the present study firefighting team, rescue team, and ambulance services, alongside the Japanese national standard values, are presented in Figure 1. The mean (standard deviation) bodily pain (48.85 ± 8.93 points) and social functioning (48.97 ± 7.42 points) scores in the present study were lower than the corresponding national average values (50.04 ± 8.17 points and 50.02 ± 7.17 points, respectively).

3.3. SF-8 item scores and participant characteristics

There was no difference in the SF-8 scores among affiliation, age, or sex groups (Table 1). Role physical ($p = 0.017$), general health ($p = 0.036$), and mental health ($p = 0.046$) scores were significantly higher in the participants that lived with family than in those that did not live with family. Physical functioning ($p = 0.005$), role physical ($p = 0.007$), bodily pain ($p = 0.024$), vitality ($p = 0.004$), social functioning ($p = 0.000$), role emotional ($p = 0.001$), mental health ($p =$

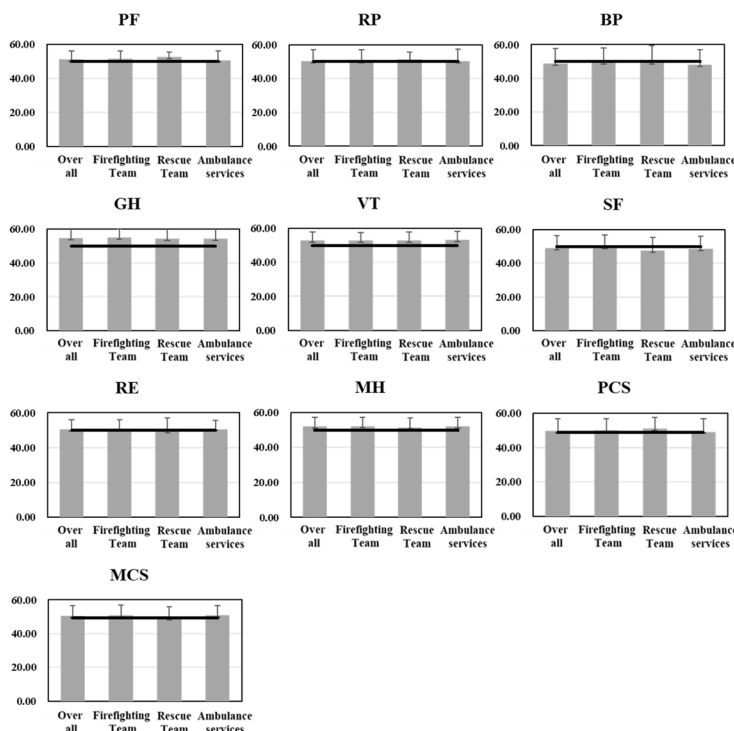


Figure 1. Comparison of SF-8 item scores with the national standard average values in Japan, stratified by firefighter and assignment. The black bold line represents the national standard average values in Japan. PF, physical functioning; RP, role physical; BP, bodily pain; GH, general health; VT, vitality; SF, social functioning; RE, role emotional; MH, mental health; PCS, physical summary scores; MCS, mental summary scores.

Table 1. Firefighter characteristics and SF-8 item scores

| Items | n | % | p-value | | | | | | | | | |
|------------------------------------|-----|------|---------|---------|--------|--------|---------|---------|---------|---------|--------|---------|
| | | | PF | RP | BP | GH | VT | SF | RE | MH | PCS | MCS |
| Affiliation | | | | | | | | | | | | |
| Firefighting team | 102 | 47.5 | 0.327 | 0.873 | 0.511 | 0.939 | 0.834 | 0.313 | 0.972 | 0.852 | 0.692 | 0.636 |
| Rescue team | 22 | 10.2 | | | | | | | | | | |
| Ambulance services | 91 | 42.3 | | | | | | | | | | |
| Age groups | | | | | | | | | | | | |
| < 20 | 2 | 1.0 | 0.340 | 0.855 | 0.355 | 0.808 | 0.257 | 0.543 | 0.426 | 0.712 | 0.501 | 0.894 |
| 20-29 | 79 | 36.7 | | | | | | | | | | |
| 30-39 | 77 | 35.8 | | | | | | | | | | |
| 40-49 | 49 | 22.8 | | | | | | | | | | |
| 50-59 | 5 | 2.3 | | | | | | | | | | |
| ≥ 60 | 3 | 1.4 | | | | | | | | | | |
| Sex | | | | | | | | | | | | |
| Male | 208 | 96.7 | 0.233 | 0.348 | 0.594 | 0.159 | 0.768 | 0.680 | 0.695 | 0.376 | 0.202 | 0.591 |
| Female | 7 | 3.3 | | | | | | | | | | |
| Living with family | | | | | | | | | | | | |
| Yes | 191 | 88.8 | 0.199 | 0.017* | 0.109 | 0.036* | 0.095 | 0.406 | 0.859 | 0.046* | 0.110 | 0.359 |
| No | 24 | 11.2 | | | | | | | | | | |
| Lack of sleep | | | | | | | | | | | | |
| Yes | 37 | 17.2 | 0.005** | 0.007** | 0.024* | 0.089 | 0.004** | 0.000** | 0.001** | 0.007** | 0.023* | 0.004** |
| No | 178 | 82.8 | | | | | | | | | | |
| Exercise frequency per week | | | | | | | | | | | | |
| 1 to 2 times | 76 | 35.4 | 0.399 | 0.568 | 0.542 | 0.030* | 0.366 | 0.281 | 0.888 | 0.824 | 0.487 | 0.961 |
| 3 to 4 times | 111 | 51.6 | | | | | | | | | | |
| ≥ 5 times | 28 | 13.0 | | | | | | | | | | |

PF, physical functioning; RP, role physical; BP, bodily pain; GH, general health; VT, vitality; SF, social functioning; RE, role emotional; MH, mental health; PCS, physical summary scores; MCS, mental summary scores; * $p < 0.05$; ** $p < 0.01$.

Table 2. SF-8 item scores stratified by COVID-19-related characteristics

| Items | n | % | p-value | | | | | | | | | |
|--|-----|------|---------|--------|--------|--------|-------|--------|---------|-------|-------|-------|
| | | | PF | RP | BP | GH | VT | SF | RE | MH | PCS | MCS |
| History of suspected COVID-19 infection | | | | | | | | | | | | |
| Yes | 28 | 13.0 | 0.408 | 0.376 | 0.024* | 0.048* | 0.130 | 0.114 | 0.083 | 0.407 | 0.171 | 0.668 |
| No | 187 | 87.0 | | | | | | | | | | |
| Experience of transporting COVID-19 patients | | | | | | | | | | | | |
| Yes | 151 | 70.2 | 0.086 | 0.207 | 0.289 | 0.729 | 0.210 | 0.028* | 0.949 | 0.770 | 0.234 | 0.729 |
| No | 64 | 29.8 | | | | | | | | | | |
| SARS-CoV-2 vaccination | | | | | | | | | | | | |
| Yes | 199 | 92.6 | 0.048* | 0.091 | 0.047* | 0.470 | 0.238 | 0.047* | 0.732 | 0.423 | 0.079 | 0.764 |
| No | 16 | 7.4 | | | | | | | | | | |
| Physical abnormalities due to the infection control | | | | | | | | | | | | |
| Yes | 30 | 14.0 | 0.062 | 0.028* | 0.046* | 0.357 | 0.079 | 0.011* | 0.003** | 0.081 | 0.123 | 0.088 |
| No | 185 | 86.0 | | | | | | | | | | |

PF, physical functioning; RP, role physical; BP, bodily pain; GH, general health; VT, vitality; SF, social functioning; RE, role emotional; MH, mental health; PCS, physical summary scores; MCS, mental summary scores; COVID-19, coronavirus disease 2019; SARS-CoV-2, severe acute respiratory syndrome coronavirus 2; * $p < 0.05$; ** $p < 0.01$.

0.007), physical summary scores ($p = 0.023$), and mental summary scores ($p = 0.004$) were significantly lower in the participants that reported insufficient sleep than in those that did not report insufficient sleep. Participants that exercised once or twice per week had significantly lower general health ($p = 0.030$) scores than the other groups.

3.4. SF-8 scores by COVID-19 status

The SF-8 scores associated with COVID-19-related items are presented in Table 2. The participants with history of

suspected infection had significantly lower bodily pain ($p = 0.024$) and general health ($p = 0.048$) scores than those without history of suspect an infection. The participants that had transported COVID-19 patients had significantly lower social functioning ($p = 0.028$) scores than those that did not transport any COVID-19 patients. The participants that had received the SARS-CoV-2 vaccine had significantly lower physical functioning ($p = 0.048$), bodily pain ($p = 0.047$), and social functioning ($p = 0.047$) scores than the participants that had not received the vaccine. The participants with physical abnormalities due to infection control had significantly lower role physical

Table 3. Regression analysis result

| Items | Partial regression coefficient | Standard partial regression coefficient | 95% CI | | p-value | |
|-------|---|---|-------------|-------------|---------|---------|
| | | | Lower limit | Upper limit | | |
| PF | Lack of sleep | -2.072 | -0.158 | -3.822 | -0.323 | 0.020* |
| | SARS-CoV-2 vaccination status | -2.164 | -0.114 | -4.680 | -0.353 | 0.092 |
| RP | Living with family | 2.518 | 0.119 | -0.262 | 5.297 | 0.076 |
| | Lack of sleep | -2.694 | -0.153 | -5.019 | -0.369 | 0.023* |
| | Physical abnormalities due to infection control measures | -3.196 | -0.119 | -5.733 | -0.660 | 0.014* |
| BP | Lack of sleep | -2.882 | -0.122 | -5.997 | 0.234 | 0.070 |
| | Suspected COVID-19 infection | -3.858 | -0.146 | -7.336 | -0.380 | 0.030* |
| | SARS-CoV-2 vaccination | -4.008 | -0.118 | -8.472 | 0.456 | 0.078 |
| | Physical abnormalities due to infection control measures | -3.030 | -0.118 | -6.428 | 0.368 | 0.080 |
| GH | Living with family | 2.643 | 0.143 | 0.207 | 5.080 | 0.034* |
| | Exercise frequency: 3-4 times/week (vs. 1-2 times/week) | 2.027 | 0.174 | 0.348 | 3.706 | 0.018* |
| | Exercise frequency ≥ 5 times/week (vs. 1-2 times/week) | 2.900 | 0.168 | 0.423 | 5.377 | 0.022* |
| | History of suspected COVID-19 infection | -2.162 | -0.125 | -4.450 | 0.127 | 0.064 |
| VT | Lack of sleep | -2.788 | -0.213 | -4.512 | -1.064 | 0.002** |
| SF | Lack of sleep | -4.001 | -0.204 | -6.629 | -1.373 | 0.003** |
| | Experience of transporting COVID-19 patients | -0.891 | -0.055 | -3.067 | 1.285 | 0.420 |
| | SARS-CoV-2 vaccination | -2.874 | -0.102 | -6.562 | 0.815 | 0.126 |
| | Physical abnormalities due to infection control measures | -3.037 | -0.142 | -5.825 | -0.250 | 0.033* |
| RE | Lack of sleep | -3.218 | -0.228 | -5.057 | -1.380 | 0.001** |
| | Physical abnormalities due to infection control measures | -2.381 | -0.155 | -4.384 | -0.378 | 0.020* |
| MH | Living with family | 2.819 | 0.173 | 0.675 | 4.963 | 0.010* |
| | Lack of sleep | -2.271 | -0.167 | -4.060 | -0.483 | 0.013* |
| PCS | Lack of sleep | -2.677 | -0.143 | -5.179 | -0.175 | 0.036* |
| MCS | Lack of sleep | -2.944 | -0.183 | -5.077 | -0.812 | 0.007** |

PF, physical functioning; RP, role physical; BP, bodily pain; GH, general health; VT, vitality; SF, social functioning; RE, role emotional; MH, mental health; PCS, physical summary scores; MCS, mental summary scores; COVID-19, coronavirus disease 2019; SARS-CoV-2, severe acute respiratory syndrome coronavirus 2; CI, confidence interval; * $p < 0.05$; ** $p < 0.01$.

($p = 0.028$), bodily pain ($p = 0.046$), social functioning ($p = 0.011$), and role emotional ($p = 0.003$) scores than the participants without any such abnormalities.

3.5. Regression analysis

Regression analysis revealed that physical functioning scores were associated with lack of sleep ($p = 0.020$). Role physical scores were associated with lack of sleep deprivation ($p = 0.023$) and physical abnormalities due to infection control ($p = 0.014$). Bodily pain scores were associated with a history of suspected infection ($p = 0.030$). General health scores were significantly associated with the co-residence status ($p = 0.034$), exercising 3-4 times/week or more (vs. 1-2 times/week) ($p = 0.018$), and exercising > 5 times/week (vs. 1-2 times a week) ($p = 0.022$). Vitality scores were associated with lack of sleep ($p = 0.002$). Social functioning scores were significantly associated with lack of sleep ($p = 0.003$) and physical abnormalities due to infection control measures ($p = 0.033$). Role emotional scores were significantly associated with the experience of lack of sleep ($p = 0.001$) and physical abnormalities due to infection control ($p = 0.020$). Mental health scores were significantly related to living with family ($p = 0.010$) and perceived lack of sleep ($p = 0.013$). There was a significant relationship between physical summary scores and lack of sleep ($p = 0.036$). There was a significant relationship between

mental summary scores and lack of sleep ($p = 0.007$) (Table 3). Multicollinearity between each independent variable was not identified.

4. Discussion

This study investigated factors affecting HRQOL among firefighters affiliated with a single organization during the fourth COVID-19 epidemic in Japan. Lack of sleep, exercise habits, living with family members, history of suspected COVID-19 infection, and physical abnormality due to infection control measures are associated with HRQOL of firefighters. This is the first study to investigate the HRQOL of firefighters in the context of the COVID-19 pandemic in Japan.

In simple comparisons, bodily pain and social functioning scores of the present study participants were lower than those of the general Japanese population. A previous study noted that firefighters had a higher prevalence of musculoskeletal symptoms than the general population due to occupational stress (10). The present study subjects may have experienced extra workload and increased burden of infection control due to the COVID-19 pandemic, which may have led to physical pain. This evidence suggests that firefighters may require interventions to ease their physical and mental burdens. The low social functioning scores indicate that firefighters have reduced social interaction with family,

friends, and neighbors, which may affect their social functioning during the COVID-19 pandemic. Therefore, the requirement to self-isolate to prevent infection spread may be a source of concern for firefighters. However, to the best of our knowledge, only a limited number of studies have examined health-related quality of life using the scale we used (SF-8) in firefighter team, rescue team, and ambulance services. In addition, prior studies (11) did not present data for each subitem such as bodily pain and social functioning for firefighters. Therefore, it was difficult to compare data from this study with data from before the COVID-19 pandemic.

We hypothesized that the COVID-19 outbreak would have a particularly detrimental effect on HRQOL of paramedics who have frequent contact with suspected infected patients. However, in the present study, there was no difference in the SF-8 scores among the participants affiliated with different divisions. Therefore, first responders requiring support during the COVID-19 pandemic include all ambulance, fire-fighting, and rescue teams. Firefighters respond to emergency calls, including fires, and rescue and ambulance calls. In Japan, there are numerous fire department; firefighters are trained and expected to respond to emergency calls.

Prolonged COVID-19 pandemic may increase the risk to physical and psychological illness, including burnout (12,13). This finding suggests the need for interventions to protect the HRQOL of first responders, such as firefighters. Social isolation has been identified as a risk factor for death (14), which is a cause of concern during the COVID-19 pandemic. In the present study, the firefighters who lived with their families had higher general health and mental health scores, suggesting that family support increases HRQOL and helps their physical and mental health.

Stress is a major cause of insomnia (15). Frontline staff managing patients with suspected or confirmed COVID-19 diagnosis report high rates of insomnia, anxiety, and depression (16,17). In the present study, physical functioning, role physical, vitality, social functioning, role emotional, mental health, physical summary scores, and mental summary scores were affected by the lack of sleep. Firefighters suffer from sleep disorders due to the nature of their work (18). In addition, the response to the COVID-19 pandemic required that working hours be extended, reducing rest and sleep time, both of which may have affected the SF-8 item scores.

Physical infection control measures affected role physical, social functioning, and role emotional scores possibly due to their increased use when responding to emergency calls during the COVID-19 pandemic. Previous studies have reported the negative impact of personal protective equipment use on the physical and mental health of healthcare workers (19). Wearing personal protective equipment above and beyond that required for routine activities may exacerbate physical

and mental fatigue and affect performance due to factors such as heat stress, hearing and vision impairment, and restricted movement (19). Although the use of personal protective gear during the COVID-19 pandemic is necessary to manage infection risks, it may also affect physical and mental health.

Exercise habits had positive effects on general health scores. Physical activity and exercise help reduce the levels of anxiety, stress, and depression, and improve overall physical and mental health (20). The present findings suggest that even among the participants that were required to change their lifestyle and social habits, engaging in exercise may help reduce the levels of depression and anxiety, and maintain well-being during the COVID-19 pandemic.

In this study, firefighters with a history of suspected COVID-19 infection were found to have lower bodily pain scores. Suspected COVID-19 infection increases the levels of stress and anxiety and may cause disruptions to the activities of daily living. Meanwhile, stress and anxiety can develop into subjective symptoms of pain, which may affect job performance. Previous studies have examined the impact of the COVID-19 pandemic on pain levels (21). Cases of suspected infection may be impossible to avoid among firefighters; however, support systems for suspected cases should be strengthened to help reduce work- and life-related stress levels.

This study had several limitations. First, this study had a small sample size and was based at a single center, which limits the generalizability of the present findings. Second, lack of sleep, living with family members, and exercise habits may contribute to HRQOL outside of the COVID-19 pandemic. Third, this study was cross-sectional, observing effects in June 2021, and precluding any conclusions about changes over time. Finally, the SF-8 questionnaire measures HRQOL by retrospectively assessing each item during the previous month; consequently, the present study did not assess the entire period between the initial COVID-19 outbreak and it becoming a pandemic.

However, the strength of this study is that it is first to examine the determinants of HRQOL among firefighters in Japan during the pandemic. The present findings may be used to design future interventions aimed at supporting first responders providing pre-hospital care in contexts associated with high risks of infection.

5. Conclusions

In the present study, factors affecting HRQOL among firefighters during the COVID-19 pandemic were lack of sleep, exercise habits, living with family members, history of suspected COVID-19 infection, and physical abnormalities due to infection control measures. The present findings may inform the development of interventions aimed at supporting first responders, such as firefighters, in future pandemics.

Acknowledgements

We greatly appreciate all firefighters for their participation in this study. We would like to thank Editage (www.editage.com) for English language editing.

Funding: This work was supported by the Chubu University under Grant [number 21M09R].

Conflict of Interest: The authors have no conflicts of interest to disclose.

References

- Zhu N, Zhang D, Wang W, *et al.* A novel coronavirus from patients with pneumonia in China, 2019. *N Engl J Med.* 2020; 382:727-733.
- Gualano MR, Lo Moro G, Voglino G, Bert F, Siliquini R. Effects of Covid-19 lockdown on mental health and sleep disturbances in Italy. *Int J Environ Res Public Health.* 2020; 17:4779
- Caban-Martinez AJ, Schaefer-Solle N, Santiago K, Louzado-Feliciano P, Brotons A, Gonzalez M, Issenberg SB, Kobetz E. Epidemiology of SARS-CoV-2 antibodies among firefighters/paramedics of a US fire department: a cross-sectional study. *Occup Environ Med.* 2020; 77:857-861.
- Prezant DJ, Zeig-Owens R, Schwartz T, Liu Y, Hurwitz K, Beecher S, Weiden MD. Medical leave associated with COVID-19 among emergency medical system responders and firefighters in New York city. *JAMA Netw Open.* 2020; 3:e2016094.
- DePierro J, Lowe S, Katz C. Lessons learned from 9/11: Mental health perspectives on the COVID-19 pandemic. *Psychiatry Res.* 2020; 288:113024.
- Skoda EM, Teufel M, Stang A, Jöckel KH, Junne F, Weismüller B, Hetkamp M, Musche V, Kohler H, Dörrle N, Schweda A, Bäuerle A. Psychological burden of healthcare professionals in Germany during the acute phase of the COVID-19 pandemic: differences and similarities in the international context. *J Public Health (Oxf).* 2020; 42:688-695.
- Lefante JJ, Harmon GN, Ashby KM, Barnard D, Webber LS. Use of the SF-8 to assess health-related quality of life for a chronically ill, low-income population participating in the Central Louisiana Medication Access Program (CMAP). *Qual Life Res.* 2005; 14:665-673.
- Kiyohara K, Itani Y, Kawamura T, Matsumoto Y, Takahashi Y. Changes in the SF-8 scores among healthy non-smoking school teachers after the enforcement of a smoke-free school policy: a comparison by passive smoke status. *Health Qual Life Outcomes.* 2010; 8:44.
- Tokuda Y, Okubo T, Ohde S, Jacobs J, Takahashi O, Omata F, Yanai H, Hinohara S, Fukui T. Assessing items on the SF-8 Japanese version for health-related quality of life: a psychometric analysis based on the nominal categories model of item response theory. *Value Health.* 2009; 12:568-573.
- Kim MG, Kim KS, Ryoo JH, Yoo SW. Relationship between occupational stress and work-related musculoskeletal disorders in Korean male firefighters. *Ann Occup Environ Med.* 2013; 25:9.
- Vinnikov D, Tulekov Z, Akylzhanov A, Romanova Z, Dushpanova A, Kalmatayeva Z. Age and work duration do not predict burnout in firefighters. *BMC Public Health.* 2019; 19:308.
- Soto-Rubio A, Giménez-Espert MDC, Prado-Gascó V. Effect of emotional intelligence and psychosocial risks on burnout, job satisfaction, and nurses' health during the COVID-19 pandemic. *Int J Environ Res Public Health.* 2020; 17:7998.
- Smith TD, DeJoy DM, Dyal MA, Huang G. Impact of work pressure, work stress and work-family conflict on firefighter burnout. *Arch Environ Occup Health.* 2019; 74:215-222.
- Elovainio M, Hakulinen C, Pulkki-Råback L, Virtanen M, Josefsson K, Jokela M, Vahtera J, Kivimäki M. Contribution of risk factors to excess mortality in isolated and lonely individuals: an analysis of data from the UK Biobank cohort study. *The Lancet Public Health.* 2017; 2:e260-e266.
- Kalmbach DA, Anderson JR, Drake CL. The impact of stress on sleep: Pathogenic sleep reactivity as a vulnerability to insomnia and circadian disorders. *J Sleep Res.* 2018; 27:e12710.
- Firew T, Sano ED, Lee JW, Flores S, Lang K, Salman K, Greene MC, Chang BP. Protecting the front line: A cross-sectional survey analysis of the occupational factors contributing to healthcare workers' infection and psychological distress during the COVID-19 pandemic in the USA. *BMJ Open.* 2020; 10:e042752.
- Zhang C, Yang L, Liu S, Ma S, Wang Y, Cai Z, Du H, Li R, Kang L, Su M, Zhang J, Liu Z, Zhang B. Survey of insomnia and related social psychological factors among medical staff involved in the 2019 novel coronavirus disease outbreak. *Front Psychiatry.* 2020; 11:306.
- Khan WAA, Conduit R, Kennedy GA, Abdullah Alslamah A, Ahmad Alsuwayeh M, Jackson ML. Sleep and mental health among paramedics from Australia and Saudi Arabia: A comparison study. *Clocks Sleep.* 2020; 2:246-257.
- Ruskin KJ, Ruskin AC, Musselman BT, Harvey JR, Nesthus TE, O'Connor M. COVID-19, personal protective equipment, and human performance. *Anesthesiology.* 2021; 134:518-525.
- Peluso MA, Guerra de Andrade LH. Physical activity and mental health: The association between exercise and mood. *Clinics (Sao Paulo).* 2005; 60:61-70.
- Majumdar P, Biswas A, Sahu S. COVID-19 pandemic and lockdown: Cause of sleep disruption, depression, somatic pain, and increased screen exposure of office workers and students of India. *Chronobiol Int.* 2020; 37:1191-1200.

Received November 8, 2022; Revised January 21, 2023; Accepted January 24, 2023.

[§]These authors contributed equally to this work.

*Address correspondence to:

Morihiro Ito, Department of Biomedical Sciences, College of Life and Health Sciences, Chubu University, 1200 Matsumoto-cho, Kasugai, Aichi 487-8501, Japan.

E-mail: m-ito@isc.chubu.ac.jp

Released online in J-STAGE as advance publication February 2, 2023.

Verification study on the catheterization of an upper arm vein using the new long peripheral intravenous catheter to reduce catheter failure incidence: A randomized controlled trial

Ryoko Murayama^{1,2}, Mari Abe-Doi^{1,3}, Yosuke Masamoto⁴, Kosuke Kashiwabara⁵,
Chieko Komiyama^{6,7}, Hiromi Sanada^{3,8}, Mineo Kurokawa^{4,*}

¹Department of Advanced Nursing Technology, Graduate School of Medicine, The University of Tokyo, Tokyo, Japan;

²Research Center for Implementation Nursing Science Initiative, Fujita Health University, Aichi, Japan;

³Department of Gerontological Nursing/Wound Care Management, Graduate School of Medicine, The University of Tokyo, Tokyo, Japan;

⁴Department of Hematology and Oncology, The University of Tokyo Hospital, Tokyo, Japan;

⁵Clinical Research Promotion Center, The University of Tokyo Hospital, Tokyo, Japan;

⁶Nursing Department, The University of Tokyo Hospital, Tokyo, Japan;

⁷Lifelong Learning Center IUHW, International University of Health and Welfare, Tokyo, Japan;

⁸Ishikawa Prefectural Nursing University, Ishikawa, Japan.

SUMMARY Intravenous infusion using a peripheral intravenous catheter (PIVC) is often complicated by catheter failure (CF). We hypothesized that catheterization of an upper arm vein instead of a forearm vein may help prevent CF. This study was designed to compare the incidence of CF in patients receiving hyper-stimulant drugs when catheters are placed in the forearm using short PIVCs (SPCs) with that when catheters are placed in the upper arm using the new long PIVCs. Patients admitted to a university hospital in Tokyo, Japan were enrolled in this study and were assigned to the SPC or the new long PIVC group. The primary outcome was the incidence of CF until 7 days. The secondary outcomes were the number of CFs per 1,000 days, the duration of the indwelling catheter, and the presence of thrombi and subcutaneous edema. Forty-seven patients were analyzed (median age, 67.0 years). The incidence of CF was 0% in the new long PIVCs and 32.0% (8 catheters) in the SPCs ($p = 0.007$), and the number of CF per 1,000 days was 0/1,000 and 81.7/1,000 days, respectively ($p = 0.001$). A significant difference in the duration of the indwelling catheter until CF occurrence was observed between the two groups ($p = 0.004$). Thrombi and subcutaneous edema were observed more frequently in the SPC group ($p < 0.001$). Catheterization of an upper arm vein using the new long PIVC to administer a hyper-stimulant drug might reduce CF compared with catheterization of a forearm vein using SPC.

Keywords Catheter failure, vascular access device, adverse event, catheterization site, intravenous infusion therapy

1. Introduction

Intravenous infusion therapy is a widely used treatment modality worldwide, with peripheral intravenous catheter (PIVC) devices being used frequently, in > 70% of hospitalized patients (1,2). Despite the usefulness of intravenous infusion therapy, catheter failures (CFs) are common, characterized by signs and symptoms, including redness, swelling, pain, and occlusion (insufficient infusion volume), and CF makes it difficult to continue infusion *via* PIVCs (3). The incidence rates of CF have been reported to range from 30-69% (4-6). We previously reported that approximately 18% of

catheters were removed because of CF in adult inpatient wards at a tertiary university hospital in Japan (7). CFs lead to patient suffering, healthcare provider workload, and higher healthcare costs; thus, the prevention of CFs is critically important (8).

The main cause of CF is damage to vascular endothelial cells due to mechanical stimulation by the catheters and chemical stimulation by the infusate (9-12). To minimize mechanical and chemical stimulation to vascular endothelial cells, it is recommended that the catheter is placed in a vessel with a larger diameter and abundant blood flow. The veins of the upper arm can meet these conditions better than those of the forearm

(13). However, no guidelines recommend a specific venous site in the upper arm for PIVC placement during chemotherapy even though forearm veins are exposed to chemical stimuli, such as irritants and vesicant drugs. To compare different insertion sites, different PIVCs are needed; PIVCs with sufficient length (long PIVC: 6-15 cm in length) (14) should be used for upper arm veins, which are generally deeper than forearm veins, to reach the blood-flow-rich axillary area, whereas short peripheral catheters (SPCs) are sufficient and suitable for forearm veins.

This study designed to compare the incidence of CFs between different insertion sites in patients receiving hyper-stimulant drugs: SPCs placed in a forearm vein versus new long PIVCs instead into an upper arm vein.

2. Methods

2.1. Trial design

This study adopted a parallel group open-label randomized trial design. Randomization was performed using the stratified permuted block method, where the stratification factor was the administration of anticancer drugs or other irritant drugs.

2.2. Study setting and participants

This study was conducted at the Hematology and Oncology Department of the University of Tokyo Hospital, Tokyo, Japan, between August 2021 and March 2022. The inclusion criteria were as follows: hospitalized patients over 19 years old who underwent the first catheterization at the hospitalization and had planned administration of hyper-stimulant drugs, such as those with an osmotic pressure ratio ≥ 3 , or irritant or vesicant drugs, including anticancer drugs. The exclusion criteria were as follows: patients who were scheduled for a chemotherapeutic regimen with continuous administration of vesicant drugs for more than 24 h, those with skin disorders at the planned puncture site, those with preexisting peripheral neuropathy, those with a history of thrombosis, those with stage \geq stage G3a chronic kidney disease, those with abnormal blood coagulation test or bleeding tendency (prothrombin-international normalized ratio (PT-INR) ≥ 1.5 ; activated partial thromboplastin time (APTT) ≥ 36.1 s, or the use of anticoagulant or antiplatelet drugs), and those who were scheduled to undergo invasive procedures (e.g., endoscopy and bronchoscopy). Other patients judged to be inappropriate for participation in this study by the physician in charge were also excluded.

All participants were given the explanation for this study, read the study's description, and signed a consent form. The study protocol was approved by the Research Ethics Committee of the Graduate School of Medicine and Institutional Review Board, The University of Tokyo

(2021502SP). The trial protocol was registered and published in the Japan Registry of Clinical Trials: jRCT (protocol number: jRCTs032210224).

2.3. Intervention

The participants were assigned to the long PIVC group (New-PIVC group) placed in the upper arm vein and the short PIVC group (SPC group) placed in a forearm vein.

Long PIVC group (New-PIVC group) We used new-PIVCs (Terumo Corp. Tokyo, Japan) as long PIVCs (New-PIVCs). Because there are no approved long catheters in Japan and the safety of these new-PIVCs has been confirmed, we decided to use them, although they are unapproved vascular access devices (VAD) (15). The catheter length was 88 mm to enable us to reach the upper arm vein and place the catheter tip near the vicinity of the axillary vein. The size was 22 gauge (outer diameter: 0.9 mm); the catheter was made of polyurethane and did not have a built-in guidewire. With the two-person method, trained nurses performed the catheterization procedure using a tourniquet and applied the aseptic/no-touch technique with 1% chlorhexidine alcohol under ultrasound guidance.

Short PIVC group (SPC group) We used plastic cannula-type sterile puncture needles (Surshield[®] Surflo[®] ii, Terumo Corp. Tokyo, Japan) as short PIVCs (SPCs). The length/gauge of the catheter was 25 mm/22 gauge (outer diameter: 0.9 mm) or 19 mm/24 gauge (outer diameter: 0.7 mm). Physicians performed the catheterization procedure with a tourniquet and applied the aseptic/no-touch technique with 0.2% chlorhexidine gluconate or 81.4 vol% ethanol under inspection and palpation, according to the usual routine practice of the department.

2.4. Outcomes

The primary outcome of this study was the incidence of CF. CF was defined as unscheduled catheter removal due to signs and symptoms such as pain, swelling, redness, and occlusion before the completion of treatment until 7 days (24 h \times 7 days), which was judged by physicians or staff nurses.

The secondary outcomes were the number of CFs per 1,000 days, the duration of the indwelling catheter until CF occurrence, and the presence of a thrombus in the vessel and subcutaneous edema. Catheter placement and pain when the needle was punctured, during the insertion of the catheter and during postural changes during catheter placement were subjectively evaluated. Although the period of indwelling was set at 24 h \times 7 days in the protocol, there were cases in which the catheter continued to be used thereafter within the day of removal, at the discretion of the physician in charge. In such cases, the survival analysis was censored at 24 h \times 7 days. Ultrasonographic images were obtained to

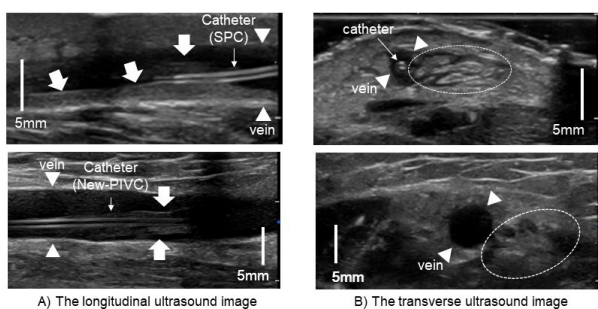


Figure 1. Samples of cases with the intravenous thrombus or the subcutaneous edema: SPCs on top; New-PIVCs on bottom. (A) Allow shows the intravenous thrombus: a marked echogenic mass with an uneven surface on the vessel wall or surround body or tip of catheter (16). **(B)** Dotted circle shows the subcutaneous edema (Mild or Severe): 1) Normal: the superficial fascia was clearly confirmed with no thickened subcutaneous fat layer, 2) Mild: the superficial fascia was confirmed with an unclear layered structure and a thickened subcutaneous fat layer, 3) Severe: a thickened subcutaneous fat layer was confirmed by a homogeneous cobblestone appearance in the subcutaneous fat layer, caused by excessive fluid in the interstitium (17).

detect thrombi in the vessel and subcutaneous edema at catheter removal. These images of subcutaneous tissue and vessel between the puncture point and catheter tip were taken using ultrasonography with two-dimensional linear-array transducers (6-13 MHz, FC1-X VA; Fujifilm, Tokyo, Japan) by research nurses trained for probe manipulation and interpretation of an image by a sonographer. Intravenous thrombi and subcutaneous tissue were assessed based on the classification described previously (Figure 1) (16,17). The removed catheter was documented photographically, and the angle of the base of the catheter was measured using ImageJ (National Institutes of Health: NIH). Painful catheterization was subjectively evaluated and confirmed using questionnaires with the visual analog scale.

We obtained data on the patients' characteristics (*i.e.*, diagnosis, medical history, oral medication, age, sex, body mass index, and the number of past regimens), blood test data on admission (*i.e.*, total protein, albumin, hematocrit, platelet count, differential white blood cell counts, C-reactive protein, prothrombin time, PT-INR, APTT, and fibrinogen), the length of hospital stay, and the rate and dosage of the infusate from the clinical records. We obtained data on the catheters and their insertion procedures, including catheter size, the number of punctures, and the distance between the elbow joint and the puncture point.

2.5. Sample size

We set the rate of CF occurrence as 5% in the New-PIVC group and 40% in the SPC group, with an effect size of 35%, according to our previous studies, which showed a CF incidence of 43.2% using SPCs (12) and 0% using the new PIVCs inserted into the upper arm vein (no events in eight cases) (15). With a two-sided statistical significance level of 0.05, and a power of 0.8,

we estimated that the number of indwelling catheters needed would be 26 for each group.

2.6. Randomization and blinding

The Electronic Data Capture (EDC) system (ViedocTM 4) of the University Hospital Clinical Trial Alliance Clinical Research Support System was applied for an assignment; therefore, sequence generation and allocation concealment mechanisms were conducted automatically. While the staff nurses, physicians, and patients were not blinded because this was difficult due to the nature of the intervention, the research nurses interpreting the ultrasound images were blinded.

2.7. Research procedure

Informed consent was obtained from the patients with confirmed eligibility, who were subsequently assigned to either group by the EDC system. The patients in the New-PIVC group underwent the catheterization procedure in the treatment room, and those in the SPC group underwent the catheterization procedure at the bedside. After catheter fixation, a photograph of the insertion site was taken, and the patient responded to the subjective evaluation questionnaire. Staff nurses observed the puncture site and the surrounding area thrice a day until 24 h after catheter removal, and the researchers macroscopically observed the same area and interviewed patients and staff nurses once a day to get information on the signs and symptoms of CFs. When the catheter required removal, the insertion site was documented by photographs, and the vessel and subcutaneous tissues were observed using ultrasonography at removal. The research nurses took a photograph of the removed catheter for analysis.

2.8. Statistical analysis

Data were analyzed using Statistical Package for the Social Sciences (ver. 23.0; IBM Corp., Armonk, NY, USA) and SAS (ver. 9.4; SAS Institute Inc., Cary, NC, USA). Statistical significance was set at a two-tailed p -value < 0.05 .

Continuous variables were expressed as means with standard deviations (SD) or medians with interquartile ranges (IQR). Statistical differences in the nominal variables between the two groups were tested using Pearson's chi-square test or Fisher's exact test, and those in the continuous variables were tested using Student's t -test or Mann-Whitney U -test after the confirmation of normal distribution.

The incidence rate of CFs and the number of CFs per 1,000 days were calculated as the number of CFs divided by the number of catheters used for infusion of irritant drugs (%) and per 1,000 catheter days. The risk difference and its two-sided 95% confidence interval

(CI) were calculated. Furthermore, the difference in CFs per 1,000 catheter days between the two groups was calculated using Poisson regression in which the treatment arm was included as a covariate. The duration of the indwelling catheter until CF occurrence in each group was shown using the Kaplan-Meier method. Survival was compared between the groups using the log-rank (Mantel-Cox) test.

3. Results

3.1. Participant flow

The number of patients who agreed to participate in the study was 52. Two of them did not meet the inclusion criteria; therefore, 50 patients were enrolled in this study and were randomly assigned to the New-PIVC ($n = 25$) or SPC ($n = 25$) groups. Three patients were excluded because one did not start the infusion of irritant drugs *via* the New-PIVC, one failed the new-PIVC placement, and one started anticoagulants. Finally, 47 patients (22 in the New-PIVC group and 25 in the SPC group) were analyzed (Figure 2).

3.2. Baseline characteristics

The median age of the patients was 67.0 ± 28.0 years; of the 47 patients, 61.7% were male, and their median body mass index was $22.0 \pm 5.7 \text{ kg/m}^2$. The data on blood tests were as follows: PT-INR was 1.00 ± 0.07 , and APTT was 28.44 ± 3.12 s. Malignant lymphoma accounted for 72.3% of the diagnoses of all patients. The baseline characteristics were generally comparable between the groups (Table 1).

Indwelling catheter sizes were 22 gauge (40.0%) and 24 gauge (60.0%) in the SPC group. All the new-

PIVCs were placed in the basilic vein in the upper arm; 18 (72.0%) catheters among the SPCs were placed in the cephalic vein in the forearm. The mean distance between the elbow joint and the puncture point was 93.0 ± 25.8 mm in the New-PIVC group. Anticancer drugs were administered to all patients, except for two patients in the SPC group who received amino acid and glucose injections with electrolytes and vitamin B1 (BFLUID®). The rate of successful initial puncture of the new-PIVCs and the SPCs did not differ (18 (81.8%) vs. 13 (52.0%); $p = 0.063$) (Table 1).

3.3. Outcome measures

The incidence of CF was 0% in the New-PIVC group and 32.0% (8 catheters) in the SPC group; the difference between the two groups was significant ($p = 0.007$). The risk difference between the New-PIVC and SPC groups was -32.0% with a 95% CI of -50.3 to -13.7% . There was a case in which a catheter made of different materials was used, and the analysis excluding that case ($n = 46$) also showed a significant difference between the New-PIVC (0 cases) and SPC (7 cases, 29.2%) group ($p = 0.013$). The risk difference was -32.0% with a 95% CI of -50.3 to -13.7% .

The number of CFs per 1,000 days was 0/1,000 days (95% CI: 0-24.0/1,000 days) in the New-PIVC group and 81.7/1,000 days (95% CI: 35.2-160.8/1,000 days) in the SPC group ($p = 0.001$). The median duration of the indwelling catheter was $8,112.5 \pm 7,045.0$ min in the New-PIVC group ($n = 22$) and $4,665.0 \pm 5,693.0$ min in the SPC group ($n = 25$) ($p = 0.141$) (Table 2). In the Kaplan-Meier analysis of the duration of the indwelling catheter until CF occurrence, a significant difference in the results of the log-rank test was observed ($p = 0.004$) (Figure 3).

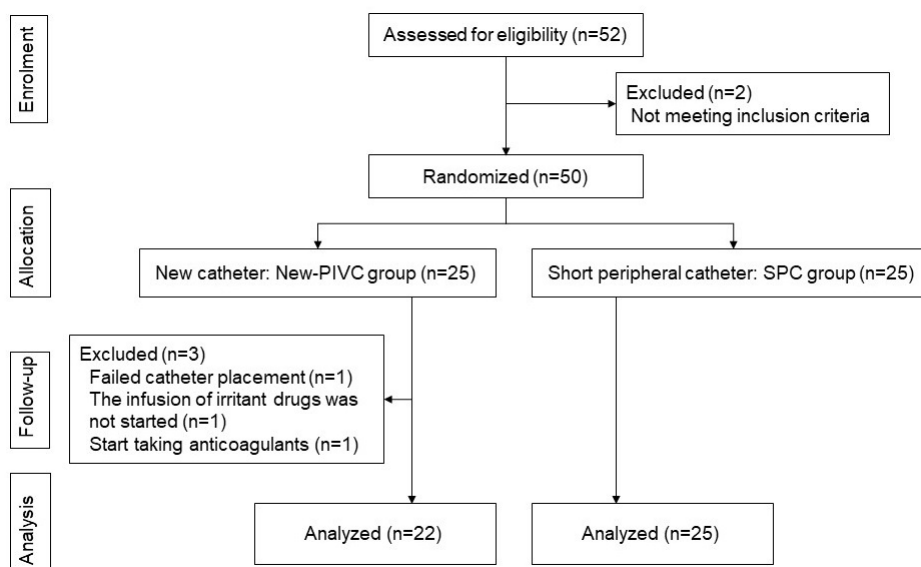


Figure 2. Study flow diagram.

Table 1. Patient and catheter characteristics

| Items | All (n = 47) | New-PIVCs ^{a)} (n = 22) | SPCs ^{a)} (n = 25) | p-value |
|---|-------------------------------|-------------------------------------|--------------------------------|-----------------------|
| Age (years) | 67.0 (28.0) | 71.0 (32.0) | 66.0 (20.0) | 0.693 ^{b)} |
| Sex (male) | 29 (61.7) | 11 (50.0) | 18 (72.0) | 0.144 ^{d)} |
| Body Mass Index (kg/m ²) | 22.0 (5.7) | 21.7 (4.1) | 22.6 (6.0) | 0.201 ^{b)} |
| Length of hospital stay | 23.0 (14.0) | 23.5 (16.5) | 23.0 (13.0) | 0.881 ^{b)} |
| Number of regimens (past) | 2.0 (6.0) | 2.0 (5.3) | 2.0 (6.0) | 0.965 ^{b)} |
| Blood test items ^{b)} : mean (SD) | | | | |
| Total protein (g/dL): mean (SD) | 6.77 (0.76) | 6.83 (0.56) | 6.72 (0.91) | 0.621 ^{d)} |
| Albumin (g/dL) | 4.10 (0.70) | 4.15 (0.63) | 4.10 (0.80) | 0.486 ^{b)} |
| Hematocrit (%): mean (SD) | 34.81 (5.46) | 36.12 (4.92) | 33.66 (5.75) | 0.125 ^{d)} |
| Blood platelet count (×10 ⁴ /μL) | 23.20 (15.60) | 23.75 (14.90) | 21.80 (15.65) | 0.609 ^{b)} |
| White blood cell count (×10 ³ /μL) | 4.60 (3.40) | 4.80 (2.73) | 4.50 (4.85) | 0.949 ^{b)} |
| C-reactive protein (mg/dL) | 0.30 (0.92) | 0.14 (0.39) | 0.46 (1.29) | 0.117 ^{b)} |
| Prothrombin (%): mean (SD) | 101.63 (12.59) | 105.47 (12.02) | 98.26 (12.33) | 0.049 ^{d)} |
| PT-INR ^{c)} : mean (SD) | 1.00 (0.07) | 0.98 (0.06) | 1.02 (0.07) | 0.046 ^{d)} |
| APTT (seconds) ^{d)} : mean (SD) | 28.44 (3.12) | 28.09 (2.97) | 28.74 (3.27) | 0.480 ^{d)} |
| Fibrinogen (mg/dL): mean (SD) | 345.57 (103.32) ^{e)} | 329.43 (91.58) ^{e)} | 359.12 (112.29) | 0.337 ^{d)} |
| Diagnoses ^{e)} | | | | |
| Malignant Lymphoma | 34 (72.3) | 15 (68.2) | 19 (76.0) | |
| DLBCL | | 9 (40.9) | 8 (32.0) | |
| FL | | 2 (9.1) | 4 (16.0) | |
| PCNSL | | 2 (9.1) | 0 (0.0) | |
| BL | | 1 (4.5) | 0 (0.0) | |
| MZL | | 1 (4.5) | 2 (8.0) | |
| CLL | | 0 (0.0) | 2 (8.0) | |
| cALCL | | 0 (0.0) | 1 (4.0) | |
| PIOL | | 0 (0.0) | 1 (4.0) | |
| WM | | 0 (0.0) | 1 (4.0) | |
| Leukemia | 13 (27.7) | 7 (31.8) | 6 (24.0) | |
| AML | | 6 (27.3) | 4 (16.0) | |
| MDS | | 1 (4.5) | 2 (8.0) | |
| Catheter size: gauge (G): 22 G / 24 G (%) | | 22 (100) / 0 | 10 (40.0) / 15 (60.0) | < 0.001 ^{d)} |
| Number of successful initial punctures | 31 (66.0) | 18 (81.8) | 13 (52.0) | 0.063 ^{d)} |
| Catheterized vein | | | | |
| Basilic | 25 (53.2) | 22 (100.0) | 3 (12.0) | |
| Cephalic | 18 (38.3) | 0 | 18 (72.0) | |
| Others (median: 3, hand: 1) | 4 (8.5) | 0 | 4 (16.0) | |
| Distance between the elbow joint and the puncture point (mm): mean (SD) | | 93.0 (25.8) | 105.6 (41.0) | 0.210 ^{d)} |
| Total volume of irritant drugs: (mL) | | 910.0 (1470.0) | 800.0 (640.0) | 0.455 ^{b)} |
| Administrated irritant drugs | | | | |
| Anticancer drugs | | 22 | 23 | |
| BFLUID ^{f)} | | 0 | 2 | |

Note. Median (IQR) or n (%); IQR, interquartile range; SD, standard deviation. ^{a)}New-PIVCs, the new peripheral intravenous catheter group; SPCs: the short peripheral intravenous catheter group. ^{b)}Blood test values on the closest day before catheter placement. ^{c)}PT-INR, prothrombin time and/or international normalized ratio. ^{d)}APTT, activated partial thromboplastin time. ^{e)}DLBCL, diffuse large B-cell lymphoma; FL, follicular lymphoma; PCNSL, primary central nervous system lymphoma; BL, Burkitt lymphoma; MZL, marginal zone lymphoma; CLL, chronic lymphocytic leukemia; cALCL, primary cutaneous anaplastic large cell lymphoma; PIOL, primary intraocular lymphoma; WM, primary macroglobulinemia/Waldenström macroglobulinemia; AML, acute myeloid leukemia; MDS, myelodysplastic syndromes. ^{f)}n = 46 (in all), n = 21 (in New-PIVCs). ^{g)}BFLUID (amino acid and glucose injection with electrolytes and vitamin B1). ^{h)}Mann-Whitney U-test. ⁱ⁾Fisher's exact test. ^{j)}t-test.

Table 2. Outcome measures

| Items | New-PIVCs (n = 22) | SPCs (n = 25) | p-value |
|---|-----------------------|--------------------------|-----------------------|
| Catheter failure (CF): n (%) | 0 (0.0) | 8 (32.0) | 0.007 ^{a)} |
| CF per 1000 days (95%CI) | 0 (0-24.0) | 81.7 (35.2-160.8) | 0.001 ^{b)} |
| Catheter dwelling time: median ± IQR (min) | 8112.5 ± 7045.0 | 4665.0 ± 5693.0 | 0.141 ^{c)} |
| Presence of the thrombus in the vessel: n (%) | 10 (45.5) | 22 (95.7) ^{d)} | < 0.001 ^{a)} |
| Presence of the mild or severe subcutaneous edema: n (%) | 4 (18.2) | 18 (78.3) ^{d)} | < 0.001 ^{a)} |
| The angle of the base of the removed catheter: mean ± SD (degrees) | 20.0 ± 7.2 | 10.2 ± 6.3 ^{d)} | < 0.001 ^{d)} |
| Subjective assessment of catheter placement: median (range) ^{e)} | | | |
| Pain when the needle punctures the skin surface | 10.5 (0-54.0) | 36.0 (9.0-89.0) | < 0.001 ^{c)} |
| Pain when inserting a catheter into a blood vessel | 0.5 (0-37.0) | 14.0 (0-88.0) | 0.008 ^{c)} |
| Painful due to posture during catheter placement | 0 (0-52.0) | 0 (0-26.0) | 0.039 ^{c)} |

Note. ^{a)}Fisher's exact test; ^{b)}Poisson regression; ^{c)}Mann-Whitney U-test; ^{d)}t-test. ^{e)}visual analogue scale: 0, no pain; 100, maximum pain. ^{f)}n = 23; ^{g)}n = 22.

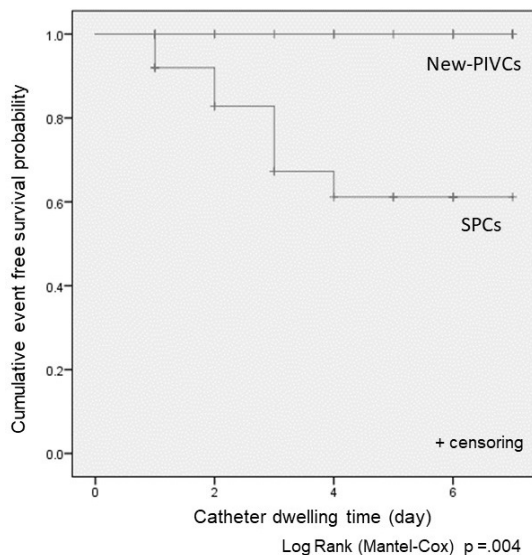


Figure 3. The duration of the indwelling catheter until catheter failure occurrence.

The number of patients for whom ultrasonographic images were obtained at catheter removal was 22 in the New-PIVC group and 23 in the SPC group. The frequency rate of thrombosis at catheter removal was 45.5% in the New-PIVC group and 95.7% in the SPC group ($p < 0.001$). Subcutaneous edema was observed in 18.2% and 78.3% of the patients of the New-PIVC and SPC group, respectively ($p < 0.001$). The signs and symptoms of CF seen in the SPC group were occlusion (insufficient infusion volume or inability, $n = 6$) and redness, swelling, and pain ($n = 2$). Catheter-related bloodstream infections, thrombophlebitis, and extravasation did not occur.

The number of patients for whom the catheter was removed was 22 in the New-PIVC group and 22 in the SPC group. The mean angle of the base of the removed New-PIVCs and SPCs differed significantly ($20.0^\circ \pm 7.2^\circ$ vs. $10.2^\circ \pm 6.3^\circ$; $p < 0.001$) (Table 2).

According to the visual analog scale (100 points is the maximum pain), the pain scores due to needle puncture on the skin surface and catheter insertion into the vessel in the New-PIVC group were lower than those in the SPC group ($p < 0.001$, and $p = 0.008$, respectively). Pain score associated with postural changes during catheter placement was higher in the New-PIVC group than in the SPC group ($p = 0.039$) (Table 2).

4. Discussion

This study revealed that the incidence of CF can be reduced by catheterizing the upper arm vein using a new long catheter instead of catheterizing the forearm vein using a short catheter in patients receiving hyper-stimulant drugs. The results suggest that CF is reduced by selecting the upper arm vein instead of the forearm vein for PIVC placement, particularly when a chemical

stimulus is likely to damage vascular endothelial cells. Therefore, the characteristics of the upper arm vein (deep and invisible or unpalpable) should be considered in selecting VAD and catheterization should be assisted by visualization devices.

Recently, the PIV5RightsTMBundle was proposed to prevent complications associated with catheter placement and to preserve vessels (18). Although there have been reports of high puncture success rates, long indwelling periods, and decreased complications with the PIV5RightsTMBundle, it has been highlighted that vessel selection in terms of blood flow (hemodilution ratio) was not considered (19). Blood vessels are probably repeatedly exposed to chemical stimuli, particularly when irritant or vesicant agents are used in chemotherapy. The patients in this study had been treated with anticancer drugs in the past. Therefore, for vascular preservation, indwelling and infusing at sites with high blood flow volume (e.g., an upper arm vein among upper extremity) seems important to reduce drug exposure. Although there have been several reports investigating the differences in CF incidence and catheter survival time when PIVCs using different catheter lengths were placed, few studies have directly compared whether the upper arm or forearm was a more appropriate insertion site to prevent CFs. Additionally, few reports have clearly described the irritancy of infusates (20,21). Therefore, in this study, we compared the incidence of CFs between patients receiving hyper-stimulant drugs *via* the upper arm and those receiving hyper-stimulant drugs *via* the forearm.

Notably, no CFs occurred in the 22 patients in the New-PIVC group, whereas CFs occurred in 32.0% of the patients in the SPC group, which are similar to the incidence rates reported previously (22,23). Six of the eight CF cases in the SPC group were occlusions (insufficient infusion volume or inability). Significantly higher rates of thrombus formation and subcutaneous edema formation at the time of catheter removal were observed in the SPC group using ultrasonography. These results suggest that mechanical and chemical stimuli to the forearm vessel are more severe than those to the upper arm vessel, possibly reflecting a more profound damage to endothelial cells.

Based on the results of this study, the upper arm should also be considered a site for catheter placement, at least in some cases. There seem to be three points to consider for catheterization into a vein in the upper arm. First, the angle of the base of the removed New-PIVCs was significantly larger than that of the removed SPCs because the needle reached the deep vessel. If external forces are applied to the catheter hub after fixation, through the movement of the subcutaneous tissue with joint movement or muscle contraction, the angle of the base of the catheter may further increase, leading to kinking of the catheter (15). Therefore, the site of catheter fixation should be far from the elbow joint

appropriately. Second, the pain score associated with needle puncture and catheter insertion into the vessel was lower in the New-PIVC group than in the SPC group. In contrast, pain due to postural changes during catheter placement was higher in the New-PIVC group than in the SPC group. Although, the median pain score was zero, some patients were uncomfortable during the catheterization of the upper arm vein. Therefore, we must consider the posture of the patient during catheter insertion at the upper arm. Third, the visualizing device (*i.e.*, ultrasonography), as well as proper training of the operators, is needed to appropriately reach the upper arm vein.

5. Limitations

The external validity of the results should be considered because most irritants administered in this study were anticancer drugs, and the patients had hematologic and oncological diseases. Although catheter placement in the upper arm vein has been shown to be effective in preventing CF caused by vancomycin (24), its effect on other irritating agents (*e.g.*, peripheral parenteral nutrition agents) is unknown. Blom JW *et al.* reported that patients with cancer have a significantly increased risk of venous thrombosis, and those harboring factor V Leiden and prothrombin 20210A mutations appeared to have an even higher risk (25). Therefore, whether the difference in patient background and the quality of infused drugs may affect the risk reduction of CF in catheterization at the upper arm is unclear. However, it is noteworthy that the risk of CF was attenuated by catheterization at the upper arm, in especially high-risk patients harboring hematologic malignancy and undergoing high-risk medications, considering this is a quite prevalent clinical situation.

There was no echo-assisted catheter placement in the SPC group in our study. If ultrasonography had been used, the SPC group might have shown a higher puncture success rate (26) and reduced mechanical stimulation, which may have reduced the occurrence of CF (22, 27). However, the way how the SPCs were placed reflects the daily practice in the real world, possibly increasing the impact of our research in everyday clinical practice.

6. Conclusions

It was demonstrated that the use of the new long catheter inserted into the upper arm vein to administer a hyper-irritant drug could significantly reduce the occurrence of CF compared with the use of a short catheter inserted into the forearm vein.

Acknowledgements

The authors thank the head nurse Toshie Yamashita for managing the research environment of the wards.

Funding: The new catheter used in this study was developed in a collaborative research with Terumo Corp., which provided funding for the collaborative research. This work was supported by JSPS KAKENHI Grant Number JP20H03976.

Conflict of Interest: RM and MA-D belong to a laboratory (Department of Advanced Nursing Technology, Graduate School of Medicine, The University of Tokyo) supported by Terumo Corporation. Other authors declare that there are no conflicts of interest. The new catheter was provided to this study free of charge from Terumo Corp.

References

1. Chen S, O'Malley M, Chopra V. How common are indwelling devices in hospitalized adults? A contemporary point prevalence study in a tertiary care hospital. *Am J Infect Control.* 2021; 49:194-197.
2. Alexandrou E, Ray-Barruel G, Carr PJ, Frost SA, Inwood S, Higgins N, Lin F, Alberto L, Mermel L, Rickard CM, OMG Study Group. Use of Short peripheral intravenous catheters: characteristics, management, and outcomes worldwide. *J Hosp Med.* 2018; 13.
3. Dychter SS, Gold DA, Carson D, Haller M. Intravenous therapy: A review of complications and economic considerations of peripheral access. *J Infus Nurs.* 2012; 35:84-91.
4. Blanco-Mavillard I, Pedro-Gómez JE, Rodríguez-Calero MÁ, Bennasar-Veny M, Parra-García G, Fernández-Fernández I, Bujalance-Hoyos J, Moya-Suárez AB, Cobo-Sánchez JL, Ferrer-Cruz F, Castro-Sánchez E. Multimodal intervention for preventing peripheral intravenous catheter failure in adults (PREBACP): A multicentre, cluster-randomised, controlled trial. *Lancet Haematol.* 2021; 8:e637-e647.
5. Marsh N, Webster J, Larsen E, Cooke M, Mihala G, Rickard CM. Observational study of peripheral intravenous catheter outcomes in adult hospitalized patients: a multivariable analysis of peripheral intravenous catheter failure. *J Hosp Med.* 2018; 13:83-89.
6. Bolton D. Improving peripheral cannulation practice at an NHS Trust. *Br J Nurs.* 2010; 19:1346-1350.
7. Murayama R, Uchida M, Oe M, Takahashi T, Oya M, Komiyama C, Sanada H. Removal of peripheral intravenous catheters due to catheter failures among adult patients. *J Infus Nurs.* 2017; 40:224-231.
8. Liu C, Chen L, Kong D, Lyu F, Luan L, Yang L. Incidence, risk factors and medical cost of peripheral intravenous catheter-related complications in hospitalised adult patients. *J Vasc Access.* 2022; 23:57-66.
9. Tanabe H, Takahashi T, Murayama R, Yabunaka K, Oe M, Matsui Y, Arai R, Uchida M, Komiyama C, Sanada H. Using ultrasonography for vessel diameter assessment to prevent infiltration. *J Infus Nurs.* 2016; 39:105-111.
10. Murayama R, Takahashi T, Tanabe H, Nakagami G, Tanabe H, Yabunaka K, Arai R, Komiyama C, Uchida M, Sanada H. The relationship between the tip position of an indwelling venous catheter and the subcutaneous edema. *Biosci Trends.* 2015; 9:414-419.
11. Tanabe H, Murayama R, Yabunaka K, Oe M, Takahashi T, Komiyama C, Sanada H. Low-angled peripheral

- intravenous catheter tip placement decreases phlebitis. *J Vasc Access*. 2016; 17:542-547.
12. Shintani Y, Murayama R, Abe-Doi M, Sanada H. Incidence, causes, and timing of peripheral intravenous catheter failure related to insertion timing in the treatment cycle in patients with hematological malignancies: a prospective descriptive study. *Jpn J Nurs Sci*. 2022; e12484.
 13. Takahashi T, Shintani Y, Murayama R, Noguchi H, Abe-Doi M, Koudounas S, Nakagami G, Mori T, Sanada H. Ultrasonographic measurement of blood flow of peripheral vein in the upper limb of healthy participants: A pilot study. *J Jpn WOCM*. 2021; 25:576-584.
 14. Qin KR, Ensor N, Barnes R, Englin A, Nataraja R, Pacilliet M. Long peripheral catheters for intravenous access in adults and children: a systematic review of the literature. *J Vasc Access*. 2021; 22:767-777.
 15. Murayama R, Oyama H, Abe-Doi M, Masamoto Y, Kashiwabara K, Tobe H, Komiyama C, Sanada H, Kurokawa M. Safety verification of a new peripheral intravenous catheter placed in the upper arm vein for administration of drugs with high irritant potential. *Drug Discov Ther*. 2022; 16:128-134.
 16. Yabunaka K, Murayama R, Takahashi T, Tanabe H, Kawamoto A, Oe M, Arai R, Sanada H. Ultrasonographic appearance of infusion *via* the peripheral intravenous catheters. *J Nurs Sci Eng*. 2015; 2:40-46.
 17. Yabunaka K, Murayama R, Tanabe H, Takahashi T, Oe M, Oya M, Fujioka M, Sanada H. Ultrasonographic classification of subcutaneous edema caused by infusion *via* peripheral intravenous catheter. *J Med Ultrasound*. 2016; 24:60-65.
 18. Steere L, Ficara C, Davis M, Moureau N. Reaching one peripheral intravenous catheter (PIVC) per patient visit with lean multimodal strategy: the PIV5Rights™ Bundle. *J Assoc Vasc Access*. 2019; 24:31-43.
 19. Foor JS, Moureau NL, Gibbons D, Gibson SM. Investigative study of hemodilution ratio: 4Vs for vein diameter, valve, velocity, and volumetric blood flow as factors for optimal forearm vein selection for intravenous infusion. *J Vasc Access*. 2022.
 20. Bahl A, Hang B, Brackney A, Joseph S, Karabon P, Mohammad A, Nnanabu I, Shotkin P. Standard long IV catheters versus extended dwell catheters: A randomized comparison of ultrasound-guided catheter survival. *Am J Emerg Med*. 2019; 37:715-721.
 21. Elia F, Ferrari G, Molino P, Converso M, Filippi GD, Milan A, Aprà F. Standard-length catheters *vs* long catheters in ultrasound-guided peripheral vein cannulation. *Am J Emerg Med*. 2012; 30:712-716.
 22. Takahashi T, Murayama R, Abe-Doi M, Miyahara-Kaneko M, Kanno C, Miwa Nakamura M, Mizuno M, Komiyama C, Sanada H. Preventing peripheral intravenous catheter failure by reducing mechanical irritation. *Sci Rep*. 2020; 10:1550.
 23. Rickard CM, Webster J, Wallis MC, Marsh N, McGrail MR, French V, Foster L, Gallagher P, Gowardman JR, Zhang L, McClymont A, Whitby M. Routine versus clinically indicated replacement of peripheral intravenous catheters: A randomised controlled equivalence trial. *Lancet*. 2012; 22; 380:1066-1074.
 24. Caparas JV, Hung HS. Vancomycin administration through a novel midline catheter: Summary of a 5-year, 1086-patient experience in an urban community hospital. *J Assoc Vasc Access*. 2017; 22:38-41.
 25. Blom JW, Doggen CJM, Osanto S, Rosendaal FR. Malignancies, prothrombotic mutations, and the risk of venous thrombosis. *J Am Med Assoc*. 2005; 293:715-722.
 26. van Loon FHJ, Buise MP, Claassen JFF, Dierick-van Daele ATM, Bouwman ARA. Comparison of ultrasound guidance with palpation and direct visualisation for peripheral vein cannulation in adult patients: A systematic review and meta-analysis. *Br J Anaesth*. 2018; 121:358-366.
 27. Takahashi T, Murayama R, Oe M, Nakagami G, Tanabe H, Yabunaka K, Arai R, Komiyama C, Uchida M, Sanada H. Is thrombus with subcutaneous edema detected by ultrasonography related to short peripheral catheter failure? A prospective observational study. *J Infus Nurs*. 2017; 40:313-322.

Received November 26, 2022; Revised January 31, 2023; Accepted February 22, 2023.

**Address correspondence to:*

Mineo Kurokawa, Department of Hematology and Oncology, The University of Tokyo Hospital, 7-3-1 Hongo, Bunkyo-Ku, Tokyo 113-8655, Japan.
E-mail: kurokawa@m.u-tokyo.ac.jp

Released online in J-STAGE as advance publication February 28, 2023.

Age distribution and disease severity of COVID-19 patients continued to change in a time-dependent manner from May 2021 to April 2022 in the regional core hospital in Japan

Futoshi Kawaura^{1,2}, Takuya Kishi^{2,*}, Tadashi Yamamoto^{1,2}, Shiki Nakayama^{1,2}, Taku Goto¹, Reimi Tsurusawa¹, Toshio Katagiri^{1,2}, Kohei Yamanouchi^{1,2}, Ayako Matsuo¹, Naomi Kobayashi-Watanabe¹, Tomohiro Imamura², Yoshitaka Hirooka², Kuniyasu Takagi^{1,2}, Tsukuru Umemura^{1,2}, Kazuma Fujimoto², Shinichiro Hayashi¹, Ayako Takamori³

¹ The Kouhou-kai Takagi Hospital, Okawa, Japan;

² International University of Health and Welfare Graduate School of Medicine, Okawa, Japan;

³ Clinical Research Center, Saga University Hospital, Saga, Japan.

SUMMARY The present retrospective study aimed to examine the real-world data regarding time-dependent changes in the age distribution of patients with coronavirus disease 2019 (COVID-19) as well as the severity and infectivity in a regional core hospital in Japan. Patients with COVID-19 who visited the fever outpatient branch in Takagi Hospital during phase I (May 1 to December 31, 2021), and during phase II (January 1 to April 30, 2022) were evaluated. The age distribution of outpatients and the characteristics of inpatients aged > 75 years were compared between phases I and II. The age distribution of outpatients shifted from the older generation in phase I to the younger generation in phase II ($p < 0.01$). Disease severity might be reduced in a time-dependent manner with a decrease in the hospitalization rate (phase I: 145/368 (39.4%); phase II: 104/1496 (7.0%); $p < 0.01$) and mortality rate (phase I: 10/368 (2.7%); phase II: 7/1496 (0.5%); $p < 0.01$). The number of patients increased in phase II (374.0/month) compared to that in phase I (36.8/month). Regarding the older inpatients, the disease severity of COVID-19 and hospitalization days were reduced in phase II compared to those in phase I ($p < 0.01$, each). In conclusion, the present study suggests a change in the age distribution of patients with COVID-19, a decrease in toxicity, and an increase in infectivity of severe acute respiratory syndrome coronavirus 2 in a time-dependent manner.

Keywords SARS-CoV-2, severe acute respiratory syndrome coronavirus 2, coronavirus disease 2019, mortality, infectivity

1. Introduction

Coronavirus disease 2019 (COVID-19), caused by severe acute respiratory syndrome coronavirus 2 (SARS-CoV-2), was detected in China in 2019 (1). The infection was limited in the regional area in the primary stage (2,3), but since then has been progressing rapidly and widely worldwide (4,5). Disease severity and the high infectivity of COVID-19 have serious consequences (6,7). With the rapid progress in COVID-19 infection, vaccinations and medications for COVID-19 have been developed and adapted widely (8-10). However, the pandemic and explosive infection of COVID-19 was not controlled until August 2022.

With repeated epidemics, SARS-CoV-2 has evolved from alpha and delta variants to the omicron variant. These mutations have induced several changes in the pathology of COVID-19 and policies for the treatment and prevention of the disease (10-13). Epidemiological data from the world, as well as Japan, suggest that the initial stage of COVID-19 mainly affected the middle and older generations, and rarely the young generations, including children (14,15). This trend has shifted over time, with COVID-19 being more prevalent among younger generations and children (16). Recent epidemiological reports suggested that COVID-19 may be becoming a milder illness in a time-dependent manner in recent times, while infectivity may be

increasing (17).

The present study aimed to examine real-world clinical data regarding time-dependent changes in the age distribution of patients with COVID-19 and the severity and infectivity of the disease in Kouhou-kai Takagi Hospital, which is the regional core hospital in Japan and treats patients at the mild and moderate stages of COVID-19, as well as non-severe patients. The data were compared with those from phase I (May 1, 2021, to December 31, 2021), and phase II (January 1, 2022, to April 30, 2022).

2. Methods

The present retrospective study included patients with COVID-19 who visited the fever outpatient branch of Kouhou-kai Takagi Hospital between May 1, 2021, and April 30, 2022. The patients were divided into two groups: phase I (May 1, 2021, to December 31, 2021) and phase II (January 1, 2022, to April 30, 2022). Takagi Hospital is the regional core hospital in Okawa city and the surrounding cities (population of approximately 150,000); most patients with COVID-19 visit Takagi Hospital, including those with mild and moderate disease severity. COVID-19 diagnosis in all patients was confirmed by SARS-CoV-2 polymerase chain reaction (PCR); loop-mediated isothermal amplification (LAMP) and quantitative antigen tests were also included (18,19). Ribonucleic acid (RNA) extraction was done using the Loopamp Viral RNA Extraction Kit (Eiken Chemical, Tokyo, Japan). The collected nasopharyngeal sample was stirred several times using a Loopamp Viral RNA Extraction Reagent. The LAMP assay was performed using 10 µL of the sample or solution alone (negative control) with Primer Mix 2019-nCoV (15 µL). The reaction was allowed to proceed for 2 min with an RNA amplification reagent in a Loopamp Realtime Turbidimeter (Eiken Chemical). The threshold time was recorded for detecting SARS-CoV-2 virus RNA (18).

Disease severity was evaluated according to the severity classification and management of the Japan Ministry of Health Labour and Welfare COVID-19 clinical practice guide (20): mild, no dyspnea + no pneumonia + $\geq 96\%$ of oxygen saturation; moderate I, dyspnea + pneumonia + 93% to 96% of oxygen saturation; moderate II, dyspnea + pneumonia + $\leq 93\%$ of oxygen saturation; and severe, patients who required medical therapy in the intensive care unit and/or with a ventilator. Patients classified as severe did not visit Takagi Hospital, but a higher-functioning hospital. The age distribution of patients who visited the outpatient branch and those who were admitted to Takagi Hospital was examined. The hospitalization criteria were: disease severity levels of moderate I or II; and those with mild severity > 75 years, severe comorbidity, and impossibility of eating

with illness. The characteristics of the hospitalized patients (> 75 years old) were evaluated, including blood tests, age, sex, height, body weight, mortality, comorbidity, performance status, disease severity, therapeutic medicines, and duration of hospitalization. The therapeutic medicines for COVID-19 infection treatment used in Takagi Hospital during the examined period were remdesivir, dexamethasone, favipiravir, tocilizumab, and neutralizing antibodies. The general condition of the patients was evaluated by the Eastern Cooperative Oncology Group Performance Status at admission (21) as follows: status 0: fully active, able to carry on all pre-disease performance without restriction; status 1: restricted in physically strenuous activity but ambulatory and able to carry out work of a light sedentary nature like light housework and office work; status 2: ambulatory and capable of all self-care but unable to carry out any work activities up, and approximately more than 50% of waking hours; status 3: capable of only limited self-care, and confined to bed or chair for more than 50% of waking hours; status 4: wholly disabled and unable to carry out any self-care, and confined to bed or chair.

The Kouhou-kai Ethical Committee approved this study (#430, May 2021). The data between phases I and II were compared using the Chi-squared or Fisher's exact test for categorical variables and the Student's *t*-test for continuous variables. JMP Pro 16 was used for all the analyses. Statistical significance was defined as $p < 0.05$.

3. Results

Table 1 shows the age distribution of the patients with COVID-19 who visited the fever outpatient branch in Takagi Hospital in phase I and phase II. The number of patients increased ten times in phase II (phase I: 36.8/month; phase II: 374.0/month). In phase I, the

Table 1. Age distribution of the patients with COVID-19 detected by the PCR who visited the fever outpatient branch in the Takagi hospital during phase I (May 1, 2021 to December 31, 2021) and phase II (January 1, 2022 to April 30, 2022)

| Age (years old) | Phase I (n) | Phase II (n) ** |
|-----------------|-------------|-----------------|
| 0-9 | 16 (4.3%) | 183 (12.2%) |
| 10-19 | 29 (7.9%) | 256 (17.1%) |
| 20-29 | 45 (12.2%) | 276 (18.4%) |
| 30-39 | 36 (9.8%) | 197 (13.2%) |
| 40-49 | 41 (11.1%) | 172 (11.5%) |
| 50-59 | 77 (20.9%) | 122 (8.2%) |
| 60-69 | 22 (6.0%) | 90 (6.0%) |
| 70-79 | 32 (8.7%) | 88 (5.9%) |
| 80-89 | 54 (14.7%) | 79 (5.3%) |
| 90 ≤ | 16 (4.3%) | 33 (2.2%) |
| Total | 368 | 1496 |

** $p < 0.01$: age distribution was different between phases I and II. PCR: SARS-CoV-2 polymerase chain reaction. n, number of patients.

prominent age group infected with COVID-19 were the middle-aged and older generations, and the number of children affected was limited. In contrast, the phase II included the middle-aged and younger generations, including children, and the change observed in the age distribution was significant ($p < 0.01$).

The number of inpatients hospitalized during phases I and II is shown in Table 2. Patients in Phase I ranged

Table 2. Age distribution of the COVID-19 patients who hospitalized the Takagi hospital during phase I (May 1, 2021 to December 31, 2021) and phase II (January 1, 2022 to April 30, 2022)

| Age (years old) | Phase I (n) | Phase II (n) ** |
|---|-----------------|--------------------|
| 0-19 | 17 (0: 0%) | 1 (0) |
| 20-49 | 47 (0: 0%) | 12 (0) |
| 50-74 | 32 (0: 0%) | 30 (0) |
| 75 ≤ | 49 (10: 20.4%) | 61 (7: 11.5%) |
| Hospitalization rate (inpatients/outpatients) | 145/368 (39.4%) | 104/1496 (7.0%) ** |

** $p < 0.01$: administration ratio to the hospital among the outpatients was decreased in phase II. n, number of patients.

in age from the elderly to the young. In phase II ($p < 0.01$), inpatients were mostly from the middle and older generations. Mortality in patients was limited to older generations (> 75 years old) in both phases at Takagi Hospital. The hospitalization ratio (inpatient/outpatient) decreased markedly in phase II ($p < 0.01$) when compared with that in phase I.

The patient characteristics of the older inpatients (≥ 75 years) with COVID-19 are shown in Table 3. The number of patients and mortality rate were not different between phases I and II. The mortality rate calculated with the outpatients decreased in phase II ($p < 0.01$), whereas the mortality rate calculated with the inpatients did not differ between phases I and II. Disease severity was high ($p < 0.01$), and hospitalization days were prolonged ($p < 0.01$) in phase I. The therapeutic approach changed between the two phases. Remdesivir was more frequently administered to patients in phase II ($p < 0.01$), and neutralizing antibodies were more available in phase II. The prescription rate of dexamethasone decreased in phase II, and tocilizumab was rarely prescribed in this phase (p

Table 3. Patient-characteristics of aged COVID-19 patients more than 75 years old who hospitalized the Takagi hospital during phase I (May 1, 2021 to December 31, 2021) and phase II (January 1, 2022 to April 30, 2022)

| Items | Phase I | Phase II | <i>p</i> value |
|---|---------------|---------------|----------------|
| Total number of aged patients (n) | 49 | 61 | |
| Mortality (n) | 10 | 7 | |
| Mortality rate | | | |
| Mortality/aged inpatients | 10/49 (20.4%) | 7/61 (11.5%) | 0.2 |
| Mortality/total inpatients | 10/145 (6.9%) | 7/104 (6.7%) | 1 |
| Mortality/total outpatients | 10/368 (2.7%) | 7/1496 (0.5%) | < 0.01 |
| Mortality caused by COVID-19 | 3 | 1 | 0.33 |
| Age (years old) | 85 ± 6.2 | 86 ± 6.1 | 0.84 |
| Genders (males/females) | 17/32 | 27/34 | 0.30 |
| Height (cm) | 153.0 ± 9.4 | 152.0 ± 10.2 | 0.50 |
| Body weight (kg) | 46.2 ± 12.0 | 45.4 ± 11.3 | 0.88 |
| Serum total protein (g/dl) | 6.6 ± 0.7 | 6.5 ± 0.8 | 0.81 |
| Serum albumin (g/dl) | 3.2 ± 0.6 | 3.2 ± 0.6 | 0.85 |
| Hemoglobin (g/dl) | 12.2 ± 1.3 | 11.7 ± 1.9 | 0.08 |
| White blood cells (/μl) | 4390 ± 3292 | 5250 ± 3056 | 0.29 |
| CRP (mg/dl) | 3.9 ± 5.6 | 1.3 ± 4.8 | 0.07 |
| Creatinine (mg/dl) | 0.69 ± 0.43 | 0.84 ± 0.20 | 0.03 |
| Disease severity (mild/moderate I/ moderate II/severe) at hospitalization | 2/15/32/0 | 24/23/14/0 | < 0.01 |
| Performance status (0/1/2/3/4) | 7/3/6/15/16 | 0/5/17/23/16 | 0.35 |
| Hospitalized duration (days) | 20.0 ± 10.7 | 12.0 ± 6.3 | < 0.01 |
| Comorbidities (n) | | | |
| Cardiovascular diseases | 25 | 35 | 0.77 |
| Cerebrovascular diseases | 17 | 19 | 0.72 |
| Renal diseases | 1 | 8 | 0.08 |
| Respiratory diseases | 11 | 10 | 0.49 |
| Gastrointestinal diseases | 0 | 2 | 0.51 |
| Diabetes mellitus | 11 | 10 | 0.49 |
| Dementia | 25 | 22 | 0.15 |
| Others | 19 | 35 | 0.17 |
| Therapeutic medicines for COVID-19 (n) | | | |
| Remdesivir | 19 | 45 | < 0.01 |
| Dexamethasone | 43 | 16 | < 0.01 |
| Favipiravir | 2 | 0 | 0.20 |
| Tocilizumab | 41 | 3 | < 0.01 |
| Neutralizing antibodies | 1 | 5 | 0.22 |

Data are mean ± SD. n, number of patients.

< 0.01, each). The other factors did not differ between the two phases. Table 4 shows the causes of death in the inpatients. Most patients were > 85 years, and three patients in phase I and one in phase II died directly due to COVID-19. Three of four patients who died directly due to COVID-19 had renal dysfunction with a high creatinine value. Other patients in phase I died from bacterial pneumonia, including aspiration pneumonia, and those in phase II died because of bacterial pneumonia and comorbidities, including hepatocellular and gastrointestinal bleeding. In phase II, five of seven patients who died did not receive COVID-19 vaccination, whereas the vaccination information was unavailable for the patients who died in phase I.

4. Discussion

The present study demonstrated that *i*) the age distribution of the patients suffering from COVID-19 moved from the older to the younger generation, including children, concomitant with the variants of SARS-CoV-2; *ii*) the disease severity of the COVID-19 infection might be reduced in a time-dependent manner, which was demonstrated by the decrease in the hospitalization and mortality rates; *iii*) the increase in the number of the patients in present times suggested that infectivity of COVID-19 might be enhanced, whereas the virus toxicity might be attenuated.

Several epidemiological reports worldwide and in Japan have demonstrated that age distribution has changed in a time-dependent manner (14,15). At the start of the COVID-19 pandemic, most patients with COVID-19 were adults, and the infection concomitant with the COVID-19 variant progression spread to the

younger generation and children (16). The infection trend in the epidemiological reports showed that SARS-CoV-2 variants were alpha and delta in phase I (May 1, 2021, to December 31, 2021) and omicron in phase II (2022 January 1, 2022, to April 30, 2022) (10-13).

The present study demonstrated that the hospitalization (39.4% in phase I, 7.0% in phase II) and mortality (2.7% in phase I, 0.5% in phase II) rates were decreased in the present times, which suggested that the viral toxicity was diminished in a time-dependent manner. In addition, the ratio of direct deaths caused by COVID-19 tended to decrease in phase II, where most patients died due to severe comorbidities. This observation is equivalent to that reported in several official releases of epidemiological data and clinical reports (4,15,17,20,22-26).

The present data of the time-dependent increase in the number of patients per month (phase I: 36.8/month, phase II: 374.0/month) suggested increased infectivity of COVID-19, although the toxicity of the virus was reduced, and this tendency was demonstrated in the official epidemiological data worldwide (4,20). An accurate diagnosis of COVID-19 tended to not be performed, and accuracy in recording the number of cases has not been demonstrated in most countries because of the marked increase in the number of patients and the dramatic decrease in mortality directly caused by COVID-19.

The limitations of the present study were as follows: the data were examined in a single regional institute in Japan, the number of patients was limited, and the patients with severe illness due to COVID-19 were excluded and hospitalized in an advanced medical institution because the patients with mild/moderate

Table 4. Characteristics of the fetal patients during phase I (May 1, 2021 to December 31, 2021) and phase II (2022 January 1, 2022 to April 30, 2022)

| Age | Gender | PS | Disease severity | Hospital stay | Cause of death | Vaccination | Cr |
|----------|--------|----|------------------|---------------|---------------------------|-------------|------|
| Phase I | | | | | | | |
| 85 | female | 4 | moderate I | 43 days | aspiration pneumonia | N.A. | 0.68 |
| 96 | female | 4 | moderate II | 52 days | aspiration pneumonia | N.A. | 0.69 |
| 86 | male | 4 | moderate II | 29 days | aspiration pneumonia | N.A. | 0.76 |
| 88 | male | 4 | moderate II | 17 days | bacterial pneumonia | N.A. | 0.93 |
| 98 | female | 4 | moderate I | 23 days | aspiration pneumonia | N.A. | 0.37 |
| 92 | male | 4 | moderate II | 33 days | aspiration pneumonia | + | 0.74 |
| 85 | female | 4 | moderate II | 17 days | bacterial pneumonia | + | 0.38 |
| 92 | female | 3 | moderate II | 9 days | COVID-19 | N.A. | 2.31 |
| 90 | male | 3 | moderate II | 10 days | COVID-19 | N.A. | 1.45 |
| 87 | female | 4 | moderate II | 13 days | COVID-19 | N.A. | 0.65 |
| Phase II | | | | | | | |
| 87 | male | 4 | moderate I | 12 days | hepatocellular carcinoma | - | 0.84 |
| 86 | male | 4 | moderate I | 10 days | hepatocellular carcinoma | - | 1.50 |
| 75 | male | 3 | moderate II | 31 days | bacterial sepsis | + | 0.84 |
| 99 | female | 3 | mild | 8 days | gastrointestinal bleeding | - | 1.52 |
| 91 | female | 3 | mild | 4 days | bacterial sepsis | - | 0.52 |
| 93 | female | 4 | mild | 17 days | bacterial pneumonia | - | 0.72 |
| 92 | female | 4 | moderate II | 2 days | COVID-19 | + | 2.87 |

PS: performance status. Cr: creatinine. N.A.: the patient data of vaccination of COVID-19 was not available. +: vaccination received. -: vaccination not received.

COVID-19 visited the fever outpatient branch of Takagi Hospital. The effect of vaccination was not indicated in the present study, as information on vaccination in phase I was unavailable. However, five of seven patients who died did not receive vaccination in phase II. At last, although we checked the variants of SARS-CoV-2 in several patients in Phase I and II, we could not fully define that patients in Phase I were mainly infected with alpha and delta variants while patients in Phase II were mainly infected with omicron variant.

5. Conclusion

The present retrospective study in a regional core hospital in Japan demonstrated a change in the age distribution of patients with COVID-19, a decrease in toxicity, and an increase in infectivity in a time-dependent manner.

Acknowledgements

We appreciate all the medical staff at Takagi Hospital for the medical treatment and care of patients with COVID-19.

Funding: None.

Conflict of Interest: The authors have no conflicts of interest to disclose.

References

- Zhu N, Zhang D, Wang W, *et al.* A novel coronavirus from patients with pneumonia in China, 2019. *N Engl J Med.* 2020; 382:727-733.
- Hoshiyama T, Wada T, Nihonyanagi N, Kameda R, Yamaoka-Tojo M, Fukuda M, Ako J, Yamaoka K, Takayama Y. Clinical and microbiological features of asymptomatic SARS-CoV-2 infection and mild COVID-19 in seven crewmembers of a cruise ship. *Intern Med.* 2020; 59:3135-3140.
- Kurihara S, Nakajima M, Kaszynski RH, Yamamoto Y, Santo K, Takane R, Tokuno H, Ishihata A, Ando H, Miwa M, Hamada S, Nakano T, Shimokawa M, Goto H, Yamaguchi Y. Prevalence of COVID-19 mimics in the emergency department. *Intern Med.* 2021; 60:3087-3092.
- World Health Organization. WHO coronavirus disease (COVID-19) dashboard. 2022. <https://covid19.who.int> (accessed December 3, 2022).
- Li Q, Guan X, Wu P, *et al.* Early transmission dynamics in Wuhan, China, of novel coronavirus-infected pneumonia. *N Engl J Med.* 2020; 382:1199-1207.
- Magesh S, John D, Li WT, Mattingly-App A, Jain S, Chang EY, Ongkeko WM. Disparities in COVID-19 outcomes by race, ethnicity, and socioeconomic status: A systematic review and meta-analysis. *JAMA Netw Open.* 2021; 4:e2134147.
- Feikin DR, Higdon MM, Abu-Raddad LJ, Andrews N, Araos R, Goldberg Y, Groome MJ, Huppert A, O'Brien KL, Smith PG, Wilder-Smith A, Zeger S, Deloria Knoll M, Patel MK. Duration of effectiveness of vaccines against SARS-CoV-2 infection and COVID-19 disease: results of a systematic review and meta-regression. *Lancet.* 2022; 399:924-944.
- Heath PT, Galiza EP, Baxter DN, *et al.* Safety and efficacy of NVX-CoV2373 Covid-19 vaccine. *N Engl J Med.* 2021; 385:1172-1183.
- Lopez Bernal J, Gower C, Andrews N; Public Health England Delta Variant Vaccine Effectiveness Study Group. Effectiveness of Covid-19 vaccines against the B.1.617.2 (Delta) variant. *N Engl J Med.* 2021; 385:585-594.
- Arbel R, Hammerman A, Sergienko R, Friger M, Peretz A, Netzer D, Yaron S. BNT162b2 vaccine booster and mortality due to Covid-19. *N Engl J Med.* 2021; 385:2413-2420.
- Guo Y, Han J, Zhang Y, He J, Yu W, Zhang X, Wu J, Zhang S, Kong Y, Guo Y, Lin Y, Zhang J. SARS-CoV-2 omicron variant: epidemiological features, biological characteristics, and clinical significance. *Front Immunol.* 2022; 13:877101.
- Zeng B, Gao L, Zhou Q, Yu K, Sun F. Effectiveness of COVID-19 vaccines against SARS-CoV-2 variants of concern: a systematic review and meta-analysis. *BMC Med.* 2022; 20:200.
- Tian D, Sun Y, Xu H, Ye Q. The emergence and epidemic characteristics of the highly mutated SARS-CoV-2 omicron variant. *J Med Virol.* 2022; 94:2376-2383.
- Rahman S, Montero MTV, Rowe K, Kirton R, Kunik F Jr. Epidemiology, pathogenesis, clinical presentations diagnosis and treatment of COVID-19: A review of current evidence. *Expert Rev Clin Pharmacol.* 2021; 14:601-621.
- Ministry of Health Labour and Welfare. Coronavirus (COVID-19). https://www.mhlw.go.jp/stf/seisakunitsuite/bunya/0000164708_00079.html (accessed December 3, 2022).
- Martin B, DeWitt PE, Russell S, *et al.* Characteristics, outcomes, and severity risk factors associated with SARS-CoV-2 infection among children in the US National COVID cohort Collaborative. *JAMA Netw Open.* 2022; 5:e2143151.
- Duong BV, Larpruenrudw P, Fang T, Hossain SI, Saha SC, Gu Y, Islam MS. Is the SARS CoV-2 omicron variant deadlier and more transmissible than delta variant? *Int J Environ Res Public Health.* 2022; 19:4586.
- Notomi T, Okayama H, Masubuchi H, Yonekawa T, Watanabe K, Amino N, Hase T. Loop-mediated isothermal amplification of DNA. *Nucleic Acids Res.* 2000; 28:E63.
- Kitagawa Y, Orihara Y, Kawamura R, Imai K, Sakai J, Tarumoto N, Matsuoka M, Takeuchi S, Maesaki S, Maeda T. Evaluation of rapid diagnosis of novel coronavirus disease (COVID-19) using loop-mediated isothermal amplification. *J Clin Virol.* 2020; 129:104446.
- Ministry of Health Labour and Welfare. COVID-19 clinical practice guide, 8th edition. <https://www.mhlw.go.jp/content/000936655.pdf> (accessed October 5, 2022).
- Oken MM, Creech RH, Tormey DC, Horton J, Davis TE, McFadden ET, Carbone PP. Toxicity and response criteria of the Eastern Cooperative Oncology Group. *Am J Clin Oncol.* 1982; 5:649-655.
- Matsunaga N, Hayakawa K, Asai Y, *et al.* Clinical characteristics of the first three waves of hospitalized patients with COVID-19 in Japan prior to the widespread use of vaccination: a nationwide observational study. *Lancet Reg Health West Pac.* 2022; 22:100421.

23. Simoni L, Alimehmeti I, Ceka A, Tafaj EA, Gina M, Panariti A, Xhafaj F, Dibra A, Goda A. Ongoing COVID-19 pandemic effects on admissions and in-hospital outcomes in patients with ST-elevation myocardial infarction (STEMI): An Albanian observational Study. *Cureus*. 2022; 14:e26813.
24. D'Arminio Monforte A, Tavelli A, Bai F, *et al*. Declining mortality rate of hospitalised patients in the second wave of the COVID-19 epidemics in Italy: Risk factors and the age-specific patterns. *Life (Basel)*. 2021; 11:979.
25. Shi HJ, Nham E, Kim B, *et al*. Clinical characteristics and risk factors for mortality in critical coronavirus disease 2019 patients 50 years of age or younger during the delta wave: comparison with patients > 50 years in Korea. *J Korean Med Sci*. 2022; 37:e175.
26. Demetriou CA, Achilleos S, Quattrocchi A, *et al*. Impact

of the COVID-19 pandemic on total, sex- and age-specific all-cause mortality in 20 countries worldwide during 2020: results from the C-MOR project. *Int J Epidemiol*. 2022; dyac170.

Received December 2, 2022; Revised February 10, 2022; Accepted February 24, 2023.

**Address correspondence to:*

Takuya Kishi, International University of Health and Welfare Graduate School of Medicine (Cardiology) 137-1 Enokizu, Okawa, Fukuoka, 831-0016, Japan.
E-mail: tkishi@iuhw.ac.jp

Released online in J-STAGE as advance publication February 26, 2023.

Continuous ingestion of sodium chloride solution promotes allergen absorption and may exacerbate allergy symptoms on ovalbumin-induced food allergy in mice

Mamoru Tanaka*, Rui Lu, Hana Kozai

Department of Food and Nutrition Sciences, College of Bioscience and Biotechnology, Chubu University, Kasugai, Aichi, Japan.

SUMMARY Various studies have reported relationships between salt intake and diseases, such as hypertension, cardiovascular disease, stroke, gastric cancer, and bronchial asthma. However, no reports exist on the relationship between salt intake and food allergies. In this study, we investigated the effect of continuous ingestion of sodium chloride (NaCl) on allergy symptoms using a mouse model of food allergy. BALB/c mice were divided into four groups of 6-8 animals each. The control-water group (CW) and sensitization-water group (SW) groups were provided free access to water, and the control-1% NaCl group (CS) and sensitization-1% NaCl group (SS) groups were provided a 1% NaCl solution. The SW and SS groups were sensitized with 50 µg ovalbumin (OVA) at 2 timepoints by intraperitoneal injection. After oral administration of OVA, anaphylactic response was measured and blood was collected. The mice were sacrificed, and serum levels of OVA and anti-OVA immunoglobulin (Ig)E and IgG1 were measured by enzyme-linked immunosorbent assays. The sodium ion (Na⁺) concentrations in duodenal and jejunal extracts were measured using a Na⁺ ion meter. The results suggested that continuous ingestion of a 1% NaCl solution for 36 days promoted allergen absorption and may have aggravated allergy symptoms in the mice. However, NaCl ingestion did not affect Na⁺ concentrations in the small intestine or OVA-specific antibody production.

Keywords Food allergy, sodium chloride, BALB/c mice, absorption, allergy symptoms

1. Introduction

Excessive salt intake may induce hypertension, and, if the blood pressure remains high, the blood vessels and heart may be strained, resulting in the progression of arteriosclerosis and cardiac hypertrophy. Consequently, studies on the relationship between dietary salt intake and disease have focused mainly on life-style related conditions, such as stroke, myocardial infarction, and heart failure (1). The sodium ion (Na⁺) attracts water, which increases the amount of water and blood flow in the human body (1). Therefore, it is postulated that the absorption of allergens may be promoted. In addition, it has been suggested that the small-intestinal epithelial cells may be damaged by an increase in Na⁺ concentration in the gastrointestinal tract. Damage to epithelial cells in the small intestine induced by wheat gliadin (2), acute exercise (3), and aspirin intake (4) has been reported to increase absorption of allergens. However, to our knowledge, there have been no studies on the relationship between salt intake and allergies. We hypothesized that, when food is digested, Na⁺ will

damage small-intestinal epithelial cells and increase the absorption of undigested and partially digested allergens, which may exacerbate allergy symptoms. In this study, we investigated the effect of continuous ingestion of a sodium chloride (NaCl) solution on allergy symptoms using a mouse model of food allergy.

2. Materials and Methods

2.1. Animal and sensitization

All experiments were performed in accordance with the guidelines for animal experimentation and approved by the Animal Experimental Committee of the Chubu University (authorization number: 201910003). Female, 5-week-old BALB/cCrSlc mice (15-20 g in weight) were obtained from Japan SLC, Inc. (Hamamatsu, Shizuoka, Japan). Mice were housed at 22 ± 2°C with 50 ± 10% relative humidity and a 12-h light-dark cycle in a specific pathogen-free facility. The animals were provided a standard diet and water *ad libitum*. After acclimating for 6 days, the mice (*n* = 29) were divided into four groups

and provided with either water or 1% NaCl (prepared in water). The mice were grouped as follows: control-water group (CW), control-1% NaCl group (CS), sensitization-water group (SW), and sensitization-1% NaCl group (SS). The sensitized mice were injected intraperitoneally with 50 µg of ovalbumin (OVA; A5503, Sigma-Aldrich, St. Louis, MO, USA) and 4 mg of aluminum hydroxide (Imject™ Alum; Thermo Fisher Scientific, Waltham, MA, USA) emulsified in 0.2 mL of phosphate-buffered saline (PBS), pH 7.0, on days 14 and 21. The unsensitized animals received aluminum hydroxide in PBS as the vehicle control.

2.2. Animal protocol

Thirty-six days after the beginning of the experiment, all mice (11 weeks old) were orally administered 10 mg of OVA in 0.5 mL of PBS each. Thirty minutes after the oral administration, rectal temperatures were measured using an endorectal probe and AD-1687 Weighing Environment Logger (A&D Co., Toshima-Ku, Tokyo, Japan) to evaluate allergic responses. The mice were anesthetized with isoflurane to collect whole blood from the portal vein and then sacrificed to collect the duodenal and jejunal contents. Serum was separated from the blood by centrifugation at $700 \times g$ for 15 min. The small intestines were divided into six equal parts. The duodenum (upper one-sixth of the intestine) and jejunum (second and third sections of the upper intestine) were extracted with 1 mL of deionized water. Supernatants were prepared from the duodenal and jejunal extracts by centrifugation at $700 \times g$ for 15 min. All samples were stored at -20°C or lower.

2.3. Enzyme-linked immunosorbent assay (ELISA)

The OVA-specific immunoglobulin (Ig)E and IgG1 levels in mouse serum were evaluated by ELISA as described previously (2). Flat-bottomed microtiter plates were precoated with 100 µL of OVA (10 µg/mL) in a carbonate buffer (pH 9.6) and incubated overnight at 4°C . After the wells were washed with PBS containing 0.05% Tween 20 (PBS-T), 1% bovine serum albumin (BSA) in PBS-T was added to each well, and the plate was incubated for 1 h at 37°C . BSA and Tween 20 were obtained from Wako Pure Chemical Industries (Chuo-ku, Osaka, Japan). Each serum sample was diluted 100-fold (specific IgE) or 1000-fold (specific IgG1) with 1% BSA/PBS-T and 100 µL aliquots were added to each well. The plate was incubated for 1 h at 37°C and each well was washed five times with PBS-T. Aliquots (100 µL) of either horseradish peroxidase (HRP)-conjugated IgG anti-mouse IgE (diluted 1:1,000; Santa Cruz Biotechnology, Dallas, Texas, USA) or HRP-conjugated IgG anti-mouse IgG1 (diluted 1:5000; Santa Cruz) were added to the appropriate wells and incubated for 1 h at 37°C . The wells were washed five times with PBS-T, and

100 µL of *o*-phenyldiamine (0.4 mg/mL) in a citrate-phosphate buffer (pH 5.0) containing 0.006% H_2O_2 (aq.) was added to each well. Color development was measured by colorimetric photometry at 490 nm.

The FASPEK Egg (Ovalbumin) ELISA Kit (OVA) was purchased from Morinaga Institute of Biological Science, Inc. (Yokohama, Kanagawa, Japan). The levels of OVA in mouse serum were measured according to the manufacturer's instructions.

2.4. Measurement of Na^+ concentration

The Na^+ concentration was determined using a LAQUAtwin Na-11 Na^+ ion meter (HORIBA Scientific, Minami-Ku, Kyoto, Japan).

2.5. Statistical analysis

Data are expressed as the mean \pm SEM. All statistical analyses were performed using SPSS Statistics software, version 25.0 (IBM Japan, Chuo-Ku, Tokyo, Japan). Analysis of variance (ANOVA) with Tukey's post hoc test was used to determine differences between the control and treated groups of mice. Data were considered to be significantly different with p -values < 0.05 .

3. Results and Discussion

In the present study, we used a mouse model of OVA-induced food allergy to investigate the effect of continuous ingestion of NaCl solution on allergy symptoms, allergen concentration and anti-OVA antibodies in the serum, and Na^+ concentration in the small intestine. In this study, we did not measure water intake; however, there was no difference in body weight observed in the presence or absence of sensitization or 1% NaCl solution (data not shown).

This mouse model for food allergies is characterized by excessive production of allergen-specific IgE and IgG1 antibodies (5,6). Therefore, IgE and IgG1 levels are often used as indicators of a food allergy. The concentrations of OVA-specific IgE and IgG1 produced by the mice injected with OVA were significantly greater than the antibody levels produced by the unsensitized mice (Figures 1A and 1B). However, a significant difference in OVA-specific IgE and IgG1 levels was not observed between the SW and SS groups (Figures 1A and 1B). Our results suggest that the sensitization with OVA promoted antibody production, but there was no effect on antibody production after ingestion of 1% NaCl solution.

Next, we investigated the effect of continuous intake of 1% NaCl on allergy symptoms and the gastrointestinal tract of unsensitized and sensitized mice. It has been reported that histamine released from mast cells of allergen-sensitized mice increased vascular permeability and decreased body temperature (7). Therefore, changes

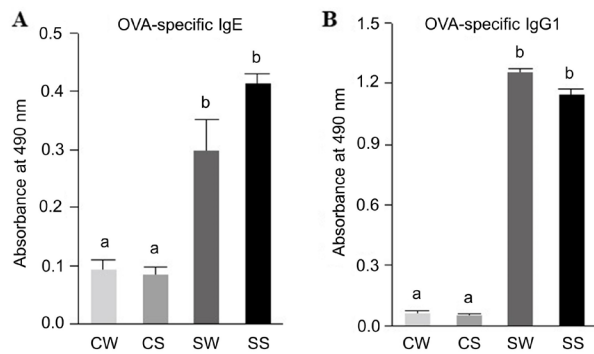


Figure 1. OVA-specific (A) IgE and (B) IgG1 levels in sera from unsensitized and OVA-sensitized mice after ingestion of water or 1% NaCl solution. CW, control-water group ($n = 6$); CS, control-1% NaCl group ($n = 8$); SW, sensitization-water group ($n = 8$); SS, sensitization-1% NaCl group ($n = 7$); OVA, ovalbumin. Data are expressed as the mean \pm SEM, $p < 0.05$ (a vs. b).

in body temperature are used commonly in the evaluation of allergies (6,7). In our study, body temperature was determined to assess anaphylaxis in the mice. The SS group had a significant decrease in rectal temperature compared with the other groups (Figure 2A). Our data suggest that NaCl ingestion exacerbates allergy symptoms after sensitization with OVA, in contrast to sensitization alone.

The concentration of OVA was significantly higher in the portal blood of mice who ingested the 1% NaCl solution compared with that in the portal blood of mice who ingested water (Figure 2B). These results indicated that NaCl intake promoted allergen absorption with or without prior sensitization with OVA. However, there were no significant differences in Na^+ concentration in the duodenal and jejunal contents between the four groups (Figure 2C).

The mechanism by which salt raises blood pressure has not been completely elucidated; however, increases in blood volume and Na^+ concentration in body fluids after salt intake may be related. It has been suggested that endogenous digitalis-like substances are involved as humoral factors and vasoactive substances. These substances are present in the adrenal gland and central nervous system, have natriuretic, vasoconstrictive, and sympathetic effects, and are increased by salt intake. In addition, it has been reported that other substances and conditions are involved in regulating high blood pressure caused by salt intake, including aldosterone, angiotensin, vasopressin, nitric oxide and vascular endothelium, oxidative stress, and Na^+ storage in the skin (1).

In our study, the difference in Na^+ concentration in the upper part of the small intestine and the degree of damage to the small intestine could not be observed. However, we propose that allergens are more easily absorbed by damaged epithelial tissue than under normal conditions. Several factors have also been reported to be involved in increased absorption of allergens

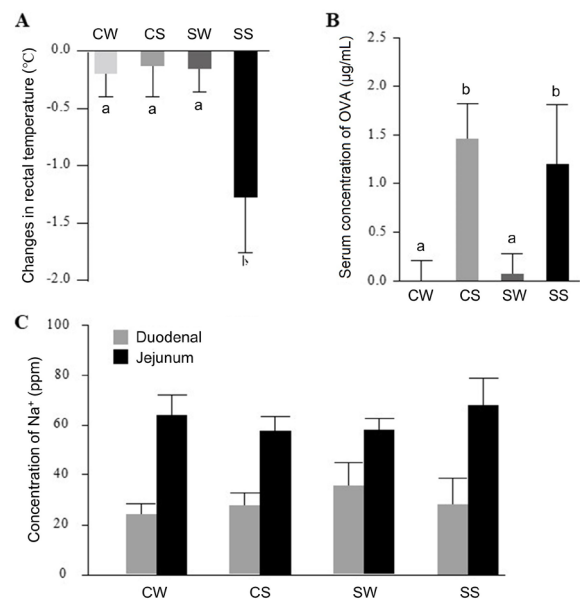


Figure 2. Effect of NaCl on changes in (A) rectal temperatures, (B) serum concentration of OVA, and (C) Na^+ concentration of duodenal and jejunal contents after oral administration of OVA in OVA-unsensitized and sensitized mice. CW, control-water group ($n = 6$); CS, control-1% NaCl group ($n = 8$); SW, sensitization-water group ($n = 8$); SS, sensitization-1% NaCl group ($n = 7$); OVA, ovalbumin. Data are expressed as the mean \pm SEM. $p < 0.05$ (a vs. b).

(2-4). Yokooji *et al.* (4) investigated the absorption mechanism of food allergens using fluorescein-labeled OVA in rats and found that the undigested allergen was absorbed through intercellular transport pathways, even in a healthy gastrointestinal tract. In addition, these authors reported that aspirin promoted the absorption of OVA by disrupting the intestinal barrier (4). The increased absorption of OVA after NaCl ingestion may be mediated by a similar mechanism involving damage to the intestinal barrier.

In conclusion, using a mouse model for food allergy, we have shown that continuous ingestion of 1% NaCl solution for 36 days promoted allergen absorption and may have exacerbated allergy symptoms. NaCl ingestion did not affect the Na^+ concentration in the small intestine or the production of allergen-specific antibodies.

Acknowledgements

We acknowledge Nozomi Kuroyanagi and Yuto Asano for their help with the laboratory analyses. We also thank Susan Zunino, PhD, from Edanz Group (<https://en-author-services.edanz.com/ac>) for editing a draft of this manuscript.

Funding: None.

Conflict of Interest: The authors have no conflicts of interest to disclose.

References

1. Kurtz TW, DiCarlo SE, Pravenec M, Morris RC Jr. The American Heart Association Scientific Statement on salt sensitivity of blood pressure: Prompting consideration of alternative conceptual frameworks for the pathogenesis of salt sensitivity? *J Hypertens*. 2017; 35:2214-2225.
2. Kozai H, Yano H, Matsuda T, Kato Y. Wheat-dependent exercise-induced anaphylaxis in mice is caused by gliadin and glutenin treatments. *Immunol Lett*. 2006 ;102:83-90.
3. Yano H, Kato Y, Matsuda T. Acute exercise induces gastrointestinal leakage of allergen in lysozyme-sensitized mice. *Eur J Appl Physiol*. 2002; 87:358-364.
4. Yokooji T, Nouma H, Matsuo H. Characterization of ovalbumin absorption pathways in the rat intestine, including the effects of aspirin. *Biol Pharm Bull*. 2014; 37:1359-1365.
5. Chen C, Sun N, Li Y, Jia X. A BALB/c mouse model for assessing the potential allergenicity of proteins: comparison of allergen dose, sensitization frequency, timepoint and sex. *Food Chem Toxicol*. 2013; 62:41-47.
6. Tanaka M, Watanabe H, Yoshimoto Y, Kozai H, Okamoto T. Anti-allergic effects of His-Ala-Gln tripeptide *in vitro* and *in vivo*. *Biosci Biotechnol Biochem*. 2017; 81:380-383.
7. Makabe-Kobayashi Y, Hori Y, Adachi T, Ishigaki-Suzuki S, Kikuchi Y, Kagaya Y, Shirato K, Nagy A, Ujike A, Takai T, Watanabe T, Ohtsu H. The control effect of histamine on body temperature and respiratory function in IgE-dependent systemic anaphylaxis. *J Allergy Clin Immunol*. 2002, 110:298-303.

Received November 6, 2022; Revised January 21, 2023; Accepted February 21, 2023.

**Address correspondence to:*

Mamoru Tanaka, Department of Food and Nutrition Sciences, College of Bioscience and Biotechnology, Chubu University, Kasugai, Aichi, Japan, 1200 Matsumoto-cho, Kasugai-city, Aichi 487-8501, Japan.

E-mail: m-tanaka@isc.chubu.ac.jp

Released online in J-STAGE as advance publication February 25, 2023.

A study of 95 infantile hemangiomas treated with propranolol: A potentially efficacious combination with laser therapy

Saori Yamada-Kanazawa^{1,*}, Shuichi Shimada¹, Wakana Nakayama¹, Soichiro Sawamura¹, Yuki Nishimura¹, Ikko Kajihara¹, Katsunari Makino¹, Jun Aoi¹, Shinichi Masuguchi¹, Fukiko Amano², Satoshi Fukushima¹

¹Department of Dermatology and Plastic Surgery, Faculty of Life Sciences, Kumamoto University, Kumamoto, Japan;

²Amano dermatology clinic, Kumamoto, Japan.

SUMMARY We studied 95 patients with infantile hemangioma (IH) treated with propranolol at the Department of Dermatology, Kumamoto University Hospital, from November 2016 to January 2022, based on sex, site, clinical classification, duration of treatment, and residual lesions after treatment. Four of the 95 patients discontinued propranolol due to side effects, and 55 completed follow-ups at our hospital. We observed that 30.1% showed complete resolution of the skin rash, while the remaining 69.8% had erythema or atrophic scarring. Complete resolution occurred in 70% of the cases with the subcutaneous type but only in 15% with the tumor type. Seventeen of the 55 patients who completed follow-ups were treated with propranolol combined with laser therapy. Combined use of propranolol and laser therapy significantly reduced severe erythema compared to the propranolol monotherapy. These results suggest that propranolol therapy in IH often leaves erythema except in the subcutaneous type and that an improvement in erythema can be expected when propranolol is combined with laser therapy.

Keywords combination therapy, infantile hemangioma, laser, propranolol, residual lesion

Infantile hemangioma (IH) is a benign tumor derived from vascular endothelial cells and characterized by neoplastic proliferation of vascular endothelial cells and resolution by apoptosis. In most cases, IH is not present at birth; it develops at 2-4 weeks and resolves spontaneously by 5-6 years of age (1,2). Léauté-Labrèze *C et al.* used propranolol in infants with IH complicated by hypertrophic obstructive cardiomyopathy and discovered by chance that the drug was remarkably effective in IH, which was reported in 2008 in a paper (3). In Japan, propranolol was approved for IH in September 2016 and is now used in many patients. In the past, IH was often treated by a wait-and-watch approach. However, the complete resolution of the hemangioma was surprisingly rare, and some residual lesions such as telangiectasia, atrophic scars, and sagging skin were often seen after resolution. With the advent of oral propranolol, the time seems ripe for aggressive therapeutic intervention to reduce residual lesions more lightly. In this study, we analyzed patients with IH who were treated with propranolol at our hospital and reported on the efficacy of the combination of propranolol and laser therapy.

Data from 95 patients with IH treated with oral propranolol therapy at the Department of Dermatology, Kumamoto University Hospital (Kumamoto, Japan) from November 2016 to January 2022 were analyzed retrospectively for sex, site, clinical classification (4), treatment duration, and residual lesions after treatment. In accordance with the Declaration of Helsinki, the institutional review board approval was obtained, and all patients provided written informed consent. The laser used was a 595-nm long-pulse dye laser (V-beam, Candela Corp. Wayland, USA). Categorical variables were expressed as frequencies and percentages and compared using the χ^2 test. All analyses were performed using SPSS version 25 (SPSS Inc., Chicago, IL, USA). All statistical tests were two-sided, and a *p*-value < 0.05 was regarded as statistically significant.

We introduced propranolol to 95 patients with IH at our hospital, and 55 completed follow-ups within the target period, 17 of whom were treated with propranolol combined with laser therapy (Figure S1, <http://www.ddtjournal.com/action/getSupplementalData.php?ID=136>). The average age for initiation of propranolol was 4 months, and the

average duration of treatment was 1 year and 2 months, regardless of concurrent laser therapy. Four patients discontinued propranolol due to side effects, which included hypotension, diarrhea, asthma-like attacks, and hypoglycemia/convulsions (Table S1, <http://www.ddtjournal.com/action/getSupplementalData>.

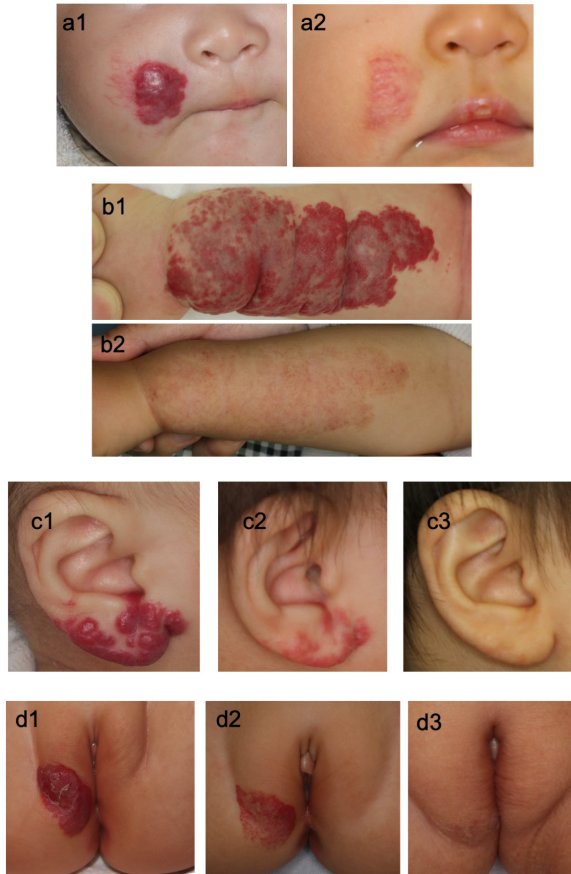


Figure 1. Residual erythema. (a, b) Cases of residual erythema after oral propranolol treatment. IH of tumor type in the right cheek: (a1) before treatment, (a2) after 6 months of oral propranolol therapy. IH of tumor type in the forearm: (b1) before treatment, (b2) after 2 years of oral propranolol therapy. (c, d) Cases of erythema improved by adding laser treatment to oral propranolol. IH of tumor type in the right auricular: (c1) before treatment, (c2) after 6 months of oral propranolol therapy, and (c3) additional laser treatment after 3 irradiations. IH of tumor type in the genitalia: (d1) before treatment, (d2) after 1 year and 2 months of oral propranolol therapy, and (d3) additional laser treatment, after 3 irradiations.

[php?ID=136](http://www.ddtjournal.com/action/getSupplementalData.php?ID=136)).

IH was more prevalent among girls, with a male-to-female ratio of 1:3.3 (boys: 23.2%, girls: 76.8%) (Table S2, <http://www.ddtjournal.com/action/getSupplementalData.php?ID=136>). About half of the patients (45.6%) had facial lesions, which are an indication for propranolol therapy due to possible subsequent functional and cosmetic problems. Most had tumor type (72.0%). Of the 55 patients who completed the follow-ups at our institution, only 30.1% had complete resolution of the skin rash, and the remaining 69.8% had erythema and atrophic scarring despite propranolol treatment (Figure 1a and 1b, Figure S2, <http://www.ddtjournal.com/action/getSupplementalData.php?ID=136>). We observed that 70% of the patients with the subcutaneous type had complete resolution with propranolol monotherapy alone. In contrast, in the non-subcutaneous type, erythema often remained, and complete resolution of the tumor type was seen in only 15 % of cases (Figure S2, <http://www.ddtjournal.com/action/getSupplementalData.php?ID=136>).

In the propranolol combined with the laser therapy group, all patients showed a reduction or disappearance of erythema (Figure 1c, d). Therefore, we performed a statistical analysis on the efficacy of the combination of propranolol and laser therapy. Regarding baseline characteristics, compared with the propranolol monotherapy group, the combined laser group was more likely to have the tumor type (85.7% vs. 52.4%, $p = 0.010$). No patients with the subcutaneous type received laser therapy due to lack of laser indications. There were no other differences in sex, number of lesions, or location between the two groups (Table S2, <http://www.ddtjournal.com/action/getSupplementalData.php?ID=136>). To determine the effect of laser therapy on residual erythema, we compared the therapeutic outcomes of the two groups by dividing the degree of residual erythema into mild and severe. The subcutaneous type was excluded from this analysis as it was not indicated for laser treatment (Table 1). No cases of severe residual erythema remained in the combined laser treatment group. Severe erythema was significantly reduced in the propranolol combined with the laser therapy group compared to the propranolol monotherapy

Table 1. Relationship between residual erythema and laser therapy

| Type of hemangioma | Degree of erythema | Propranolol monotherapy | Propranolol combined with laser | <i>p</i> -value |
|---------------------------------------|--------------------|--------------------------------|---------------------------------|-----------------|
| Plaque + Tumor (<i>n</i> = 53 IH) | mild | <i>n</i> = 32 IH 13 (40.6%) | <i>n</i> = 21 IH 9 (42.9%) | 0.872 |
| | severe | 7 (21.9%) | 0 (0%) | 0.022 |
| Plaque (<i>n</i> = 13 IH) | mild | <i>n</i> = 10 IH 5 (50.0%) | <i>n</i> = 3 IH 1 (33.3%) | 0.563 |
| | severe | 0 (0%) | 0 (0%) | - |
| Tumor (<i>n</i> = 40 IH) | mild | <i>n</i> = 22 IH 8 (36.4%) | <i>n</i> = 18 IH 8 (44.4%) | 0.604 |
| | severe | 7 (31.8%) | 0 (0%) | 0.009 |

IH, infantile hemangioma.

group (21.9% vs. 0%, $p = 0.022$). This reduction was the most prominent for the tumor type (31.8% vs. 0%, $p = 0.009$).

In this study, we presented two novel findings. First, IH, except for the subcutaneous type lesions, treated with oral propranolol monotherapy often left residual lesions such as erythema. The cause of residual erythema after propranolol treatment is not yet understood. Factors contributing to erythema include simple residual lesions, nutrient vessels, and normal blood vessels that have become more prominent due to skin stretching. Future studies using Glut-1 staining of skin biopsy from the erythematous area may help to determine the cause. Second, we found that combined use of propranolol and laser therapy significantly reduced severe residual erythema compared to the propranolol monotherapy, especially in the tumor type. Almost all cases of tumor type IH that resolved completely were treated with propranolol combined with laser therapy. Laser therapy was more reliably and rapidly effective for erythema than oral propranolol, however due to the small number of patients in this study, there was no significant difference in the plaque type or residual mild erythema. Further case studies are needed.

Recently, several papers have reported on the combination of oral propranolol and laser therapy for IH (5,6). Reddy KK *et al.* reported that patients with segmental IH of the face had earlier remission in the propranolol plus laser therapy group than in the propranolol monotherapy group (7). In the present study, there was no difference in the mean durations of propranolol treatment with or without laser therapy. We observed several patients in which the tumor had flattened and only erythema remained, was continued propranolol for a long period of time despite laser therapy. When the tumor flattens, it may be better to discontinue propranolol, to prevent its side effects, and continue with only laser treatment.

To summarize this study, propranolol therapy effectively reduced the tumor size; however, erythema persisted for a longer time than expected, while laser therapy effectively eliminated the surface erythema. We believe that a regimen that extracts the advantages of each method is recommended; initiating laser therapy as soon as an IH is detected, adding oral propranolol when a tumor forms, and discontinuing oral propranolol and continuing laser therapy alone when the tumor flattens and only erythema is present. We hope that with the

accumulation of data from future cases, the combination of propranolol and laser therapy can become the standard therapy for IH and that IH can be treated promptly with fewer residual lesions.

Funding: None.

Conflict of Interest: The authors have no conflicts of interest to disclose.

References

1. Rodríguez Bandera AI, Sebaratnam DF, Wargon O, Wong LF. Infantile hemangioma. Part 1: Epidemiology, pathogenesis, clinical presentation and assessment. *J Am Acad Dermatol.* 2021; 85:1379-1392.
2. Kaneko T, Sasaki S, Baba N, *et al.* Efficacy and safety of oral propranolol for infantile hemangioma in Japan. *Pediatr Int.* 2017; 59:869-877.
3. Léauté-Labrèze C, Dumas de la Roque E, Hubiche T, Boralevi F, Thambo JB, Taïeb A. Propranolol for severe hemangiomas of infancy. *N Engl J Med.* 2008; 358:2649-2651.
4. Nakayama H. Clinical and histological studies of the classification and the natural course of the strawberry mark. *J Dermatol.* 1981; 8:277-291.
5. Hartmann F, Lockmann A, Himpel O, Kühnle I, Hensen J, Schön MP, Thoms KM. Combination therapy of oral propranolol and combined Nd:YAG/pulsed dye laser therapy in infantile hemangiomas: a retrospective analysis of 48 treated hemangiomas in 30 children. *J Dtsch Dermatol Ges.* 2020; 18:984-993.
6. Sun X, Liu X, Lu N, Yao S, Xu X, Niu L. Short-term curative effect and safety of propranolol combined with laser in the treatment of infantile hemangiomas. *Oncol Lett.* 2018; 16:6561-6565.
7. Reddy KK, Blei F, Brauer JA, Waner M, Anolik R, Bernstein L, Brightman L, Hale E, Karen J, Weiss E, Geronemus RG. Retrospective study of the treatment of infantile hemangiomas using a combination of propranolol and pulsed dye laser. *Dermatol Surg.* 2013; 39:923-933.

Received October 17, 2023; Revised February 16, 2023; Accepted February 20, 2023.

**Address correspondence to:*

Saori Yamada-Kanazawa, Department of Dermatology and Plastic Surgery, Faculty of Life Sciences, Kumamoto University, 1-1-1 Honjo, Kumamoto, Japan.
E-mail: saoritinkerbelle@gmail.com

Released online in J-STAGE as advance publication February 25, 2023.



Drug Discoveries & Therapeutics

Guide for Authors

1. Scope of Articles

Drug Discoveries & Therapeutics (Print ISSN 1881-7831, Online ISSN 1881-784X) welcomes contributions in all fields of pharmaceutical and therapeutic research such as medicinal chemistry, pharmacology, pharmaceutical analysis, pharmaceuticals, pharmaceutical administration, and experimental and clinical studies of effects, mechanisms, or uses of various treatments. Studies in drug-related fields such as biology, biochemistry, physiology, microbiology, and immunology are also within the scope of this journal.

2. Submission Types

Original Articles should be well-documented, novel, and significant to the field as a whole. An Original Article should be arranged into the following sections: Title page, Abstract, Introduction, Materials and Methods, Results, Discussion, Acknowledgments, and References. Original articles should not exceed 5,000 words in length (excluding references) and should be limited to a maximum of 50 references. Articles may contain a maximum of 10 figures and/or tables. Supplementary Data are permitted but should be limited to information that is not essential to the general understanding of the research presented in the main text, such as unaltered blots and source data as well as other file types.

Brief Reports definitively documenting either experimental results or informative clinical observations will be considered for publication in this category. Brief Reports are not intended for publication of incomplete or preliminary findings. Brief Reports should not exceed 3,000 words in length (excluding references) and should be limited to a maximum of 4 figures and/or tables and 30 references. A Brief Report contains the same sections as an Original Article, but the Results and Discussion sections should be combined.

Reviews should present a full and up-to-date account of recent developments within an area of research. Normally, reviews should not exceed 8,000 words in length (excluding references) and should be limited to a maximum of 10 figures and/or tables and 100 references. Mini reviews are also accepted, which should not exceed 4,000 words in length (excluding references) and should be limited to a maximum of 5 figures and/or tables and 50 references.

Policy Forum articles discuss research and policy issues in areas related to life science such as public health, the medical care system, and social science and may address governmental issues at district, national, and international levels of discourse. Policy Forum articles should not exceed 3,000 words in length (excluding references) and should be limited to a maximum of 5 figures and/or tables and 30 references.

Case Reports should be detailed reports of the symptoms, signs, diagnosis, treatment, and follow-up of an individual patient. Case reports may contain a demographic profile of the patient but usually describe an unusual or novel occurrence. Unreported or unusual side effects or adverse interactions involving medications will also be considered. Case Reports should not exceed 3,000 words in length (excluding references).

Communications are short, timely pieces that spotlight new research findings or policy issues of interest to the field of global health and medical practice that are of immediate importance. Depending on their content, Communications will be published as "Comments" or

"Correspondence". Communications should not exceed 1,500 words in length (excluding references) and should be limited to a maximum of 2 figures and/or tables and 20 references.

Editorials are short, invited opinion pieces that discuss an issue of immediate importance to the fields of global health, medical practice, and basic science oriented for clinical application. Editorials should not exceed 1,000 words in length (excluding references) and should be limited to a maximum of 10 references. Editorials may contain one figure or table.

News articles should report the latest events in health sciences and medical research from around the world. News should not exceed 500 words in length.

Letters should present considered opinions in response to articles published in *Drug Discoveries & Therapeutics* in the last 6 months or issues of general interest. Letters should not exceed 800 words in length and may contain a maximum of 10 references. Letters may contain one figure or table.

3. Editorial Policies

For publishing and ethical standards, *Drug Discoveries & Therapeutics* follows the Recommendations for the Conduct, Reporting, Editing, and Publication of Scholarly Work in Medical Journals issued by the International Committee of Medical Journal Editors (ICMJE, <https://icmje.org/recommendations>), and the Principles of Transparency and Best Practice in Scholarly Publishing jointly issued by the Committee on Publication Ethics (COPE, <https://publicationethics.org/resources/guidelines-new/principles-transparency-and-best-practice-scholarly-publishing>), the Directory of Open Access Journals (DOAJ, <https://doaj.org/apply/transparency>), the Open Access Scholarly Publishers Association (OASPA, <https://oaspa.org/principles-of-transparency-and-best-practice-in-scholarly-publishing-4>), and the World Association of Medical Editors (WAME, <https://wame.org/principles-of-transparency-and-best-practice-in-scholarly-publishing>).

Drug Discoveries & Therapeutics will perform an especially prompt review to encourage innovative work. All original research will be subjected to a rigorous standard of peer review and will be edited by experienced copy editors to the highest standards.

Ethical Approval of Studies and Informed Consent: For all manuscripts reporting data from studies involving human participants or animals, formal review and approval, or formal review and waiver, by an appropriate institutional review board or ethics committee is required and should be described in the Methods section. When your manuscript contains any case details, personal information and/or images of patients or other individuals, authors must obtain appropriate written consent, permission and release in order to comply with all applicable laws and regulations concerning privacy and/or security of personal information. The consent form needs to comply with the relevant legal requirements of your particular jurisdiction, and please do not send signed consent form to *Drug Discoveries & Therapeutics* to respect your patient's and any other individual's privacy. Please instead describe the information clearly in the Methods (patient consent) section of your manuscript while retaining copies of the signed forms in the event they should be needed. Authors should also state that the study conformed to the provisions of the Declaration of Helsinki (as revised in 2013, <https://wma.net/what-we-do/medical-ethics/declaration-of-helsinki>). When reporting experiments on animals, authors should indicate whether the institutional and national guide for the care and use of laboratory animals was followed.

Reporting Clinical Trials: The ICMJE (<https://icmje.org/recommendations/browse/publishing-and-editorial-issues/clinical-trial-registration.html>) defines a clinical trial as any research project that prospectively assigns people or a group of people to an intervention, with or without concurrent comparison or control groups, to study the relationship between a health-related intervention and a health outcome. Registration of clinical trials in a public trial registry

at or before the time of first patient enrollment is a condition of consideration for publication in *Drug Discoveries & Therapeutics*, and the trial registration number will be published at the end of the Abstract. The registry must be independent of for-profit interest and publicly accessible. Reports of trials must conform to CONSORT 2010 guidelines (<https://consort-statement.org/consort-2010>). Articles reporting the results of randomized trials must include the CONSORT flow diagram showing the progress of patients throughout the trial.

Conflict of Interest: All authors are required to disclose any actual or potential conflict of interest including financial interests or relationships with other people or organizations that might raise questions of bias in the work reported. If no conflict of interest exists for each author, please state "There is no conflict of interest to disclose".

Submission Declaration: When a manuscript is considered for submission to *Drug Discoveries & Therapeutics*, the authors should confirm that 1) no part of this manuscript is currently under consideration for publication elsewhere; 2) this manuscript does not contain the same information in whole or in part as manuscripts that have been published, accepted, or are under review elsewhere, except in the form of an abstract, a letter to the editor, or part of a published lecture or academic thesis; 3) authorization for publication has been obtained from the authors' employer or institution; and 4) all contributing authors have agreed to submit this manuscript.

Initial Editorial Check: Immediately after submission, the journal's managing editor will perform an initial check of the manuscript. A suitable academic editor will be notified of the submission and invited to check the manuscript and recommend reviewers. Academic editors will check for plagiarism and duplicate publication at this stage. The journal has a formal recusal process in place to help manage potential conflicts of interest of editors. In the event that an editor has a conflict of interest with a submitted manuscript or with the authors, the manuscript, review, and editorial decisions are managed by another designated editor without a conflict of interest related to the manuscript.

Peer Review: *Drug Discoveries & Therapeutics* operates a single-anonymized review process, which means that reviewers know the names of the authors, but the authors do not know who reviewed their manuscript. All articles are evaluated objectively based on academic content. External peer review of research articles is performed by at least two reviewers, and sometimes the opinions of more reviewers are sought. Peer reviewers are selected based on their expertise and ability to provide quality, constructive, and fair reviews. For research manuscripts, the editors may, in addition, seek the opinion of a statistical reviewer. Every reviewer is expected to evaluate the manuscript in a timely, transparent, and ethical manner, following the COPE guidelines (https://publicationethics.org/files/cope-ethical-guidelines-peer-reviewers-v2_0.pdf). We ask authors for sufficient revisions (with a second round of peer review, when necessary) before a final decision is made. Consideration for publication is based on the article's originality, novelty, and scientific soundness, and the appropriateness of its analysis.

Suggested Reviewers: A list of up to 3 reviewers who are qualified to assess the scientific merit of the study is welcomed. Reviewer information including names, affiliations, addresses, and e-mail should be provided at the same time the manuscript is submitted online. Please do not suggest reviewers with known conflicts of interest, including participants or anyone with a stake in the proposed research; anyone from the same institution; former students, advisors, or research collaborators (within the last three years); or close personal contacts. Please note that the Editor-in-Chief may accept one or more of the proposed reviewers or may request a review by other qualified persons.

Language Editing: Manuscripts prepared by authors whose native language is not English should have their work proofread by a native English speaker before submission. If not, this might delay the publication of your manuscript in *Drug Discoveries & Therapeutics*.

The Editing Support Organization can provide English

proofreading, Japanese-English translation, and Chinese-English translation services to authors who want to publish in *Drug Discoveries & Therapeutics* and need assistance before submitting a manuscript. Authors can visit this organization directly at <https://www.iacmhr.com/iac-eso/support.php?lang=en>. IAC-ESO was established to facilitate manuscript preparation by researchers whose native language is not English and to help edit works intended for international academic journals.

Copyright and Reuse: Before a manuscript is accepted for publication in *Drug Discoveries & Therapeutics*, authors will be asked to sign a transfer of copyright agreement, which recognizes the common interest that both the journal and author(s) have in the protection of copyright. We accept that some authors (e.g., government employees in some countries) are unable to transfer copyright. A JOURNAL PUBLISHING AGREEMENT (JPA) form will be e-mailed to the authors by the Editorial Office and must be returned by the authors by mail, fax, or as a scan. Only forms with a hand-written signature from the corresponding author are accepted. This copyright will ensure the widest possible dissemination of information. Please note that the manuscript will not proceed to the next step in publication until the JPA Form is received. In addition, if excerpts from other copyrighted works are included, the author(s) must obtain written permission from the copyright owners and credit the source(s) in the article.

4. Cover Letter

The manuscript must be accompanied by a cover letter prepared by the corresponding author on behalf of all authors. The letter should indicate the basic findings of the work and their significance. The letter should also include a statement affirming that all authors concur with the submission and that the material submitted for publication has not been published previously or is not under consideration for publication elsewhere. The cover letter should be submitted in PDF format. For an example of Cover Letter, please visit: Download Centre (<https://www.ddtjournal.com/downcentre>).

5. Submission Checklist

The Submission Checklist should be submitted when submitting a manuscript through the Online Submission System. Please visit Download Centre (<https://www.ddtjournal.com/downcentre>) and download the Submission Checklist file. We recommend that authors use this checklist when preparing your manuscript to check that all the necessary information is included in your article (if applicable), especially with regard to Ethics Statements.

6. Manuscript Preparation

Manuscripts are suggested to be prepared in accordance with the "Recommendations for the Conduct, Reporting, Editing, and Publication of Scholarly Work in Medical Journals", as presented at <http://www.ICMJE.org>.

Manuscripts should be written in clear, grammatically correct English and submitted as a Microsoft Word file in a single-column format. Manuscripts must be paginated and typed in 12-point Times New Roman font with 24-point line spacing. Please do not embed figures in the text. Abbreviations should be used as little as possible and should be explained at first mention unless the term is a well-known abbreviation (e.g. DNA). Single words should not be abbreviated.

Title page: The title page must include 1) the title of the paper (Please note the title should be short, informative, and contain the major key words); 2) full name(s) and affiliation(s) of the author(s), 3) abbreviated names of the author(s), 4) full name, mailing address, telephone/fax numbers, and e-mail address of the corresponding author; 5) author contribution statements to specify the individual contributions of all authors to this manuscript, and 6) conflicts of interest (if you have an actual or potential conflict of interest to disclose, it must be included as a footnote on the title page of the manuscript; if no conflict of interest

exists for each author, please state "There is no conflict of interest to disclose").

Abstract: The abstract should briefly state the purpose of the study, methods, main findings, and conclusions. For article types including Original Article, Brief Report, Review, Policy Forum, and Case Report, a one-paragraph abstract consisting of no more than 250 words must be included in the manuscript. For Communications, Editorials, News, or Letters, a brief summary of main content in 150 words or fewer should be included in the manuscript. For articles reporting clinical trials, the trial registration number should be stated at the end of the Abstract. Abbreviations must be kept to a minimum and non-standard abbreviations explained in brackets at first mention. References should be avoided in the abstract. Three to six key words or phrases that do not occur in the title should be included in the Abstract page.

Introduction: The introduction should provide sufficient background information to make the article intelligible to readers in other disciplines and sufficient context clarifying the significance of the experimental findings.

Materials/Patients and Methods: The description should be brief but with sufficient detail to enable others to reproduce the experiments. Procedures that have been published previously should not be described in detail but appropriate references should simply be cited. Only new and significant modifications of previously published procedures require complete description. Names of products and manufacturers with their locations (city and state/country) should be given and sources of animals and cell lines should always be indicated. All clinical investigations must have been conducted in accordance with the Declaration of Helsinki (as revised in 2013, <https://wma.net/what-we-do/medical-ethics/declaration-of-helsinki>). All human and animal studies must have been approved by the appropriate institutional review board(s) and a specific declaration of approval must be made within this section.

Results: The description of the experimental results should be succinct but in sufficient detail to allow the experiments to be analyzed and interpreted by an independent reader. If necessary, subheadings may be used for an orderly presentation. All Figures and Tables should be referred to in the text in order, including those in the Supplementary Data.

Discussion: The data should be interpreted concisely without repeating material already presented in the Results section. Speculation is permissible, but it must be well-founded, and discussion of the wider implications of the findings is encouraged. Conclusions derived from the study should be included in this section.

Acknowledgments: All funding sources (including grant identification) should be credited in the Acknowledgments section. Authors should also describe the role of the study sponsor(s), if any, in study design; in the collection, analysis, and interpretation of data; in the writing of the report; and in the decision to submit the paper for publication. If the funding source had no such involvement, the authors should so state.

In addition, people who contributed to the work but who do not meet the criteria for authors should be listed along with their contributions.

References: References should be numbered in the order in which they appear in the text. Citing of unpublished results, personal communications, conference abstracts, and theses in the reference list is not recommended but these sources may be mentioned in the text. In the reference list, cite the names of all authors when there are fifteen or fewer authors; if there are sixteen or more authors, list the first three followed by *et al.* Names of journals should be abbreviated in the style used in *PubMed*. Authors are responsible for the accuracy of the references. The EndNote Style of *Drug Discoveries & Therapeutics* could be downloaded at **EndNote** (https://www.ddtjournal.com/examples/Drug_Discoveries_Therapeutics.ens).

Examples are given below:

Example 1 (Sample journal reference):

Nakata M, Tang W. Japan-China Joint Medical Workshop on Drug Discoveries and Therapeutics 2008: The need of Asian pharmaceutical researchers' cooperation. *Drug Discov Ther.* 2008; 2:262-263.

Example 2 (Sample journal reference with more than 15 authors):

Darby S, Hill D, Auvinen A, *et al.* Radon in homes and risk of lung cancer: Collaborative analysis of individual data from 13 European case-control studies. *BMJ.* 2005; 330:223.

Example 3 (Sample book reference):

Shalev AY. Post-traumatic stress disorder: Diagnosis, history and life course. In: *Post-traumatic Stress Disorder, Diagnosis, Management and Treatment* (Nutt DJ, Davidson JR, Zohar J, eds.). Martin Dunitz, London, UK, 2000; pp. 1-15.

Example 4 (Sample web page reference):

World Health Organization. The World Health Report 2008 – primary health care: Now more than ever. <https://apps.who.int/iris/handle/10665/43949> (accessed September 23, 2022).

Tables: All tables should be prepared in Microsoft Word or Excel and should be arranged at the end of the manuscript after the References section. Please note that tables should not in image format. All tables should have a concise title and should be numbered consecutively with Arabic numerals. If necessary, additional information should be given below the table.

Figure Legend: The figure legend should be typed on a separate page of the main manuscript and should include a short title and explanation. The legend should be concise but comprehensive and should be understood without referring to the text. Symbols used in figures must be explained. Any individually labeled figure parts or panels (A, B, *etc.*) should be specifically described by part name within the legend.

Figure Preparation: All figures should be clear and cited in numerical order in the text. Figures must fit a one- or two-column format on the journal page: 8.3 cm (3.3 in.) wide for a single column, 17.3 cm (6.8 in.) wide for a double column; maximum height: 24.0 cm (9.5 in.). Please make sure that artwork files are in an acceptable format (TIFF or JPEG) at minimum resolution (600 dpi for illustrations, graphs, and annotated artwork, and 300 dpi for micrographs and photographs). Please provide all figures as separate files. Please note that low-resolution images are one of the leading causes of article resubmission and schedule delays.

Units and Symbols: Units and symbols conforming to the International System of Units (SI) should be used for physicochemical quantities. Solidus notation (*e.g.* mg/kg, mg/mL, mol/mm²/min) should be used. Please refer to the SI Guide www.bipm.org/en/si/ for standard units.

Supplemental data: Supplemental data might be useful for supporting and enhancing your scientific research and *Drug Discoveries & Therapeutics* accepts the submission of these materials which will be only published online alongside the electronic version of your article. Supplemental files (figures, tables, and other text materials) should be prepared according to the above guidelines, numbered in Arabic numerals (*e.g.*, Figure S1, Figure S2, and Table S1, Table S2) and referred to in the text. All figures and tables should have titles and legends. All figure legends, tables and supplemental text materials should be placed at the end of the paper. Please note all of these supplemental data should be provided at the time of initial submission and note that the editors reserve the right to limit the size

and length of Supplemental Data.

7. Online Submission

Manuscripts should be submitted to *Drug Discoveries & Therapeutics* online at <https://www.ddtjournal.com/login>. Receipt of your manuscripts submitted online will be acknowledged by an e-mail from Editorial Office containing a reference number, which should be used in all future communications. If for any reason you are unable to submit a file online, please contact the Editorial Office by e-mail at office@ddtjournal.com

8. Accepted Manuscripts

Page Charge: Page charges will be levied on all manuscripts accepted for publication in *Drug Discoveries & Therapeutics* (Original Articles / Brief Reports / Reviews / Policy Forum / Communications: \$140 per page for black white pages, \$340 per page for color pages; News / Letters: a total cost of \$600). Under exceptional circumstances, the author(s) may apply to the editorial office for a waiver of the publication charges by stating the reason in the Cover Letter when the

manuscript online.

Misconduct: *Drug Discoveries & Therapeutics* takes seriously all allegations of potential misconduct and adhere to the ICMJE Guideline (<https://icmje.org/recommendations>) and COPE Guideline (https://publicationethics.org/files/Code_of_conduct_for_journal_editors.pdf). In cases of suspected research or publication misconduct, it may be necessary for the Editor or Publisher to contact and share submission details with third parties including authors' institutions and ethics committees. The corrections, retractions, or editorial expressions of concern will be performed in line with above guidelines.

(As of December 2022)

Drug Discoveries & Therapeutics
Editorial and Head Office
Pearl City Koishikawa 603,
2-4-5 Kasuga, Bunkyo-ku,
Tokyo 112-0003, Japan.
E-mail: office@ddtjournal.com

